ABSTRACT

Title of Document: NUMERICAL STUDY OF SEISMIC BEHAVIOR OF HIGH STRENGTH STEEL REPLACEABLE SHEAR LINKS

Huiling Hu
Master of Science, 2015

Directed By: Yunfeng Zhang, Professor
Department of Civil and Environmental Engineering

Eccentrically Braced Frames (EBFs) have been widely used in seismic protection and remediation in the recent years. However, the seismic behavior of shear links made of high strength steel, which are essential “fuse” elements in EBFs, are not fully understood yet. Furthermore, most existing studies either assumed no axial load or an unrealistic constant axial load. In this numerical simulation study, two steel grades (Q460 high strength structural steel (by China standard) and ASTM A992 steel for comparison) were considered for the shear link specimens and their effects on shear link’s seismic performance were numerically studied under cyclically varying lateral load along with axial force.

Finite element (FE) modeling of shear link specimens with the above two steel grades were established in a general FE analysis software – ANSYS and numerical simulations are conducted on these finite element models following monotonic and cyclic loading protocols respectively. To see whether a sustainability goal of steel structure design (by saving steel use) can be achieved or not, a feasibility study of Q460 steel shear links with various section size reduction schemes are performed in this research.

The numerical simulation results reveal that shear links made of Q460 high strength steel have satisfactory performance compared with A992 steel shear links, with additional benefits of material saving and weight reduction, often desired features for sustainable steel construction and replaceable fuse elements in seismic resistant structures.

NUMERICAL STUDY OF SEISMIC BEHAVIOR OF HIGH STRENGTH STEEL REPLACEABLE SHEAR LINKS

By

Huiling Hu

Thesis submitted to the Faculty of the Graduate School of the
University of Maryland, College Park, in partial fulfillment
of the requirements for the degree of
Master of Science
2015

Advisory Committee:
Professor Yunfeng Zhang, Chair/Advisor
Professor Chung C. Fu
Professor M. Sherif Aggour

ACKNOWLEDGEMENTS

I would like to express my gratefulness to Dr. Yunfeng Zhang, who has been advising me and guiding me through the development of this thesis. His insightfulness and encouragement are indispensable parts towards the completion of this thesis, and help me all the time when I was stuck in different challenges when doing research and writing this thesis.

I also thank Dr. Fu and Dr. Aggour for their valuable time serving on my thesis committee.

TABLE OF CONTENTS

LIST OF TABLES

LIST OF FIGURES

List of Notation

E – Elastic modulus

G – Shear modulus

F_y – Minimum yield strength

I – Moment of inertia

N – Axial Load

e – Link length

ρ – Link length ratio

γ_p – Plastic link rotation angle

A_g – Gross area

A_w – Web area

d – Overall beam depth

t_f – Flange thickness

t_w – Web thickness

V_p – Plastic shear capacity

Z – Plastic section modulus

M_p – Plastic flexural strength

K_e – Elastic stiffness

K_b – Flexural stiffness

K_s – Shear stiffness

Ω – Over-strength factor

V_{max} – Maximum shear force

V_y – Yield shear force

μ – Ductility factor

Δ_u – Ultimate displacement

Δ_y – Displacement at yield point

CHAPTER 1: INTRODUCTION

1.1. Motivation

Eccentrically braced frame (EBF) is a promising steel lateral force resisting structure system to resist seismic load. Compared to Concentrically Braced Frame (CBF) and Moment Resisting Frame (MRF), EBF has the advantage of providing high stiffness and ductility to the structure. Moreover, EBF also exhibit excellent hysteresis energy dissipation capacity. The EBFs are designed to develop inelastic actions in concentrated regions of fuse elements (i.e., link beams) under severe seismic action (e.g., under design basis earthquake), while other parts of the structure are kept elastic. As deformation-controlled fuse elements, the size of link beams has to be proportioned carefully in order that the link beams would behave satisfactorily. AISC Provision (2010) provides design procedures for EBFs from extensive experimental studies.

Wang et al. (2015) studied the experimental behavior of high strength steel under cyclic loadings. Similar to Shi et al, they are mainly concerned with the comparison between Q460 and Q345 (a type of steel in China standard, which has very similar property to ASTM A992 steel). Instead of using non-linear kinematic hardening model, a trilinear hardening model is used and yield a good matching with the experimental results. Green et al. (2002) also studied ultra-high strength steel, e.g., HPS steel. They compared the performance of high strength steel with yield stress up to 690MPa. The result shows that those steel types exhibit a less rotational capacity. Further, loading condition and material parameters have a greater impact on the performance.

Summarized by Fussell (2014), EBFs are used more and more widely in a replaceable manner: over the time, EBFs may suffer from great forces from an earthquake, where active links are damaged by design. In this case, it may be desirable if active links can be replaced with ease. However, in the conventional EBFs, it is costly and time consuming to replace the active links because it is usually the part of common floor beams. Replaceable EBFs have an extra bolted extended plates to facilitate the removal of links when necessary. In this study, the potential of reducing the size of shear links is later considered. By reducing the size, which in turn reduce the weight, of a shear link, the replacement of active links would become even easier and safer.

For replaceable shear links, it is important to keep their weight low so manual replacement can be done post-earthquake without the use of heavy lifting equipment. Therefore, it is of great significance if the size of link beams can be reduced further and made lighter without compromising its seismic performance.

1.2. Objective

The objective of this study is to investigate the potential use of shear links made of Q460 high strength steel (minimum yield stress = 460MPa by China standard, close to (but with lower strength) ASTM A70 steel) for EBFs by performing nonlinear finite element analysis. Finite element modeling of shear links were performed in a general purpose FE analysis software – ANSYS. Cyclically varying axial load is applied to a set of shear link specimens along with lateral force, in order to simulate the real loading conditions in shear links of EBFs subjected to earthquake ground motion. Moreover, the feasibility of using high strength steel for replaceable shear

link design in order to reduce the link beam size without compromising its seismic performance in comparison with conventional ASTM A992 steel shear links were also examined in this simulation study. In particular, the following tasks are planned:

1) To understand the seismic behavior of shear links made of Q460 high strength steel, finite element models of a variety of shear links with different section size and length are established in ANSYS and analyzed under cyclical lateral force in conjunction with varying axial load. In particular, four quantitative performance metrics including strength, ductility, energy dissipation, and stiffness of shear links are studied. The failure mode contours of each mode are also presented and discussed.

2) The seismic behavior of Q460 steel shear links with reduced section size are examined. The total material volume of Q460 steel (and thus weight) is expected to be reduced by ten per cent in Q460 shear link while maintaining comparable performance as those of ASTM A992 steel shear links with no apparent reduction in strength and ductility. This suggests that the weight of shear links can be reduced by using high strength steel in order to facilitate manual installation and replacement of shear links

1.3. Thesis Organization

In Chapter 2, previous experimental and numerical results on shear links are reviewed. It is popular to use shear links in seismic areas for its promising hysteric behavior. However, it is also interesting to use high strength steel for replaceable shear links, in order to reduce material use and link beam weight. As a result, the mass and size of shear links can be reduced when the high strength steel is used.

Chapter 3 describes the shear link finite element models for monotonic and cyclic load analysis. The link beam specimens for nonlinear finite element analysis are introduced. A total of five shear link models are originally designed and built in ANSYS. Next these 5 shear links are reduced in section size by 10% and 20% respectively, to examine the effect of size reduction on their seismic behavior. Model parameters including material constitutive models for large deformation hysteretic behavior are described in detail. Thus a total of 15 shear link models, with variation considered in section size, length ratio, and steel grades. To model the strain hardening for nonlinear finite element analysis, a combined constitutive model of isotropic and kinematic hardening is considered.

Chapter 4 provides a summary of the FE analysis results for both monotonic and cyclic behavior of the shear links. The seismic performance of shear links made of A992 steel and Q460 steel are compared. Furthermore, the pros and cons of applying higher strength material Q460 in shear links are also assessed. Finally recommendations regarding the use of high strength steel in shear links are made in this chapter.

Chapter 5 summarizes the conclusion and findings of this research. Potential future research is also described.

CHAPTER 2: LITERATURE REVIEW

There are three primary types of seismic-resistant steel building framed structures, that is, Moment Resisting Frames (MRFs), Concentrically Braced Frames (CBFs), and Eccentrically Brace Frames (EBFs). MRFs show a stable hysteretic behavior but requires girders much larger that requirement in order to meet the force demand. For CBFs, the energy dissipation capacity is not as high due to overall brace buckling. Moment resisting frames are assembled rectilinearly, where beams and columns are connected rigidly. In contrast, EBFs are braced frames, containing beams, columns, and braces. Unlike traditional concentrically braced frames, EBF introduces an intentional eccentricity, which makes the centerlines of braces, beams, and columns meet at different points. The framing is arranged in a way such that they are isolated by a short segment of beam at each brace. This isolated beam segment is called a "link". We are mainly concerned with EBFs and their performance as well as optimizations in the research.

A shear link in EBF is designed to perform inelastic action, and thus it needs to provide high ductility. Columns, beams and frames are designed to remain essentially elastic in a frame. Usually they are designed to be stronger than the links. A well-designed EBF should be able to combine high stiffness in the elastic range, which is the case for a concentrically braced frame, with high ductility in the inelastic range, which is a common behavior of a moment resisting frame. Because an EBF has high elastic stiffness, beam and column sizes are generally much smaller than they are in a moment resisting frame.

The main parameters of a shear link include link length e, nominal shear strength V_p, nominal plastic flexural strength M_p, and link rotation γ. The definition of link rotation angle can be found in Figure 2-1.

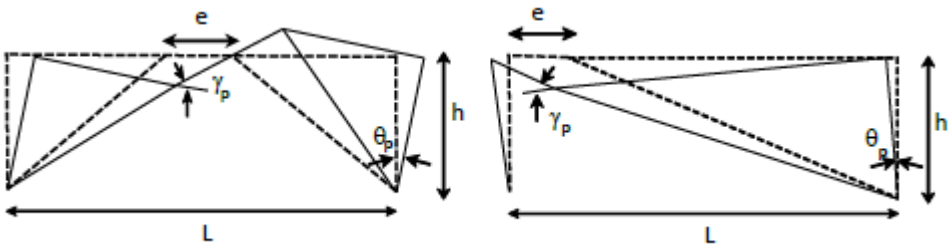

Figure 2-1 Definition of EBF rotation

Plastic deformation and changes on the yielding surface is usually dominated by hardening rules. Previously, the research community used two types of different hardening rules to model this phenomenon, which is isotropic hardening and kinematic hardening. For isotropic hardening, it assumes that for a yielding surface, only the size will be changed with plastic deformation while for kinematic hardening, it assumes that only the position, that is the center of the yielding surface will change. However, for most of the materials in real life, it is not as simple as isotropic or kinematic hardening. Rather, they behaves in a combination of those two hardening. Among existing works, Chaboche (1986) combined nonlinear kinematic hardening rules and non-linear isotropic hardening rules based on Voce hardening law achieves a good accuracy when it is used to predict the behavior of different steel structures.

Okazaki *et al.* (2004) found that the cyclic loading history used in testing and research can significantly affect the performance of a shear link. Four types of loading protocols are presented and compared in their paper. Later, one of these four

protocols is chosen as the AISC revised protocol commonly used by research communities and industries since then. In this paper, if not indicated explicitly otherwise, the cyclic loading protocol used when evaluating the performance of shear links and steel will be this revised loading protocol.

The details of these four proposed protocols are shown in the following. As we can see from Figure 2-2, the old protocol is much more severe than the new, revised protocol. The main reason is that the old protocol does not regard loading cycles in the early stages as important, which is not the case in real situation. Okazaki modified the protocol such that the loading cycles in the early stage are less severe and thus closer to the real situation. This change potentially lower the strength requirement for shear links and therefore reduce the size and material needed when building EBFs.

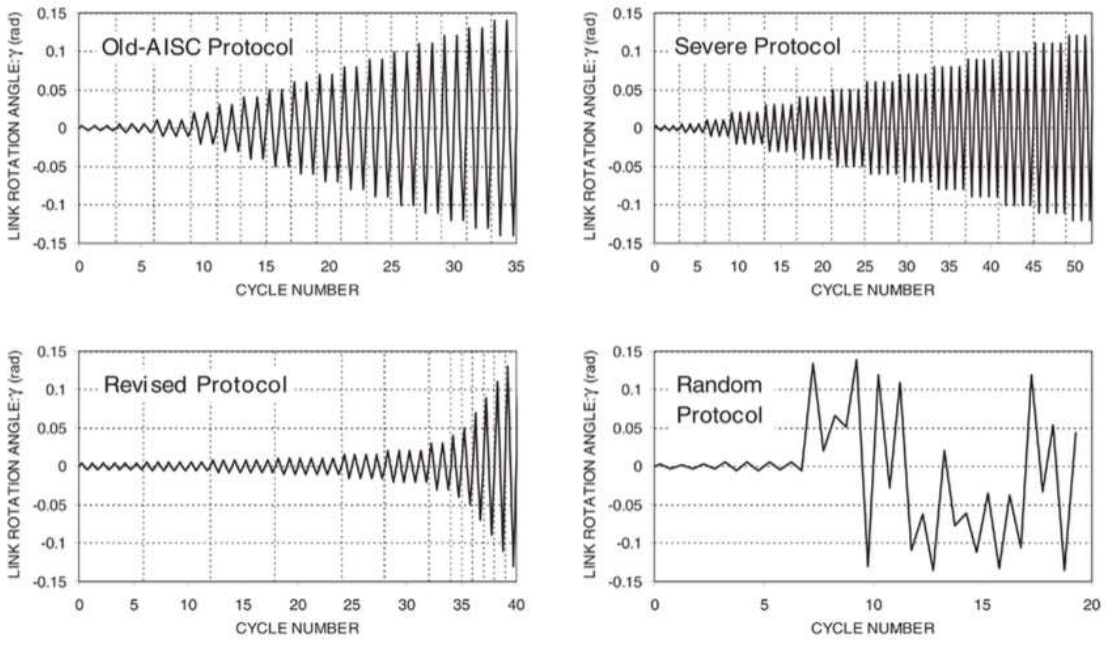

Figure 2-2. Four loading protocols discuss by Okazaki *et al.* (2004): The revised protocol is later used by ASIC (2010) revised standard

In Okazaki *et al.* (2004), cyclic loading tests were also conducted to study the behavior of link beams in steel eccentrically braced frames, thirty-seven link specimens were constructed from five different wide-flange sections, all of ASTM A992 steel, with link length varying from short shear yielding links to long flexure yielding links. The occurrence of web fracture in shear yielding link specimens that leads to further study on the cause of these fractures is also discussed. Based on the test data, a change in the flange slenderness limit is therefore proposed. They conclude that the link over-strength factor is 1.5, as assumed in the current U.S. code provisions, appears to be reasonable. The cyclic loading history used for testing was found to significantly affect link performance. Test observations also suggest new techniques for link stiffener design and detailing for link-to-column connections.

Corte *et al.* (2012) conducted analytical and numerical studies on plastic over-strength of shear links based on the experimental results from Okazaki *et al.* (2004). The validation of finite element models is confirmed by comparing the results from FE analysis with the experimental results from three types of shear links, including W10x33 (ρ=1.04), W18x40 (ρ=1.02), and W10x68 (ρ=1.25). Then, the parameters that affect the over-strength factor are analyzed and discussed. It turns out that there are three parameters of which the combination shows a huge impact on the over-strength of a shear link. These three important factors are axial force, the ratio of flange over web area, and cross section depth.

Park (1989) systemized the evaluations of ductility of structures. In this paper, he discussed the definition for the ductility of structures in seismic designs. Since the ductility factor of structures is denoted as the ratio of maximum deformation and the

deformation at yielding, the main challenge becomes how to estimate these two parameters accurately and easily. In their paper, different methods to estimating the yield deformation and the maximum available are presented and analyzed specifically. In the following figure from Park (1989), they showed 4 ways to compute yielding displacement:

Method a: The displacement when yielding happens for the first time. In order to get the yielding displacement, we first draw a tangent line to the curve starting from the origin. Then we can get the yielding displacement by finding the y coordinate of the intersection point between the curve and the tangent line.

Method b: The yield displacement of the equivalent elasto-plastic system with the same elastic stiffness and ultimate load as the real system. This method is slightly different from Method a. The first step is the same that we will get a tangent line to the curve. Then, instead of reading the intersection point directly, we will draw another horizontal line corresponding to the ultimate load. The final yielding displacement can be found by finding the intersection of these two lines.

Method c: The yield displacement with the same energy absorption as the real system. This method adopts totally a different way to find the yielding point. We first draw a line from the origin. This line, together with the curve and the ultimate protocol line mentioned above forms two areas, shown as shaded areas in the figure. The yield displacement is the y-coordinate of the point that split these two areas to have the same area.

Method d: Method d is based on reduced stiffness equivalent elasto-plastic yield. First, we need to draw the horizontal line corresponding to ultimate load. Then

another line with 70 percent of ultimate load is drawn, and this line intersects the curve at a certain point, namely P. Then we draw a line across the origin and the point P, and the finally yielding displacement is the y-coordinate of the intersection between this new line and ultimate line.

As we can see from the above description, method b is easy to compute and gives a descriptive result, so we adopted method b in this study when related parameters are calculated.

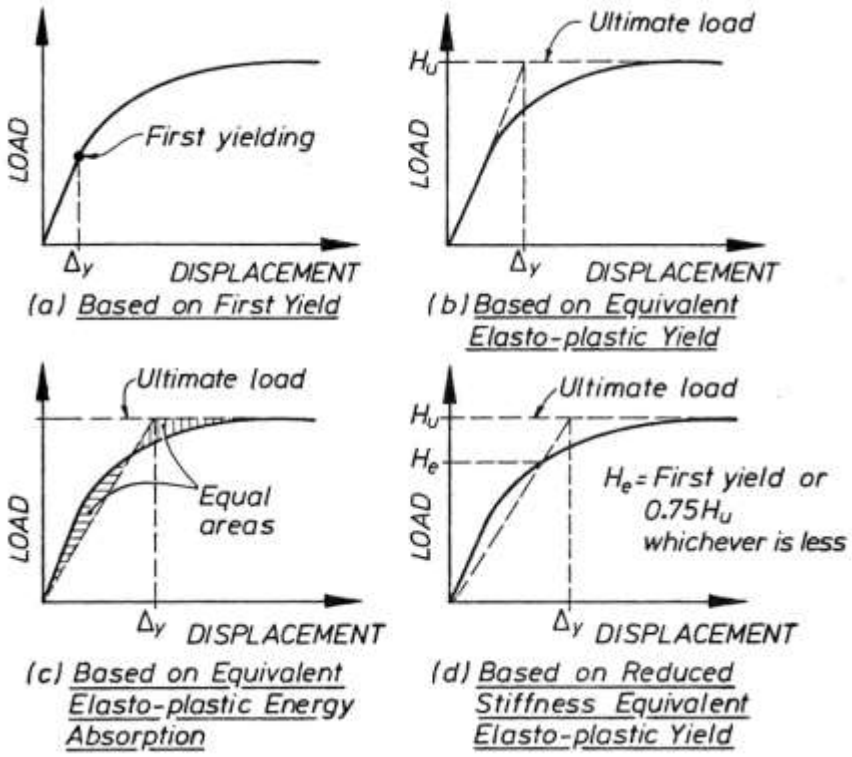

Figure 2-3 Four types of method to determine yielding displacement by Park (1989)

Dusicka *et al.* (2010) discussed the performance of five types of shear links under cyclic loadings when different grades of steels ranging from 485MPa to 100MPa are used. Their studies are classified into two categories where some experiments are

done on classically designed shear links with no stiffeners, and others experiments are performed over better, newly designed shear links where stiffeners are used in shear links. In summary, their observation is that by using better-designed shear links, a better shear deformation point around at 0.12 rad can be achieved, compared with traditional results that deforms at a much earlier point. The enhanced performance was the result of shifting the failure mode by excluding intermediate stiffeners and providing low web compactness. This combination eliminated welding and decreased measured plastic strain demands on the face of the inelastic deforming webs.

Dusicka *et al.* (2004) also investigated non-linear behavior of finite element models accounted by large displacements when studying the behavior of steel built-up shear links that had previously been tested using large-scale experiments as well as correlated the numerical results with experimental observations. They incorporated elasto-plastic as well as cyclic stress-stain material properties to the study on the influence of material behavior on the shear link response. They also compared the backbone curves recorded from the real physical experiments with the numerical models, where they get similar trend in both of the cases. They show that plastic strain concentrations are more significant compared with shear links at stiffener to web interface. Finally they conclude that FE models can be used confidently to verify and ensure that the design of shear links with different steel grades and sectional geometries behaves safely.

Dastmalchi *et al.* (2014) studied the impact of axial load on the strength and ductility of shear links. High axial load is one of the most significant parameters that affect hysteretic behavior of shear links because premature flange local buckling

might occur and results in deterioration in shear capacity, ductility, and energy dissipation of the links. They studied the effect of high axial load ratio on shear capacity and ductility of shear links by numerical simulation. After simulating twenty-two shear link specimens, they propose a reduction factor to modify the code-specified design equation. Furthermore, they also observe local buckling due to high axial load in link specimens, which precludes the shear links from providing the code-specified rotation capacity. The detrimental effect of high axial load ratio on ductility of the shear links turns out to be not uncommon from their conclusion.

Chaboche (1986) considered time-independent plasticity when cyclic loadings are applied. They mainly considered three different types of approaches used to describe kinematic behaviors:

1. Using multi-yield surfaces
2. Using only two surfaces only
3. Using nonlinear kinematic hardening rule precisely defined by differential equations.

They also considered the behaviors of materials where temperature is taken into considerations. They finally proposed a specific set of models used to describe cyclic hardening of the model, which is used widely later. However, the model has some issues to be implemented as computer programs at that stage of development, but it is no longer the case now. We defer more details of Chaboche model to Chapter 3, where the validation of the model for steel types used in this thesis is also included.

Shi *et al.* (2012) studied the performance of Q460D under seventeen different loading protocols. They also evaluated the structural responses of these experiments,

including stress–strain relationship, failure modes, ductility and hysteretic performance. Their FE analysis is based on ABAQUS through user subroutine interface UMAT.

In addition, they proposed a simple version of constitutive model for high-strength structural steels under uniaxial cyclic loadings, including monotonic loading curve, hysteresis skeleton curve and hysteresis criterion. They conclude that high strength Q460D steel behaves similar with cyclic loadings compared with normal steel in terms of plasticity, cyclic hardening or softening, average stress relaxation and Bauschinger effect. However, high-strength structural steel Q460D owns better ductility and energy dissipation capacity. They also conclude that cyclic loadings and strains amplitudes have a huge impact on the ductility. Because of this, fracture strain of steel under cyclic loading cannot be directly determined by fracture strain from monotonic loading.

Shi *et al.* (2012) compared the performance of steel structure Q235B and A992B under seismic loadings, and looked for the constitutive relationship of steel under cyclic loading. They studied totally 50 specimens of two types of steels as well as their monotonic behavior, hysteretic behavior, macro-and micro-failure modes, ductility characteristics and cumulative damage degradation. They show that the response of steel under cyclic loading and the monotonic loading are quite different, therefore, the skeleton curve under cyclic loading plays an important role for accurate numerical simulation; cyclic loops and amplitudes seriously affect the fracture ductility of specimens and the failure strain under cyclic loading cannot be determined in accordance with the monotonic loading.

Shi *et al.* (2012) studied the performance on Q460D steel structures under different monotonic and cyclic loadings. They conducted different tests on fourteen specimens of steel type Q460D, with different monotonic or cyclic loadings. Their observation shows that high strength steel behaves similarly with commonly used steels in terms of the phenomenon of yielding, deformation and ductility. The cyclic loading tests also show that high strength steel performs well under cyclic loadings. However, because of the accumulated strain, it still performs much worse than it is under monotonic loading, especially in terms of ductility. Shi et al used Ramberg-Osgood model to predict the backbone curve with success and the backbone curve also shows that the hardening happens earlier because of the accumulated stress caused by cyclic loading.

Dai *et al.* (2012) used the experiment result from Shi *et al.* (2012) on Q460 and the experiments on A992 to compare the performance difference between these two types of steel. This thesis is similar to this paper in the sense that both research focus on the same set of steel types. However, this thesis particularly focuses on the performance of the shear links when these two types of steel are used, rather than focus on the material solely. After a detailed analysis, Dai et al concluded that both types of steel behaves reasonably well under cyclic loadings to the extent that both satisfy the requirements from Chinese codes on steel. However, they also showed that Q460 performs better in terms of ductility and better at reducing the Bauschinger effect.

Li *et al.* (2014) studied the feasibility of using stainless steel for shear links. As they pointed out in the paper, in the real application of shear link, stainless steel

works better because they are better at corrosion resistant tasks, e.g. coastal regions. In particular, they studied AISI 326L stainless steel for shear links as a seismic fuse device. They also used nonlinear finite element analysis and simulations to study in detail the behavior of the ductility, over-strength ratio, as well as deformation of the shear links. They conclude that without considering residual stress in heat affected zones including the interconnections of stiffeners and webs, stainless steel shows a promising performance as seismic fuse elements.

CHAPTER 3: FINITE ELEMENT MODELING OF SHEAR LINKS

In this section, details pf the finite element model used to get the simulation results will be introduced. The FE software used for simulation is ANSYS. In the following, test specimen, model parameter, material properties, elements, loading protocol, and other factors will be discussed. All the experiments are done with ANSYS Command Line Interface, to accelerate model-building process. In the following, we also include code snippets used in building models hoping on saving future efforts on similar tasks.

3.1. Test Specimens

There are originally five sets of shear link specimens used in this thesis. In particular, three types of sections for these specimens, including W14x68, W10x33, and W10x68 are used. For sections of type W14x68, three types of specimens with different length are further used. To be more precise, their link length ratios are 1.2, 1.4, and 1.6 respectively. Details of these specimens are listed in Table 3-1 and Figure 3-7 to Figure 3-11.

In the later part of the study, the case where the size of shear link sections is further reduced by 10% and 20% respectively are also studied. Specifically, both the web thickness t_w and the flange width b_f are reduced at the same time, while other parameters of shear links are kept the same. The reason why flange thickness and depth are not reduced is because shrinking in depth will cause a significant deterioration in stiffness. Details of these specimens are listed in Table 3-2 and Table 3-3.

The shear link length e is a key parameter to controls the inelastic behavior. It is determined by considering both the fully plastic shear capacity V_p and fully plastic moment capacity M_p of the link section at the same time. The nominal link ratio is defined as the following:

$$\rho = \frac{e}{M_p/V_p}$$

The fully plastic moment capacity is calculated as

$$M_p = ZF_y,$$

and fully plastic shear capacity is calculated as

$$V_p = 0.6t_w(d - 2\ t_f\ )F_y,$$

where Z is the plastic section modulus, for section I,

$$Z = \mathrm{b}t_f(d - t_f) + 0.25t_w(\underline{\mathrm{d}} - 2t_f)^2,$$

where t_w is the thickness of web.

Specify Test specimen in ANSYS

Here the snippet of code used in ANSYS on how to specify specimens is shown. The version of ANSYS used is the latest version. If not indicated in the other way, all the codes are for the latest version of ANSYS.

```
1  sect,1,shell,,flange
2  secdata, 18.288,1,0.0,3
3  secoffset,MID
4  seccontrol,,,, , , ,
5  sect,2,shell,,web
6  secdata, 10.541,1,0,3
7  secoffset,MID
8  seccontrol,0,0,0, 0, 1, 1, 1
9  sect,3,shell,,stiffener
10 secdata, 9.525,1,0,3
11  secoffset,MID
12  seccontrol,0,0,0, 0, 1, 1, 1
13  sect,4,shell,,flange 2
14  secdata, 365.76,2,0,3
15  secoffset,MID
16  seccontrol,0,0,0, 0, 1, 1, 1
17  sect,5,shell,,web2
18  secdata, 421.64,2,0,3
19  secoffset,MID
20  seccontrol,0,0,0, 0, 1, 1, 1
```

Figure 3-1 ANSYS commands to create and specify test specimens

As seen from the code above, five types of section parameters, called flange, web, stiffener, flange2 and web2 are defined. Here, flange and web are defined as above, while stiffener is thickness of stiffeners in shear links, while flange2 and web2 are for ridged sections on the left.

3.2. Model Parameter

Model parameters include material property, which defines the type of steels used; element type, which defines how each element are modeled, boundary conditions, which set up the simulation constraints; and loadings, which can be either monotonic or cyclic. In the following the details of them with ANSYS code after each subsection

are introduced. Note that all these model parameters are got either from existing standards, or from FE simulations got from previous sections.

3.2.1. Material Property

In this research project, two sets of material properties are mainly concerned: A992 steel, which is a lower strength steel that is commonly used nowadays in different areas of applications; Q460 steel, which is a new high strength steel that is heavily used, for example, in the construction of the main gymnasium for Beijing 2008 Olympics. It is also used more and more in modern buildings, where higher strength is required.

Because of the effect of cyclic hardening, cyclic softening and Bauschinger effect, the mechanic properties of steel are quite different between the case with monotonic loading and the case with cyclic loading. Therefore, it is important to find a proper material constitutive model for numerical analysis of seismic performance of shear links, especially because the material models in ANSYS are required to be accurate. In the previous researches, different models are proposed to provide an accurate prediction of the performance, including bilinear model, nonlinear models, etc.

As mentioned in the previous sections, two types of materials will be considered in this research for shear link specimens: A992 steel and Q460 steel. For these two steels, the material properties are determined from experimental data from cyclic coupon tests by Shi *et al.* (2011).

A constitutive material model is a model combining isotropic hardening and kinematic hardening, that is, a combined hardening model. The reason why both types of the hardening are considered is because it is considered to be nonlinear and

time independent. It is also considered to be more accurate when simulating cyclic responses of steel than other models, including bilinear model or non-linear model. A constitutive model takes into account the Bauschinger effect in steel, where the yielding face will change in both size and position, and thus can predict the performance even better.

In this section, the experiment data from paper Shi *et al.* (2012) are used to calibrate parameters in the constitutive model. The finite element software ANSYS is also used to verify the accuracy of these material parameters.

Isotropic Hardening

Von Mise criterion determines the yielding condition of steel. A yielding surface is defined in the principal stress space. If the material is in elastic range, the stress state will fall within the yielding surface. On the other hand, once the material goes to an inelastic range, a new yielding surface will be formed. Both the size and the position of this new yielding surface will be changed. Figure 3-12 shows the illustration of isotropic hardening.

The isotropic hardening determines the size of yielding surface R_0, which is a function of accumulated plastic strain $\hat{\varepsilon}_p$. It is defined as follows:

$$R = R_0 + R_\infty(1 - e^{-b_{iso}\hat{\varepsilon}_p})$$

$\hat{\varepsilon}_p$ is the accumulated plastic strain, R_0, R_∞ and b_{iso} are material constants that can be calculated from experiment data, by using curve fitting.

Kinematic Hardening

The kinematic hardening defines the position of the yielding surface χ, the back stress χ can be expressed as:

$$\chi = \chi_1 + \chi_2 = \frac{C_1}{\gamma_1}(1 - e^{-\gamma_1 \epsilon_p}) + \frac{C_2}{\gamma_2}(1 - e^{-\gamma_2 \epsilon_p})$$

where ε_p is the plastic strain, which can be calculated as $\varepsilon_p = \varepsilon - \sigma/E$. C_1, γ_1, C_2, γ_2, C_3, γ_3 are parameters that can be obtained from experimental data through curve fitting. Figure 3-13 shows the illustration of isotropic hardening.

In this study, the effect of both isotropic and kinematic hardening are considered. That is, the combined strain hardening are considered. Figure 3-14 shows the illustration of this combined hardening.

Summary

The approach described in Shi *et al. (2012)* are followed, where the experimental data are used to calculate these parameters related to combined hardening model mentioned previously.

These parameters are used in finite element analysis software ANSYS to set up the material model for steels to be used in this paper.

The results of finite element simulations and experiments are compared to ensure that the constitutive model is of considerable accuracy. Table 3-4 shows the calibrated parameters for A992 steel and Q460 steel, and Figure 3-15 shows that the finite element results and experimental results are consistent within an acceptable error limit.

In the figure, the blue curve denotes the experimental data, while the green curve is the results of FE analysis. It shows great agreement, which proves the validation of the determined hardening parameters.

Note that there is a correspondence between parameters used for Chaboche model and the parameters used for ANSYS 15.0.

Specify Material properties in ANSYS

The related ANSYS code used to specify material properties are also shown. In the code, "MP" stands for material properties. In line 6, elastic modulus is specified. The Chaboche nonlinear model is also specified in line 21 and detailed parameters after that line. As shown in the code, the material model with as a combination of Chaboche model (CHAB) and Nonlinear Isotropic model (NLIS) is specified.

```
1  MPTEMP,,,,,,,,
2  MPTEMP,1,0
3  MPDE,EX,1
4  MPDE,NUXY,1
5  MPDE,PRXY,1
6  MPDATA,EX,1,,2E+005
7  MPDATA,PRXY,1,,0.3
8  MPTEMP,,,,,,,,
9  MPTEMP,1,0
10 MPDE,EX,2
11 MPDE,NUXY,2
12 MPDE,PRXY,2
13 MPDATA,EX,2,,2E+006
14 MPDATA,PRXY,2,,0.3
15 MPTEMP,,,,,,,,
16 MPTEMP,1,0
17 MPDE,EX,1
18 MPDE,PRXY,1
19 MPDATA,EX,1,,2E+005
20 MPDATA,PRXY,1,,0.3
21 TBDE,CHAB,1,,,
22 TB,CHAB,1,1,2.0,
23 TBTEMP,0
24 TBDATA,,474,4797,30.75,3794,26.19,
26 TBDE,NLIS,1,,,
27 TB,NLIS,1,1,4,
28 TBTEMP,0
29 TBDATA,,474,0,102.7,2.59,,
```

Figure 3-2 ANSYS commands for material property

3.2.2. Elements

In ANSYS, it is necessary to define element types for all structures before performing simulations under monotonic or cyclic loadings. The element type we used here is Shell 181 for all sections of the structure. It is suitable for modeling web and flange of shear link. It is a four-node element and with six degrees of freedom at each nodes: displacement in x, y and z directions, and rotation about x, y and z-axis, respectively. It is also is well suited for linear, large rotation, and/or large strain nonlinear applications. Change in shell thickness is accounted for in nonlinear analyses. In the element domain, both full and reduced integration schemes are supported. It is used to replace Shell 43, which leads to different convergence problems previously. The element type shell 181 is also suitable for large strain nonlinear application.

Specify Element Type in ANSYS

Specifying element type in ANSYS is very easy and straight forward, with the following single line of code:

```
ET,1,SHELL181
```

Figure 3-3 ANSYS commands for element type

ET stands for “element type”.

3.2.3. Boundary Conditions

As shown in the typical finite element shear link model in Figure 3-16, the right side of a shear link is rigidly restrained. Here the X, Y, Z, ROTX, ROTY, and ROT Z DOF on this side are restricted. The left side is restrained against rotations, that is, ROTX, ROTY and ROTZ. The loading added to the shear link is achieved by adding a 100mm long rigid segment on the left. To make it rigid enough, in ANSYS model, the Young's elastic module of rigid area is set to be 200000 MPa, and the thickness of flange and web plates to be 20 and 40 times of the shear link's flange and web plates.

Specify Boundary Conditions in ANSYS

```
1  NSEL, S, LOC, Z,0
2  D, ALL, ALL,0
3  NSEL, S, LOC, X,0
4  NSEL, R, LOC, Y, wh
5  NSEL, R, LOC, Z, length,totallength
6  D, ALL, ROTX, 0
7  NSEL, S, LOC, X,0
8  NSEL, R, LOC, Y, 0
9  NSEL, R, LOC, Z, length,totallength
10 D, ALL, ROTX, 0
11 NSEL, S, LOC, X, 0
12 NSEL, R, LOC, Z, totallength
13 DDELE, ALL, ALL
14 D, ALL, ROTX, 0
15 D, ALL, ROTY, 0
16 D, ALL, ROTZ, 0
```

Figure 3-4 ANSYS commands for boundary conditions

This snippet of code adds 4 boundary conditions on the shear link: line 1 to 2, line 3 to 6, line 7 to 10, and line 11 to 16. Each time we define a boundary condition, the set of nodes are selected that the boundary condition will be applied on using "NSEL", and then using "D" or "DDELE" to add or modify the displacement.

3.3. Loading Protocols

In all loadings used for FE analysis, displacement is used to control the external loadings for both monotonic case and cyclic case.

In Okazaki *et al.* (2006), four different loading protocols are proposed for cyclic tests. It is confirmed that the old AISC loading protocol aimed to promote low cycle fatigue and premature shear link failure. However, the revised protocol in *2005 AISC Seismic Provisions* is believed to be more representative of simulating seismic performance of shear links. The main parameter values of the revised loading protocols are shown in Figure 3-17 and Table 3-5.

Specify Monotonic Loads in ANSYS

In order to add monotonic loads to the shear link, constant-valued displacement on the ridged section of the shear link is needed to be applied. The ANSYS commands to achieve this is shown in the following box:

```
1  NSEL, S, LOC, Z, length
2  D, ALL, UY, displ
3  NSEL, S, LOC, Z, totallength
4  F, ALL, FZ, force
```

Figure 3-5 ANSYS commands to add monotonic loading

In addition to applying a displacement on the node with magnitude displ, predefined earlier, we also can apply a constant valued force on the axial direction.

Specify Cyclic Loads in ANSYS

In order to apply a cyclic load to the shear link, it is necessary to first load the loading protocols to ANSYS, which is achieved using line 1 to 3. Here, the value read

from loading protocol is also multiplied by the length of the shear link, to transform angle to distance needed to apply on the shear link.

```
1  *DIM,loadre,TABLE,157,1,1, , ,
2  *TREAD,LOADRE,'loadRE','txt',path_to_load, ,
3  *VOPER,LOADRE,LOADRE,MULT,length, ,
4  NSEL, S, LOC, Z, length
5  D, ALL, UY, %LOAD%
```

Figure 3-6 ANSYS commands to add cyclic loading

3.4. Effect of Axial Load

Axial load ratio refers to axial load acting on the shear links divided by nominal yield strength A_gF_y. It can be written as:

$$\text{Axial load ratio} = N/A_gF_y$$

, where N is the axial force and A_g is the cross section area of the shear link.

Axial load is an important factor in real frames structures. As in earthquakes, the lateral force will be transferred through the shear links to the related beams or columns; it is of highly significance to research the effect of axial load to shear links in seismic conditions.

Axial load is considered to vary cyclically. In this case, consider the peak ratio to be at the same scale as loading protocol, the axial load ratio added to the shear links is shown in Figure 3-18. It is considered to be more realistic than a constant axial load.

The performance when axial load is applied to the shear links is briefly investigated, and take two models among all five models had as an example.

Figure 3-19 and Figure 3-22 show that when a cyclic axial load (with peak ratio equals 0.14) is applied on the shear link, the initial stiffness are not affected, however, the stiffness after yielding will have a shrink comparing with the model that do not have axial load. The same happens to ductility too.

3.5. Validation of Shear Link Model

Before going to the analysis of different steels and shear links, the model in ANSYS needs to be validated. Since our model is constructed using ANSYS commands, all of them follow the same structure. Therefore, only one representative from five models used is validated. In particular, the result got from Okazaki *et al.* (2006) and the simulation result from ANSYS are compared.

Okazaki conducted real experiments on 10x33 shear links, with ASIC old loading protocols, which in fact invented the revised loading protocol used later as standards. Corte et al. (2013) studied plastic shear over-strength using FE simulations based on ABAQUS. In their work, the experimental results are used to validate their FE models. The experimental results from Okazaki is used since the correctness has been verified multiple times by different groups.

Most of our experiments are based on revised loading protocols. In order to compare with their results, the loading protocols are changed from the revised protocol to the old one and simulate the same loading. We extracted the data points from Okazaki *et al.* (2006) and plot them together with the simulation results in

Figure 3-23. As we can see from the figure, the two curves are very similar to each other. In particular, they share similar range of values as well as ultimate strength.

Type	b_f/mm	d/mm	t_f/mm	t_w/mm	e/mm	*Web stiffener*
W14x68 (ρ=1.2)	254	355.6	18.288	10.541	1120	4@224 mm
W14x68 (ρ=1.4)	254	355.6	18.288	10.541	1308	5@218 mm
W14x68 (ρ=1.6)	254	355.6	18.288	10.541	1486	6@212 mm
W10x33	202.2	247.0	11.0	7.4	686	4@137 mm
W10x68	256.54	264.16	19.558	11.938	1041	3@260 mm

Table 3-1 Detailed parameters for original model

Type	b_f/mm	d/mm	t_f/mm	t_w/mm	L/mm	*Web stiffener*
W14x68 (ρ=1.2)	241.3	355.6	18.288	9.487	1120	4@224 mm
W14x68 (ρ=1.4)	241.3	355.6	18.288	9.487	1308	5@218 mm
W14x68 (ρ=1.6)	241.3	355.6	18.288	9.487	1486	6@212 mm
W10x33	192.09	247.0	11.0	6.66	686	4@137 mm
W10x68	243.713	264.16	19.558	10.744	1041	3@260 mm

Table 3-2 Detailed parameters for 10% reduction model

Type	b_f/mm	d/mm	t_f/mm	t_w/mm	L/mm	*Web stiffener*
W14x68 (ρ=1.2)	228.6	355.6	18.288	8.433	1120	4@224 mm
W14x68 (ρ=1.4)	228.6	355.6	18.288	8.433	1308	5@218 mm
W14x68 (ρ=1.6)	228.6	355.6	18.288	8.433	1486	6@212 mm
W10x33	181.98	247.0	11.0	5.92	686	4@137 mm
W10x68	230.886	264.16	19.558	9.550	1041	3@260 mm

Table 3-3 Detailed parameters for 20% reduction model

Type	σ_0/MPa	σ_∞/MPa	b_{iso}	C_1/MPa	γ_1	C_2/MPa	γ_2	C_3/MPa	γ_3
A992	380	50	1.2	7993	175	7100	116	2650	60
Q460	474	102.7	2.59	4797	156	30.75	145	1498	107

Table 3-4 ANSYS parameters for A992 and Q460 in Chaboche model

Load Step	Peak Link Rotation Angle	Number of Cycles
1	0.00375	6
2	0.005	6
3	0.0075	6
4	0.01	6
5	0.015	4
6	0.02	2
7	0.03	2
8	0.04	1
9	0.05	1
10[a]	0.07	1

Table 3-5 Detailed information on revised loading protocols

[a] Continue with increments in γ of 0.02, and perform one cycle at each step until failure

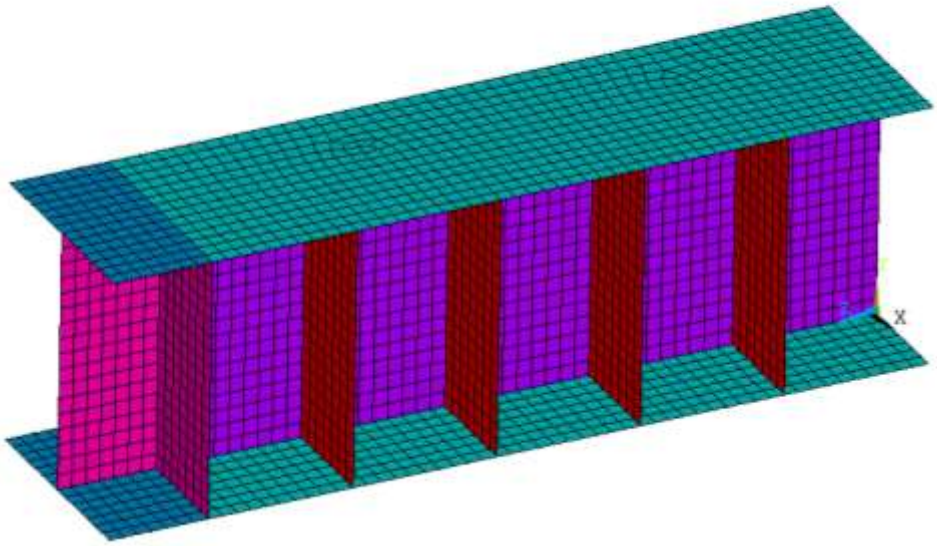

Figure 3-7 ANSYS model of W10x33 shear link beam

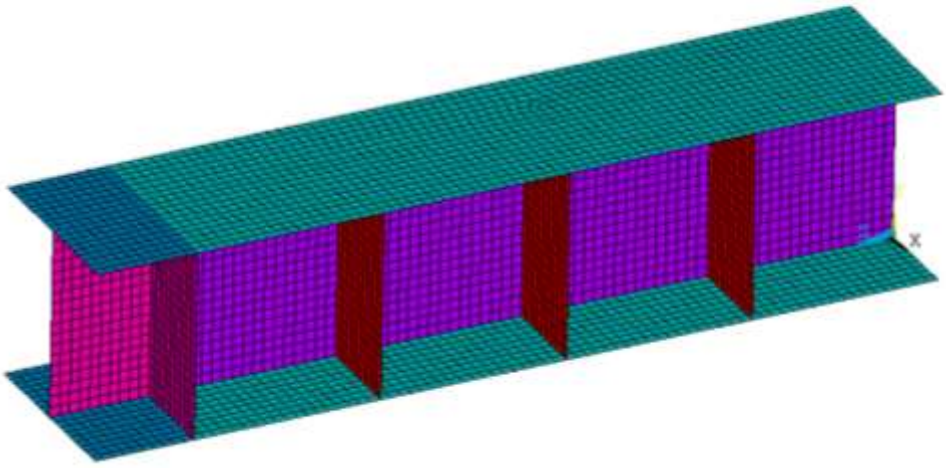

Figure 3-8 ANSYS model of W10x68 shear link beam

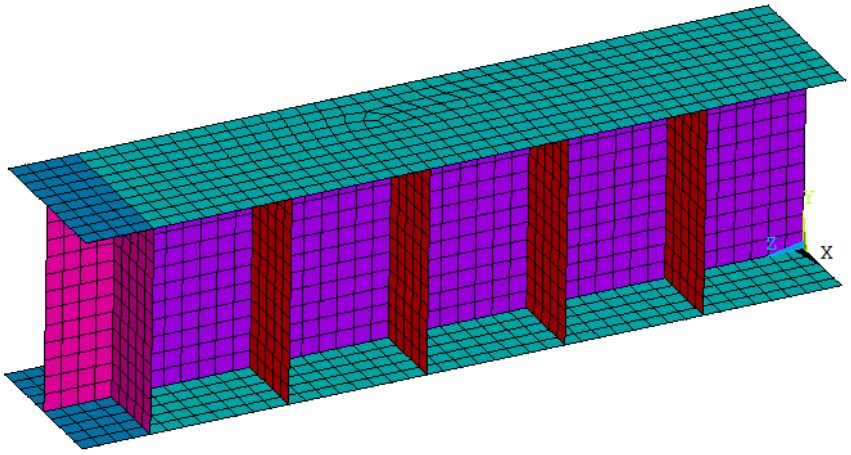

Figure 3-9 ANSYS model of W14x68 (ρ=1.2) shear link beam

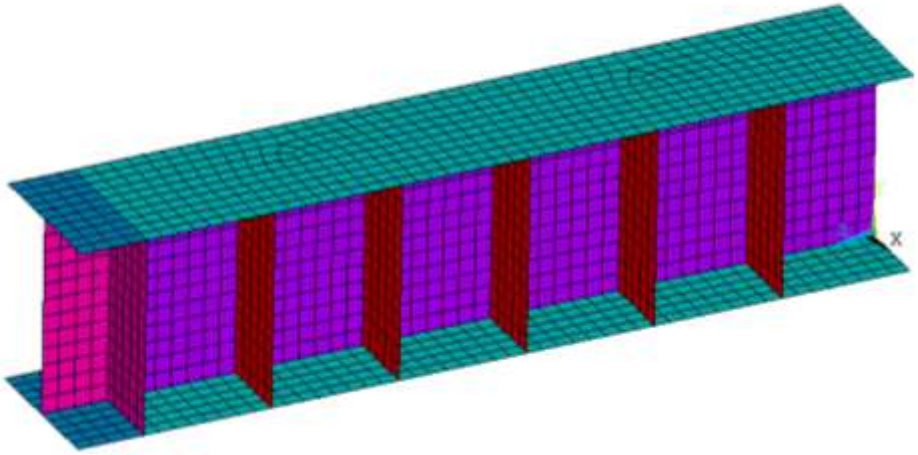

Figure 3-10 ANSYS model of W14x68 (ρ=1.4) shear link beam

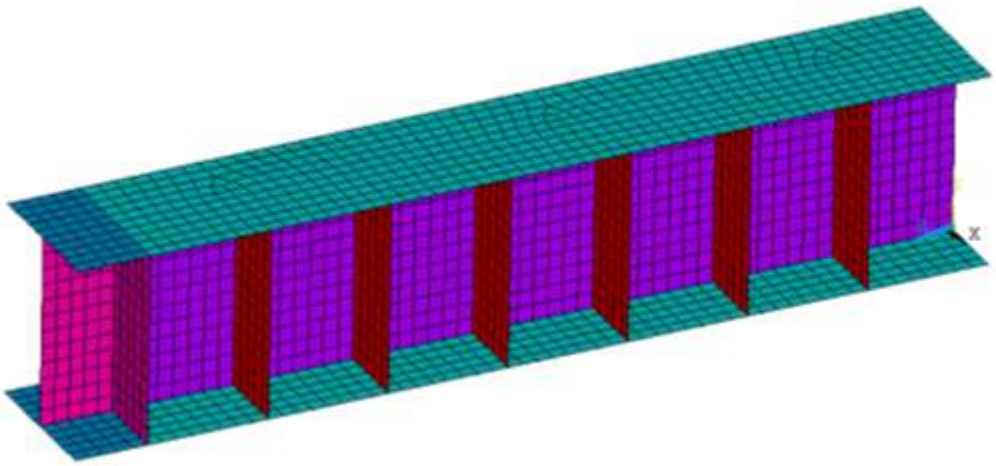

Figure 3-11 ANSYS model of W14x68 (ρ=1.6) shear link beam

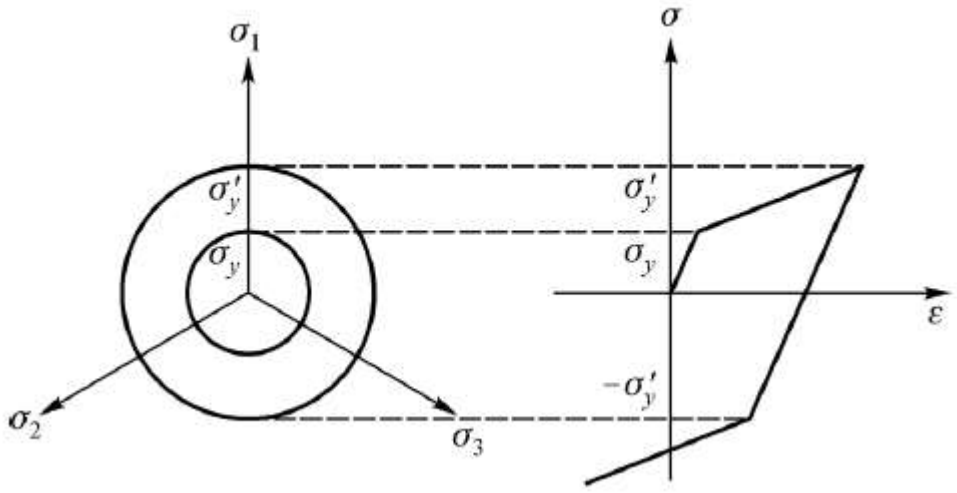

Figure 3-12 Loading surface for isotropic hardening

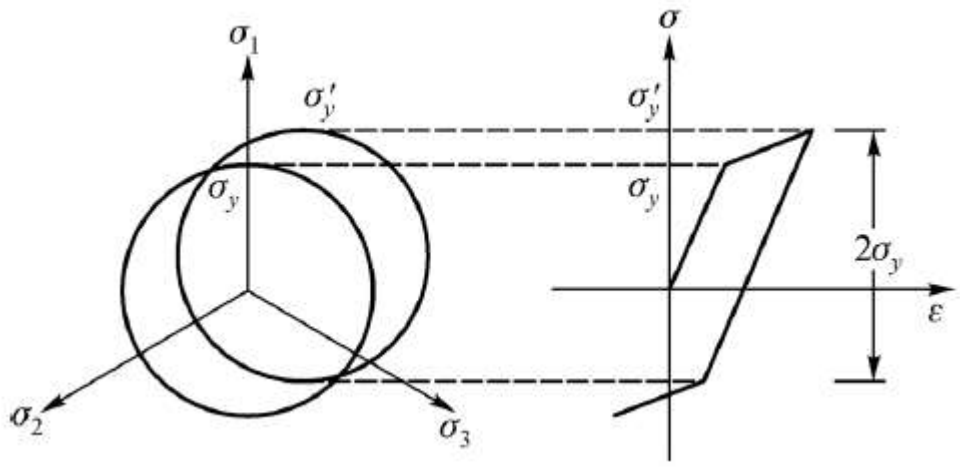

Figure 3-13 Loading surface for kinematic hardening

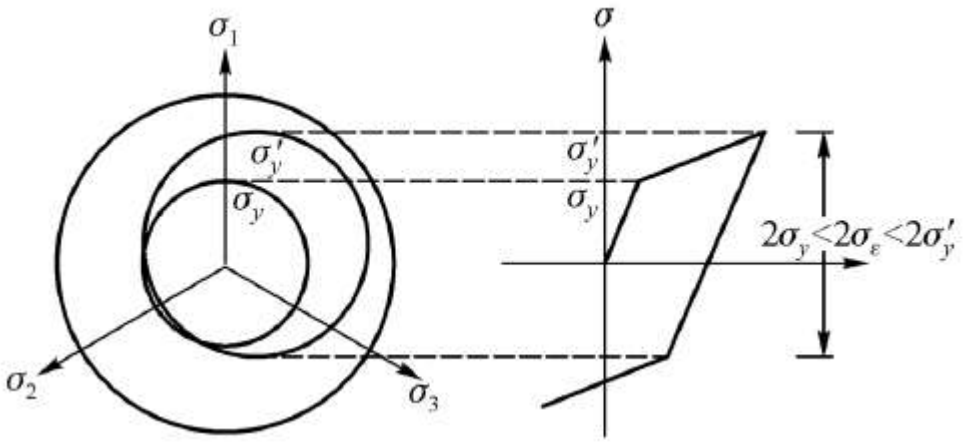

Figure 3-14 Loading surface for combined hardening

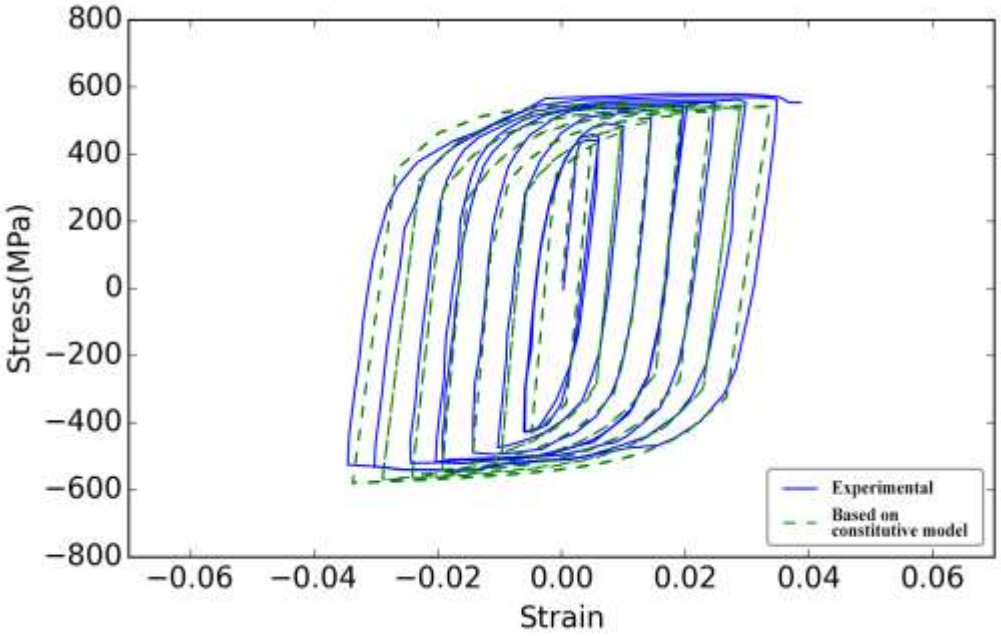

Figure 3-15 Comparison between experimental results for A992 and simulation result based on constitutive model

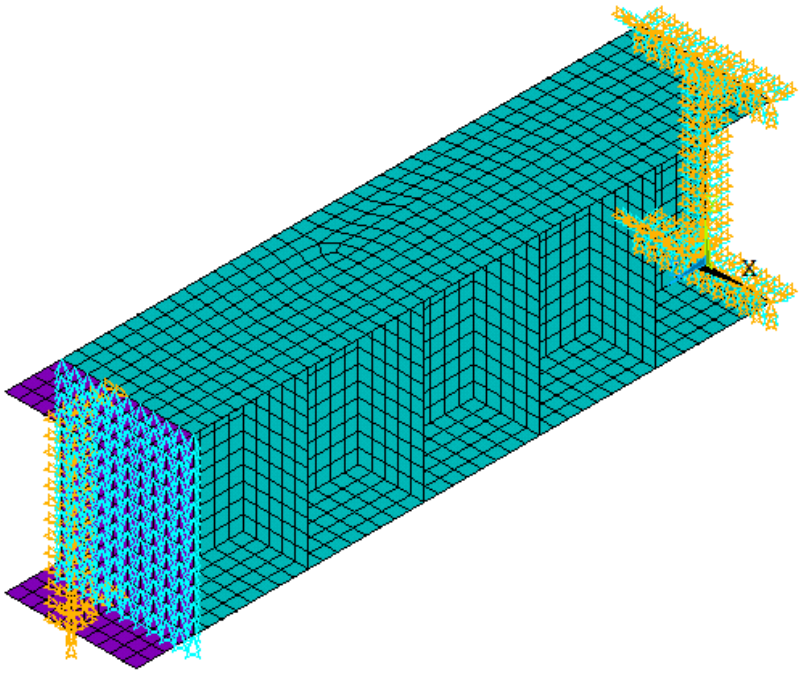

Figure 3-16 Typical FE model for shear link

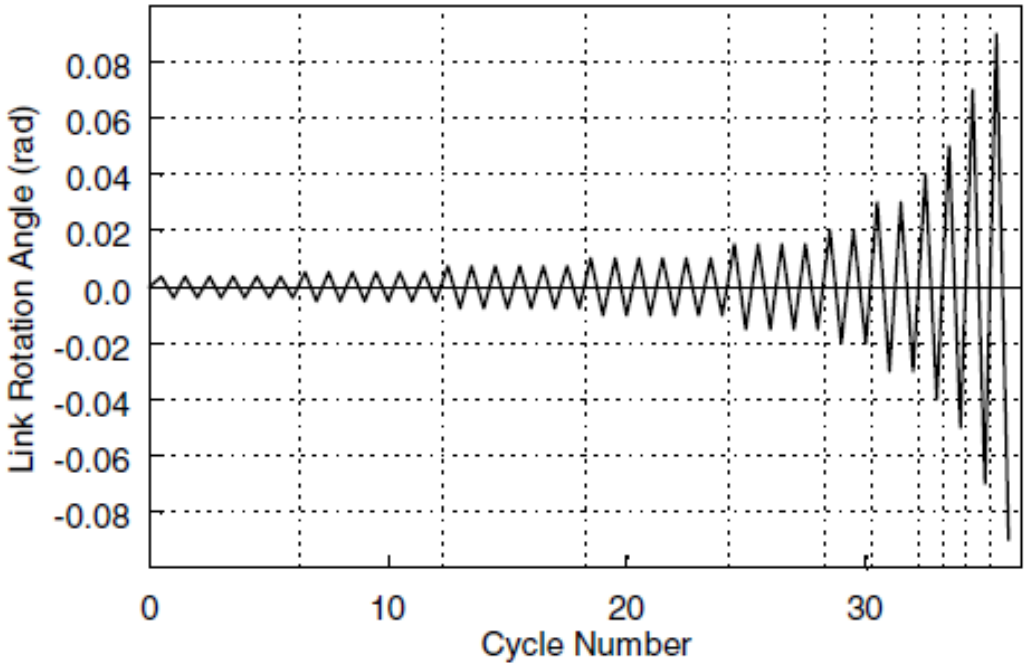

Figure 3-17 Cyclic loading protocol

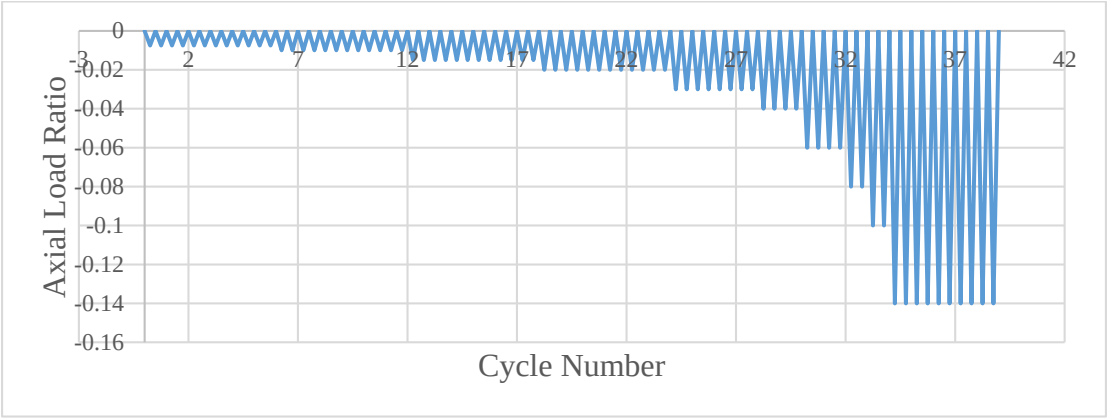

Figure 3-18 Cyclic axial load ratio

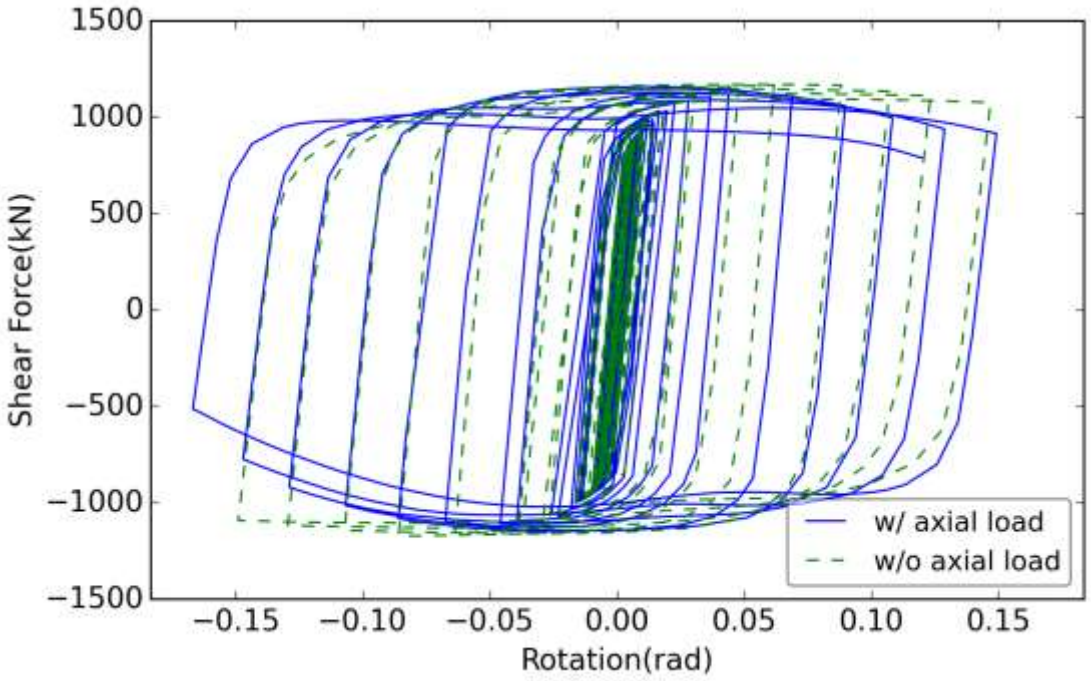

Figure 3-19 Comparing the effect of axial load for W10x68 made of Q460 steel

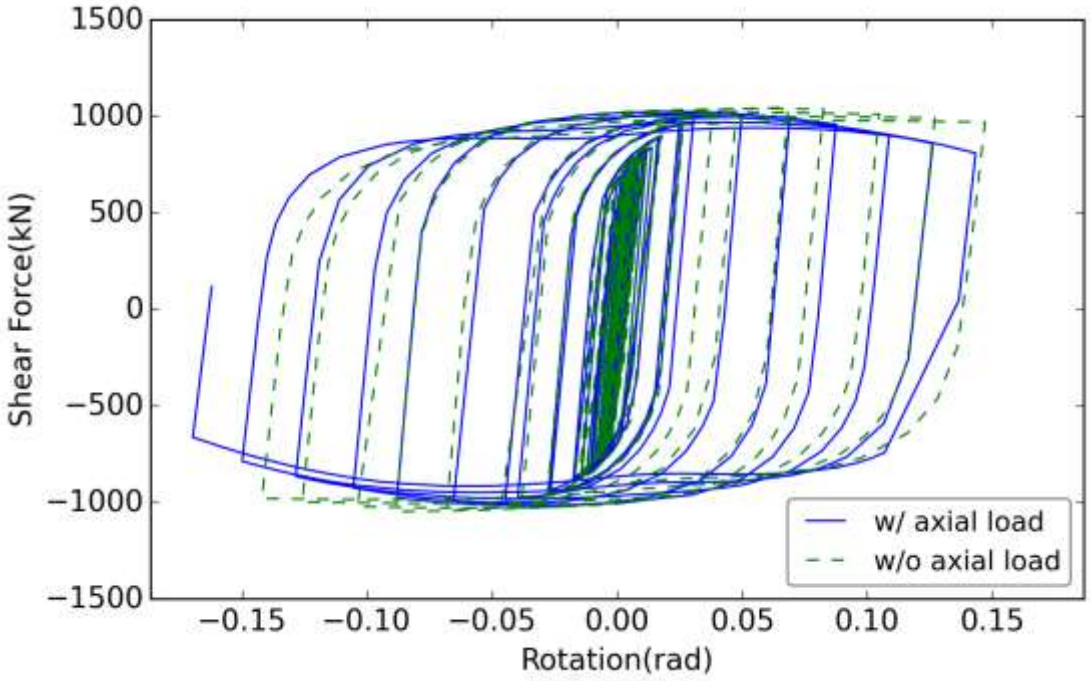

Figure 3-20 Comparing the effect of axial load for W10x68 made of A992 steel

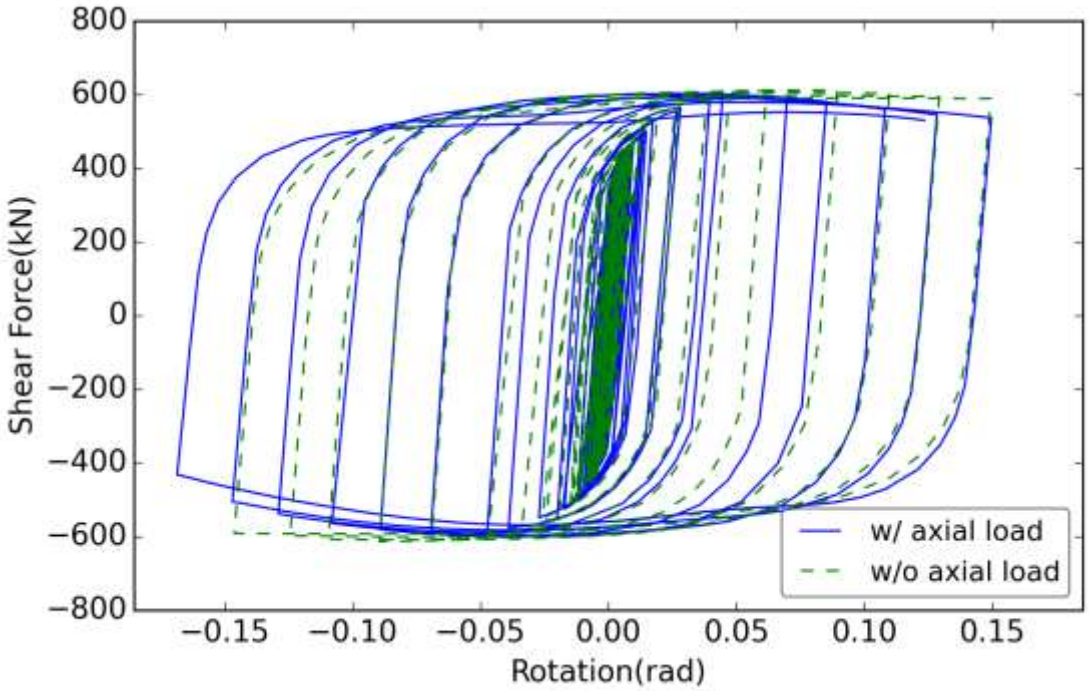

Figure 3-21 Comparing the effect of axial load for W10x33 made of A992 steel

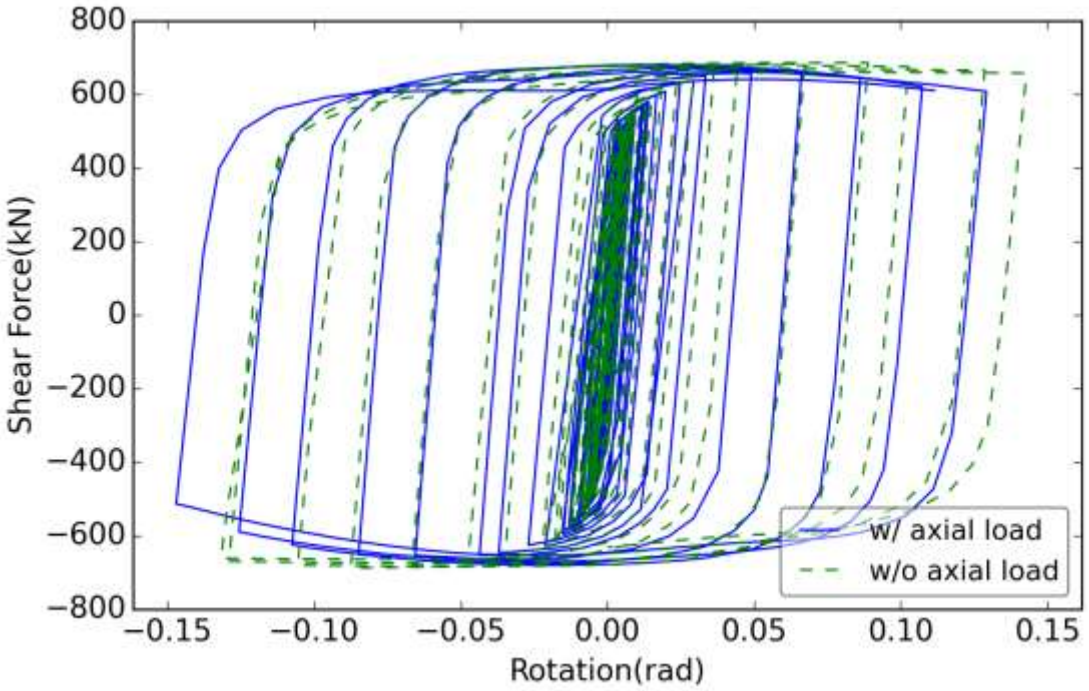

Figure 3-22 Comparing the effect of axial load for W10x33 made of Q460 steel

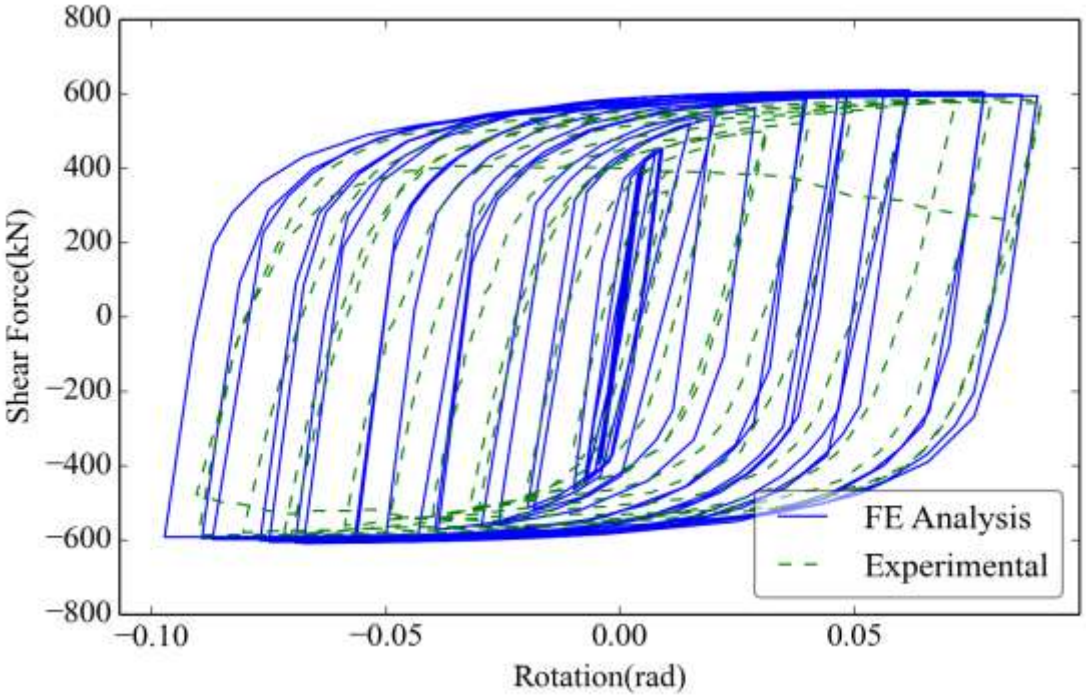

Figure 3-23 Comparison of numerical vs. experimental curves of W10x33 (Corte *et al.* 2013)

CHAPTER 4: NONLINEAR FE ANALYSIS OF Q460 SHEAR LINK

4.1. Introduction

Shear link in Eccentrically Braced Frames (EBFs) is one of the most important components in a modern building. EBFs act as fuse devices that are used to absorb the energy in a building when an earthquake happens, so that other parts of the buildings will have a smaller chance to be destroyed because there is less energy left. Shear links are usually built in a way such that it is very easy to be replaced after it is destroyed, which in turn makes it faster to maintain the building after earthquakes. If used properly, shear links can potentially reduce the overall cost of maintaining the buildings a lot while, at the same time, improve the safety of the buildings to a huge extent.

However, the use of shear links can be costly for places where earthquake happens frequently. Therefore it would be beneficial and economical if we could use less amount of steel in a shear link while achieving the similar strength, ductility, energy-dissipation capacity, and stiffness at the same time. In this section, to what extent are we able to reduce are studied in terms of the total amount of the steel used in the shear link if higher strength steel is used. To make it closer to the real scenario and applications, we added cyclic axial force that is proportional the loading added. By doing so, the simulation results are closer to the practice thus more valuable.

The performance in five different aspects, including strength, ductility, energy-dissipation, stiffness, and failure pattern contour are compared. To explore how much

steel can be reduced, the performance of A992 and Q460 to specimens where the size is reduced by 10% and 20% are also compared.

4.2. Monotonic LOAD BEHAVIOR

From Figure 4-2 to Figure 4-6, the performance of shear links of different shapes are shown. In each of the figure, four curves are included: the performance with material A992, the one with Q460, with Q460 steel and 10% reduction in size and Q460 with 10% reduction in size. As we can see from those figures, Q460 has the highest maximum shear force among all four variations, because of its higher strength. A992 is lower than Q460 after the yielding point. If the size is reduced by 10% for Q460, the curve will be very close to A992 in the later period of the loading. This means that if the size is reduced by 10%, the performance will be competitive to lower strength steel A992. However, if we reduce the size by 20%, the curve will be lower than corresponding A992 curves.

The fact that the convexity of the curve does not change as much as the maximum shear force is also observed. It can be seen see that Q460 has a higher convexity than A992. However, even if the size reduced by 20% the convexity is still much better than corresponding A992 curves. The implication and the cause of this phenomenon is not known and left as an interesting direction to explore in the future.

4.3. Cyclic LOAD BEHAVIOR

In this section, the performance of shear links when different types of steels are used are used. In particular, the following five aspects of properties are focused:

Stiffness, Shear strength, Ductility ratio, Hysteresis energy, and failure pattern contour. These are five important properties in assessing cyclic performance of shear link beams.

In addition, for each properties and each of the steel shapes, the value of four different combinations of material and size: A992, Q460, Q460 with 10% and 20% reduction in size. Specifically, the way of reducing the size is to reduce the web thickness and flange width of shear link section by 10% or 20% at the same time. In most of the case, as shown in the following, Q460 performs better than A992, and even for Q460 with 10% reduction, its performance is still competitive compared with A992. But for Q460 with 20% reduction in size, the performance in terms of certain properties are not as good as A992. The summary of different variations of models are included in Figure 4-22 to Figure 4-26.

4.3.1. Stiffness

Stiffness is a crucial parameter that affects the cyclic performance of shear links. In order to analyze the effect of using higher grade steel like Q460 on stiffness of shear link beams, five types of shear link models are simulated. There are four variations considered in each model: the original A992 shear link, the Q460 shear link with the same size, the Q460 shear link with 10% and 20% size reduction respectively.

The elastic stiffness is calculated by the following equation:

$$K_e = \frac{K_b K_s}{K_b + K_s}$$

, where K_e is the equivalent elastic stiffness, K_b is the bending stiffness and $K_b = 12EI/e^3$, E is the elastic modulus of steel, I is the moment of inertia, K_s is the shear stiffness and $K_s = GA_{tw}/e$. G is the shear modulus, A_{tw} is the area of web.

Performance Analysis

First, as shown in Table 4-1 to Table 4-5, the results from FE analysis is very close to the theoretically calculated results, which again confirms the validity of our model.

Then, the elastic stiffness of four variations of shear links are also compared, in Table 4-1 to Table 4-5 and Figure 4-7 to Figure 4-11, for those five shear links, the initial elastic stiffness values of A992 and Q460 with the same size are very similar. From Figure 4-7 to Figure 4-11 the initial stiffness values are basically the same can also be seen. After the yield point, the stiffness values are also similar. For example, for the model W14x68 with ρ=1.4, the elastic stiffness of A992 and Q460 steel shear link all equal to 133.5 kN/mm. This make sense because as seen from the aforementioned equations, the value of stiffness is not dependent on the types of steels used, but only the shape of the section.

The change of stiffness when the section is reduced is also analyzed. As shown in Table 4-1 to Table 4-5 and Figure 4-12 to Figure 4-21, the initial stiffness will reduce around 9% when the size of section has a 10% reduction, and will reduce by around 19% when the size of section has a 20% reduction. This phenomenon is not desirable, however, it is possible to increase the stiffness simply by adding more stiffeners to the shear link.

4.3.2. Shear Strength

Ultimate strength and yield strength are important factors to assess shear link beam performance. Over-strength factor is calculated as the ratio of the ultimate strength to the yield strength in cyclic testing. It can be expressed as the following equation:

$$\Omega = \frac{V_{max}}{V_y}$$

In this equation, the ultimate strength V_{max} is defined to be the maximum shear force in the cyclic curve; V_y is the yield strength of shear link, which is defined by (Park 1989).

Performance Analysis

Table 4-6 to Table 4-10 show some interesting results in terms of ultimate strength, yield strength, and over-strength factor. As seen, shear links made of Q460 have higher yield strength than the corresponding A992 shear links. This is because the yield stress of Q460 steel is higher. The ultimate strength of Q460 shear links is also higher, which means that strain hardening is more obvious in Q460 steel. The over-strength factor of A992 in different shear links range from 1.39 to 1.60, while for Q460 the over-strength factor is much less, ranging from 1.29 to 1.32. We can find that both ultimate shear link force and yielding strength of the shear link increases when high strength steel of same size are used. However, the increase of yielding strength is much higher, which leads to the decrease of over-strength ratio.

In each table from Table 4-6 to Table 4-10, the over-strength factor for Q460 with 10% and 20% reduction in size is also shown. When the size of the shear link is reduced, we can find that over-strength factor does not have much change compared with the corresponding initial Q460 steel shear links. Therefore, if only over-strength factor of the shear link is considered, even if the size of the shear link is reduced by 20%, the over-strength factor is still smaller than one in A992 steel shear links.

4.3.3. Ductility

In earthquake design, ductility is used to denote the ability of a structure to withstand large cyclic deformations in the inelastic range before it shows substantial reduction in its strength. The ductility ratio can therefore be expressed in the following:

$$\mu = \frac{\Delta_u}{\Delta_y}$$

Where Δ_u is the post-peak displacement when the load carrying capacity has undergone a 15% reduction. Δ_y is the rotation at the yield point of shear link.

In Figure 4-1, the second definition defined by Park (1989) to compute Δ_y is used from the FE analysis result. The detailed steps of how to determine the yield strength is as following:

1) The first step is the same that we will get a tangent line to the curve.
2) Then, instead of reading the intersection point directly, we will draw another horizontal line corresponding to the ultimate load.
3) The final yielding displacement can be found by finding the intersection of these two lines.

Performance Analysis

In the following table, the ductility ratio for all test cases are shown with different steel type and shapes.

One thing to note is fracture initiation failure mode is not considered in the FE models in this study, therefore, the ductility ratios in Table 4-11 are larger than the real case. Actually in some models, the loading carrying capacity never reduces by 15%

before the simulation terminates. The value of Δ_u is determined either by the last displacement value or the 15% post-peak displacement.

It can be seen that the ductility ratio of A992 is higher than the ductility ratio of Q460 shear link of same type of steel shape. This means that Q460 steel shear links have a worse ductility compared with A992 type shear links. However, this is not surprising because it is usually the case that higher strength steel performs worse than lower strength steel in terms of ductility. Furthermore, as seen that the differences between two types of shear links are not big when used in this setting.

When the size of Q460 steel shear links has 10% or 20% reduction, the ductility of shear links do not endure big decrease. Shown from Figure 4-12 to Figure 4-21, the ductility ratios fall into almost the same range when the size is reduced.

Specifically, in the case W14x68 (ρ=1.6), which can be found in Figure 4-9, the curves are obviously different from that of other models. The ductility endure a significantly decrease when A992 steel is replaced with Q460.

4.3.4. Energy Dissipation

In this subsection, how much energy can be absorbed by shear links will be discussed and how much difference will be achieved if different types of shear links are used, different types of steel as well as different length. This is a very important performance factor as, in an earthquake, it is essentially the exceeding amount of energy that destroys the buildings and if there was not enough energy, then the buildings will be in a safer situation.

First of all, a way to calculate energy from the hysteretic cycle figures is needed. We followed the approach adopted by Shi et al (2012) to calculate the energy absorption. The hysteretic energy of a shear link is defined as the sum of areas of all the hysteretic cycles, which represents the seismic energy dissipation of the shear link.

Performance Analysis

In Table 4-12, the hysteretic energy of the original 10 shear link models is calculated. The hysteretic energy of shear links using A992 steel and Q460 steel are compared, and the results show that the shear links with Q460 can absorb 9% to 20% more than the A992 shear links with the same size.

Additionally, the size of Q460 shear links are reduced to 10% and 20%, the hysteretic energy is then again compared with A992 shear links. When the section of Q460 shear links are reduced to 10%, the energy dissipation capacities are almost similar to the A992 shear links, which means from the prospective of energy dissipation capacity, the Q460 shear links with a 10% reduction in its section are of the same level with A992 shear links of the same type.

4.3.5. Failure Pattern Contour

In this section, the contour figures and failure modes of different models are further discussed. In summary, for most of the simulations done, web buckle happens before flange buckling except for W14x68 with ρ=1.6 where flange buckle happens.

Figure 4-27 to Figure 4-36 show the plastic shear strain contour of all five types of shear links made of A992 and Q460 steel, at link rotation γ = 0.015 radius (around yield point). These figures show that at the yield point with same level of shear strain, shear links made of Q460 steel have larger plastic strain area than ones made of A992

steel. This indicates that Q460 shear links can have more hysteresis energy dissipation. The deformed shapes of local buckling are also shown. Since the failure modes of A992 and Q460 shear links are similar, only the deformed shapes of Q460 link beams are presented in order to avoid redundancy.

Figure 4-37 to Figure 4-46 show the plastic shear distribution of five models made of A992 and Q460 steel at link rotation γ around 0.10 rad. For model W14x68 with ρ=1.2 and 1.4, W10x33, and W10x68, excessive strain are observed in web areas, which means that web buckling occurs in these models at 0.10 rad. However for model W14x68 with ρ=1.6, excessive plastic strain are observed at the area very close to the edge of flange, which indicates flange local buckling occurred.

Figure 4-47 to Figure 4-56 show the plastic shear distribution of models made of Q460 with 10% and 20% size reduction respectively, at around yield point with γ=0.01 rad.

Figure 4-57 to Figure 4-66 show the plastic shear distribution of models made of Q460 with 10% and 20% size reduction respectively, at around failure point γ=0.08 rad. The results also indicate that when the size of shear link beam section are reduced to 10% or 20%, failure mode will occur earlier than the corresponding original models.

4.4. Summary

The five initial shear link specimens are designed, each was made from different steel grades including ASTM A992 (345MPa) steel and Q460 (460MPa) high

strength steel. An additional set of 10 shear link specimens made of high strength steel Q460 are designed to have a 10% and 20% size reduction in section area compared with the corresponding unreduced shear link specimen. Finite element models of all these 20 shear link specimens are built in ANSYS software. ANSYS command line tool is used to automate and accelerate the simulation of models in ANSYS and discussed core snippet of the code. After validation of the model using available experimental results, their performance (in terms of five performance indices: ductility, over-strength factor, stiffness, energy absorption, and failure mode) are compared under cyclic loading and monotonic loading respectively.

The following findings can be observed from the numerical simulation results:

1. Using ANSYS with Chaboche model can accurately predict the performance of shear links of different types and steel. However, fracture initiation in shear link was not taken into account in this simulation study.

2. In general, by using Q460 high strength steel for shear links, smaller over-strength factor values and higher energy dissipation capacity are achieved compared to corresponding A992 steel shear links. Although reduced ductility due to local buckling is observed in Q460 steel shear links, this can be alleviated by adding more stiffeners. All shear links made of Q460 steel considered in this study can achieve 0.08 radian inelastic link rotation.

3. Reducing the size by 10% on Q460 shear links would yield a performance that is still comparable to that of corresponding A992 shear link. However, if the section size of shear link is reduced by 20%, its performance would further deteriorate.

W14x68 (ρ=1.2)			
Type	K_e by calculation (kN/mm)	K_e by FE analysis (kN/mm)	Ratio of reduction in K_e compared to A992
A992	175	173.4	/
Q460	175	173.4	0%
Q460, 10% Red.	158.4	157.1	9.4%
Q460, 20% Red.	138.8	140.4	19.0%

Table 4-1 Calculated and simulated results for stiffness of W14x68 (ρ=1.2) with A992, Q460, Q460 with 10% and 20% reduced section

W14x68 (ρ=1.4)			
Type	K_e by calculation (kN/mm)	K_e by FE analysis (kN/mm)	Ratio of reduction in K_e compared to A992
A992	133.4	133.5	/
Q460	133.4	133.5	0%
Q460, 10% Red.	119.5	120.9	9.4%
Q460, 20% Red.	107.3	108.0	19.1%

Table 4-2 Calculated and simulated results for stiffness of W14x68 (ρ=1.4) made of A992, Q460, Q460 with 10% and 20% reduced section

W14x68 (ρ=1.6)			
Type	K_e by calculation (kN/mm)	K_e by FE analysis (kN/mm)	Ratio of reduction in K_e compared to A992
A992	104.8	106.0	/
Q460	104.8	105.9	0.1%
Q460, 10% Red.	93.1	95.9	9.5%
Q460, 20% Red.	83	85.7	19.2%

Table 4-3 Calculated and simulated results for stiffness of W14x68 (ρ=1.6) made of A992, Q460, Q460 with 10% and 20% reduced section

W10x33 (ρ=1.07)			
Type	K_e by calculation (kN/mm)	K_e by FE analysis (kN/mm)	Ratio of reduction in K_e compared to A992
A992	150.3	146.1	/
Q460	150.3	146.1	-0.5%
Q460, 10% Red.	137.4	132.6	6.8%
Q460, 20% Red.	119.4	118.7	14.7%

Table 4-4 Calculated and simulated results for stiffness of W10x33 (ρ=1.07) made of A992, Q460, Q460 with 10% and 20% reduced section

W10x68 (ρ=1.2)			
Type	K_e by calculation (kN/mm)	K_e by FE analysis (kN/mm)	Ratio of reduction in K_e compared to A992
A992	142.3	145.2	/
Q460	142.3	154.5	-6.1%
Q460, 10% Red.	128.1	131.6	14.8%
Q460, 20% Red.	115	126.1	18.4%

Table 4-5 Calculated and simulated results for stiffness of W10x68 (ρ=1.2) made of A992, Q460, Q460 with 10% and 20% reduced section

W14x68 (ρ=1.2)			
Type	V_{max} (kN)	V_y (kN)	$\Omega = V_{max}/V_y$
A992	1208	830	1.46
Q460	1356	1034	1.31
Q460, 10% Red.	1199	922	1.30
Q460, 20% Red.	1047	833	1.26

Table 4-6 Ultimate strength, yield strength, and Over-strength factor of W14x68 (ρ=1.2) with A992, Q460, Q460 with 10% and 20% reduced section

W14x68 (ρ=1.4)			
Type	V_{max} (kN)	V_y (kN)	$\Omega = V_{max}/V_y$
A992	1205	751	1.60
Q460	1362	1058	1.29
Q460, 10% Red.	1207	940	1.28
Q460, 20% Red.	1048	830	1.26

Table 4-7 Ultimate strength, yield strength, and Over-strength factor of W14x68 (ρ=1.4) with A992, Q460, Q460 with 10% and 20% reduced section

W14x68 (ρ=1.6)			
Type	V_{max} (kN)	V_y (kN)	$\Omega = V_{max}/V_y$
A992	1198	863	1.39
Q460	1333	1033	1.29
Q460, 10% Red.	1198	938	1.28
Q460, 20% Red.	1049	837	1.25

Table 4-8 Ultimate strength, yield strength, and Over-strength factor of W14x68 (ρ=1.6) with A992, Q460, Q460 with 10% and 20% reduced section

W10x33 (ρ=1.07)			
Type	V_{max} (kN)	V_y (kN)	$\Omega = V_{max}/V_y$
A992	603	420	1.44
Q460	681	514	1.32
Q460, 10% Red.	602	455	1.32
Q460, 20% Red.	525	397	1.32

Table 4-9 Ultimate strength, yield strength, and Over-strength factor of W10x33 (ρ=1.07) with A992, Q460, Q460 with 10% and 20% reduced section

W10x68 (ρ=1.2)			
Type	V_{max} (kN)	V_y (kN)	$\Omega = V_{max}/V_y$
A992	1024	735	1.39
Q460	1158	895	1.29
Q460, 10% Red.	1021	796	1.28
Q460, 20% Red.	888	708	1.25

Table 4-10 Ultimate strength, yield strength, and Over-strength factor of W10x68 (ρ=1.2) with A992, Q460, Q460 with 10% and 20% reduced section

Link type	W14x68 (ρ=1.2)	W14x68 (ρ=1.4)	W14x68 (ρ=1.6)	W10x33 (ρ=1.07)	W10x68 (ρ=1.2)
A992	20.6	18.8	12.7	25.0	21.1
Q460	18.4	13.7	9.3	19.3	19.4
Q460, 10% Red.	15.8	13.7	9.0	17.5	18.7
Q460, 20% Red.	15.9	12.0	10.3	17.1	15.2

Table 4-11 Ductility of different types with A992, Q460, Q460 with 10% reduced section and Q460 with 20% reduced section

Link type	W14x68 (ρ=1.2) / J	W14x68 (ρ=1.4) / J	W14x68 (ρ=1.6) / J	W10x33 (ρ=1.07) / J	W10x68 (ρ=1.2) / J
A992	1544646	1740276	1864737	935929	1897651
Q460	1728023	1895462	2070106	1052377	2613403
Q460, 10% Red.	1568850	1777728	1885182	899599	1922062
Q460, 20% Red.	936203	1550626	1610739	657180	1642043

Table 4-12 Energy absorption of different types with A992, Q460, Q460 with 10% and 20% reduced section

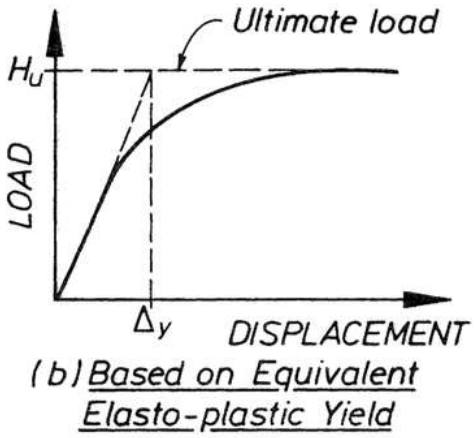

Figure 4-1 Method to compute yielding displacement, by Park (1989)

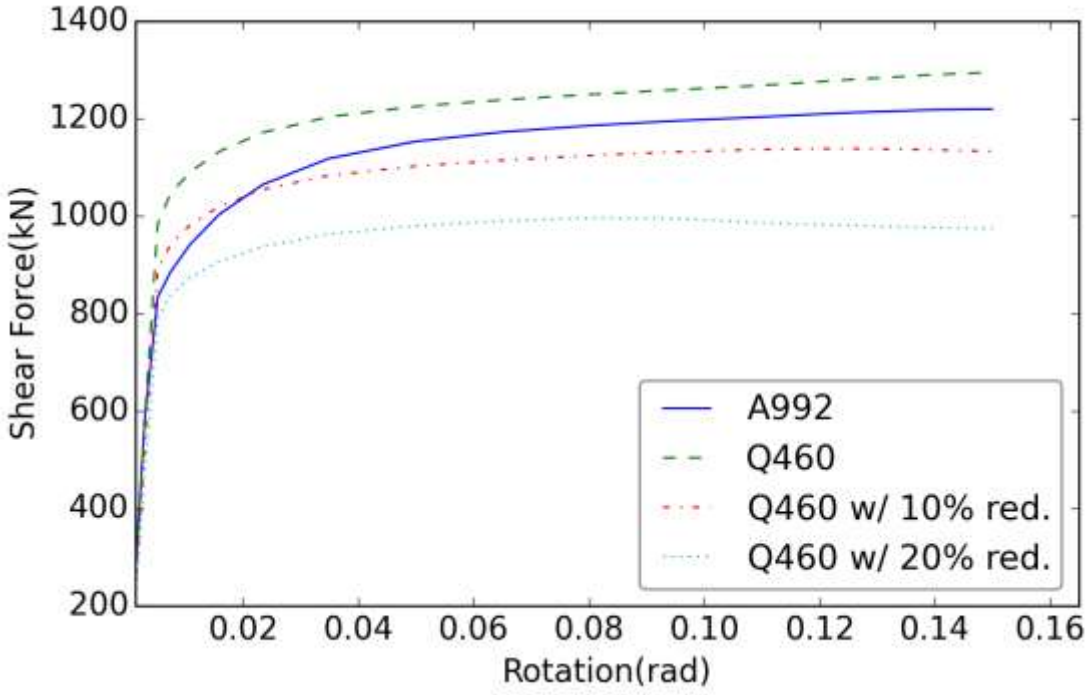

Figure 4-2 Comparison of shear link W14x68 (ρ=1.2) with A992 steel and Q460 steel under monotonic loading

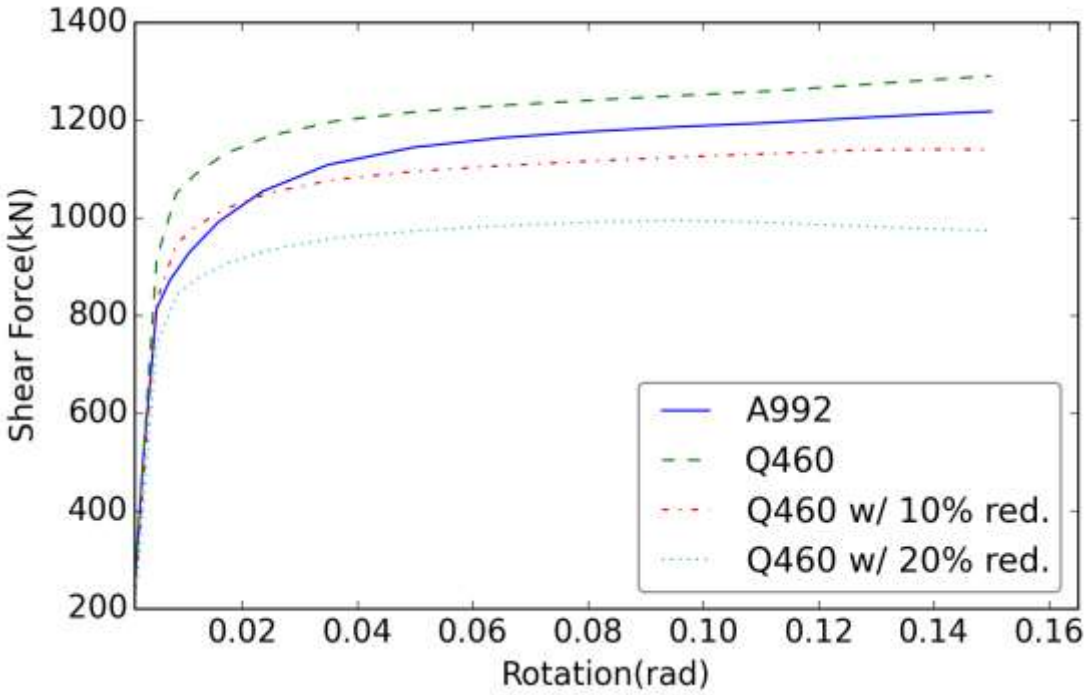

Figure 4-3 Comparison of shear link W14x68 (ρ=1.4) with A992 steel and Q460 steel under monotonic loading

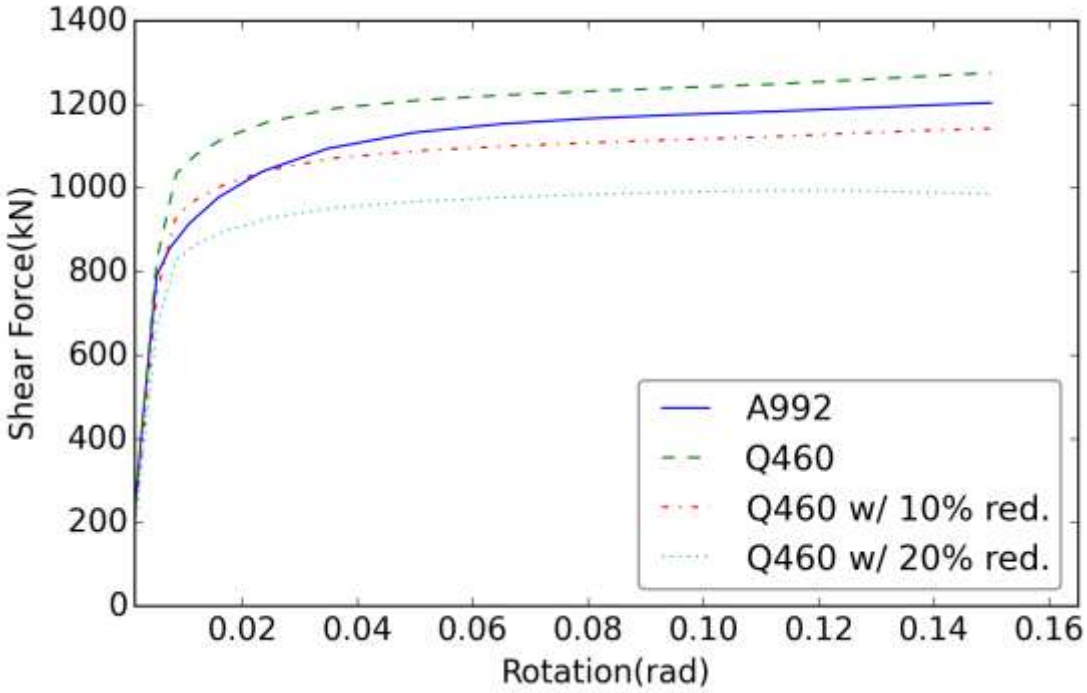

Figure 4-4 Comparison of shear link W14x68 (ρ=1.6) with A992 steel and Q460 steel under monotonic loading

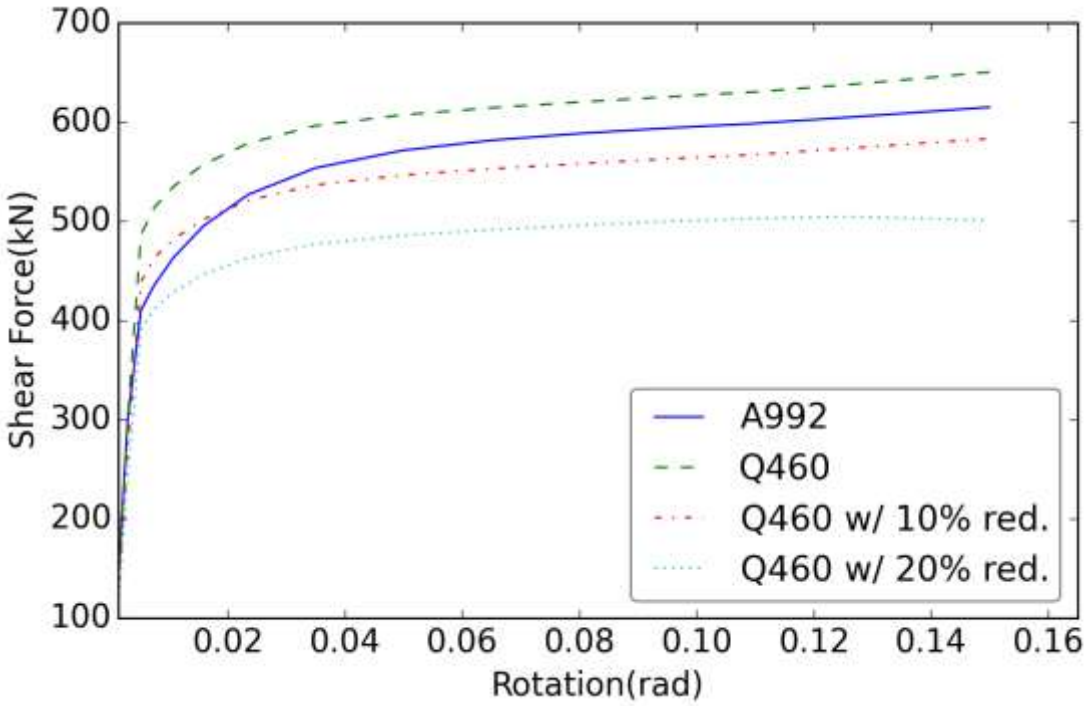

Figure 4-5 Comparison of shear link W10x33 (ρ=1.07) with A992 steel and Q460 steel under monotonic loading

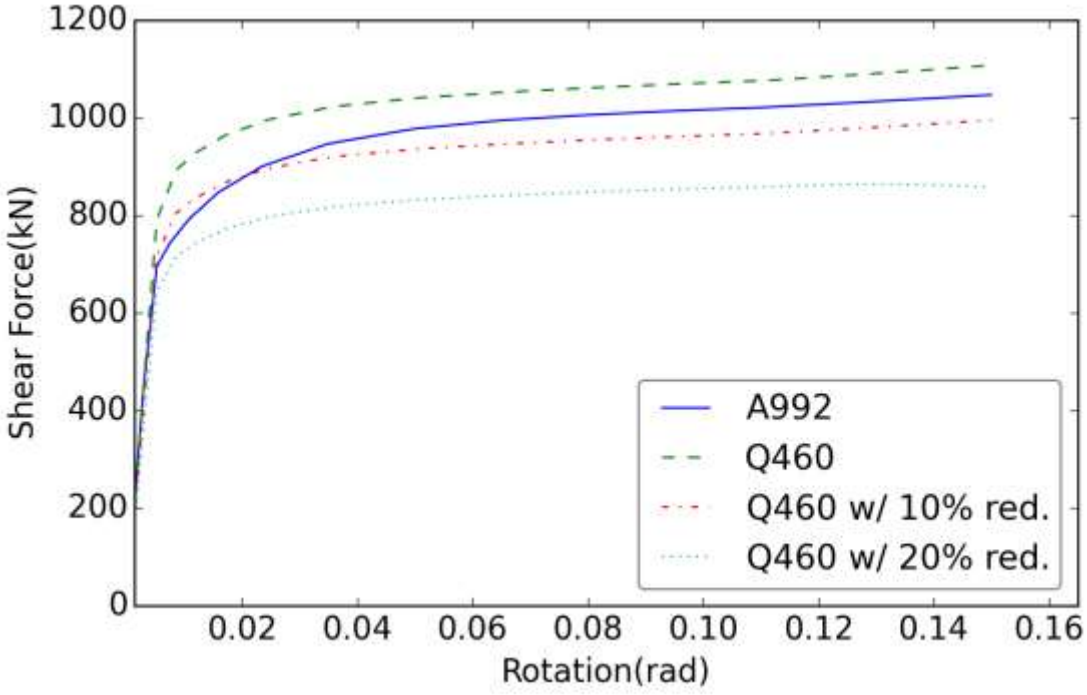

Figure 4-6 Comparison of shear link W10x68 (ρ=1.2) with A992 steel and Q460 steel under monotonic loading

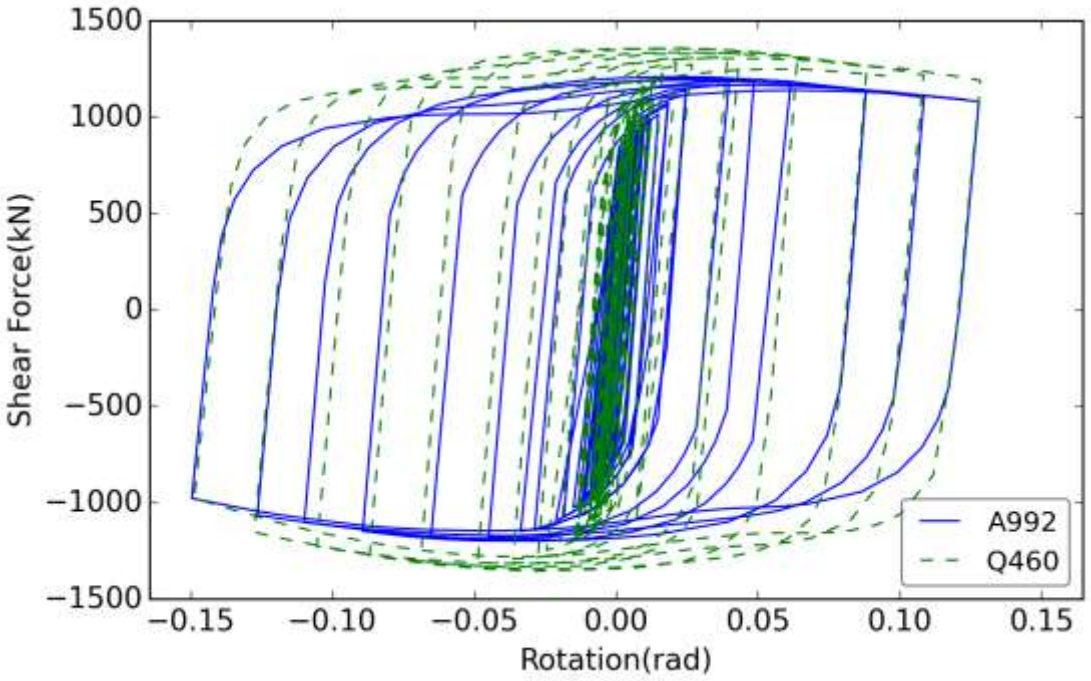

Figure 4-7 Comparison of shear link W14x68 (ρ=1.2) with A992 steel and Q460 steel under cyclic loading

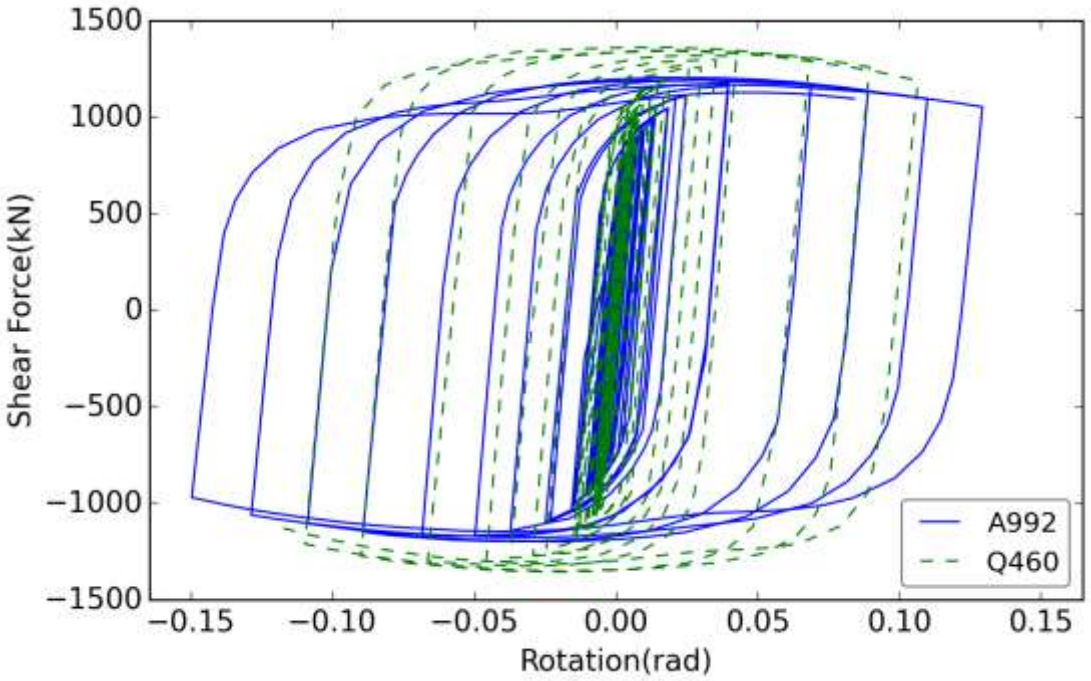

Figure 4-8 Comparison of shear link W14x68 (ρ=1.4) with A992 steel and Q460 steel under cyclic loading

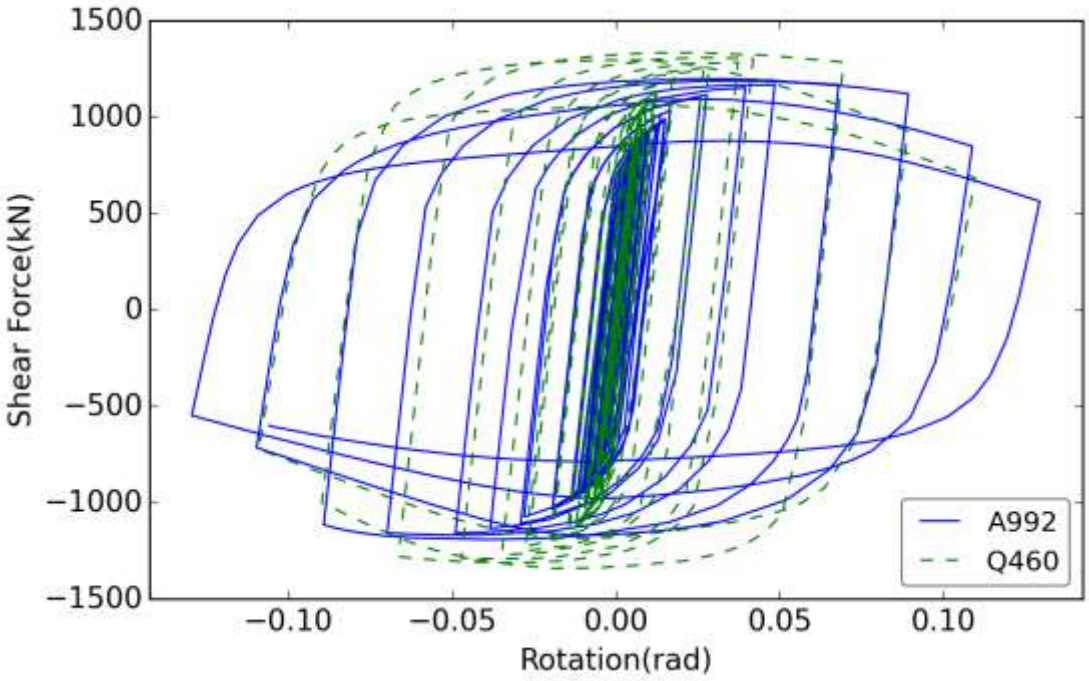

Figure 4-9 Comparison of shear link W14x68 (ρ=1.6) with A992 steel and Q460 steel under cyclic loading

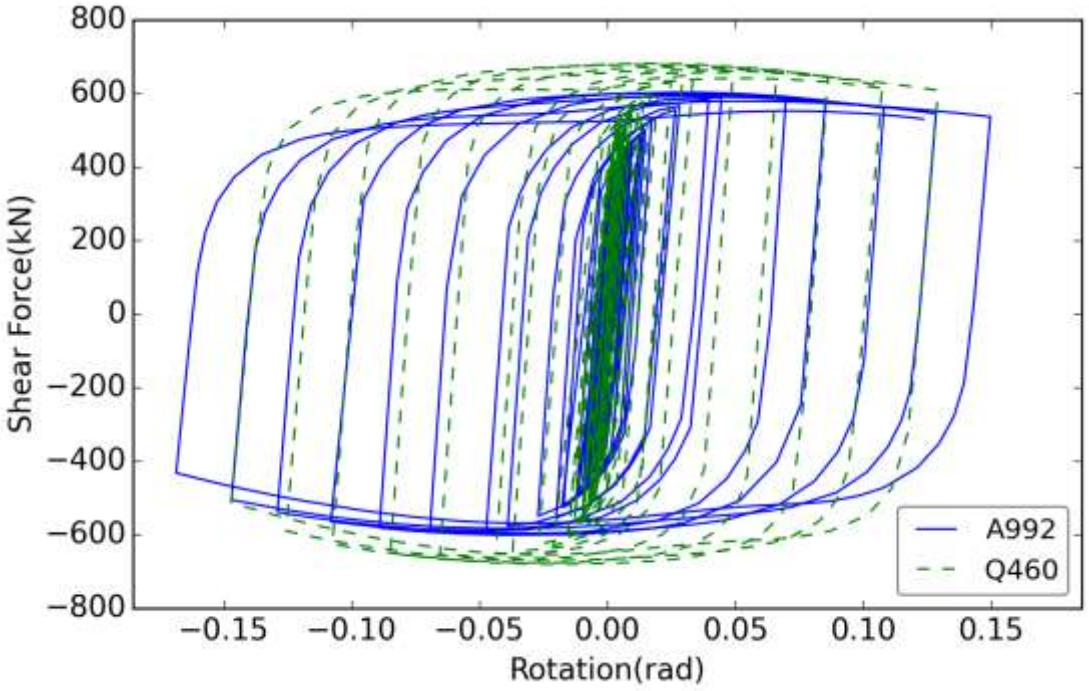

Figure 4-10 Comparison of shear link W10x33 (ρ=1.07) with A992 steel and Q460 steel under cyclic loading

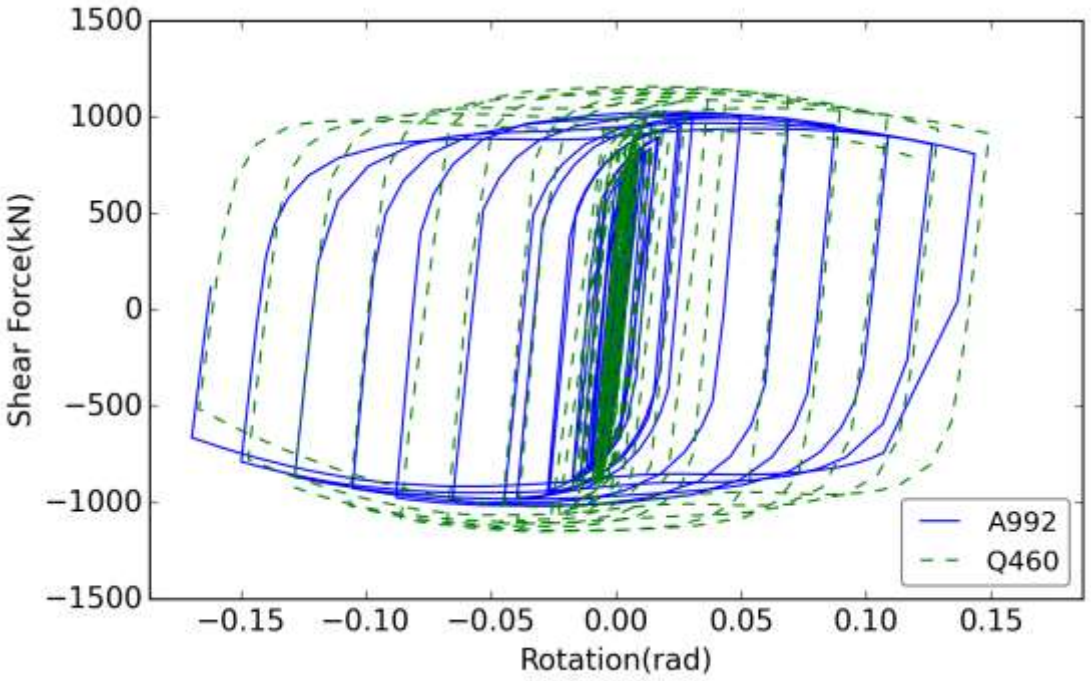

Figure 4-11 Comparison of shear link W10x68 (ρ=1.2) with A992 steel and Q460 steel under cyclic loading

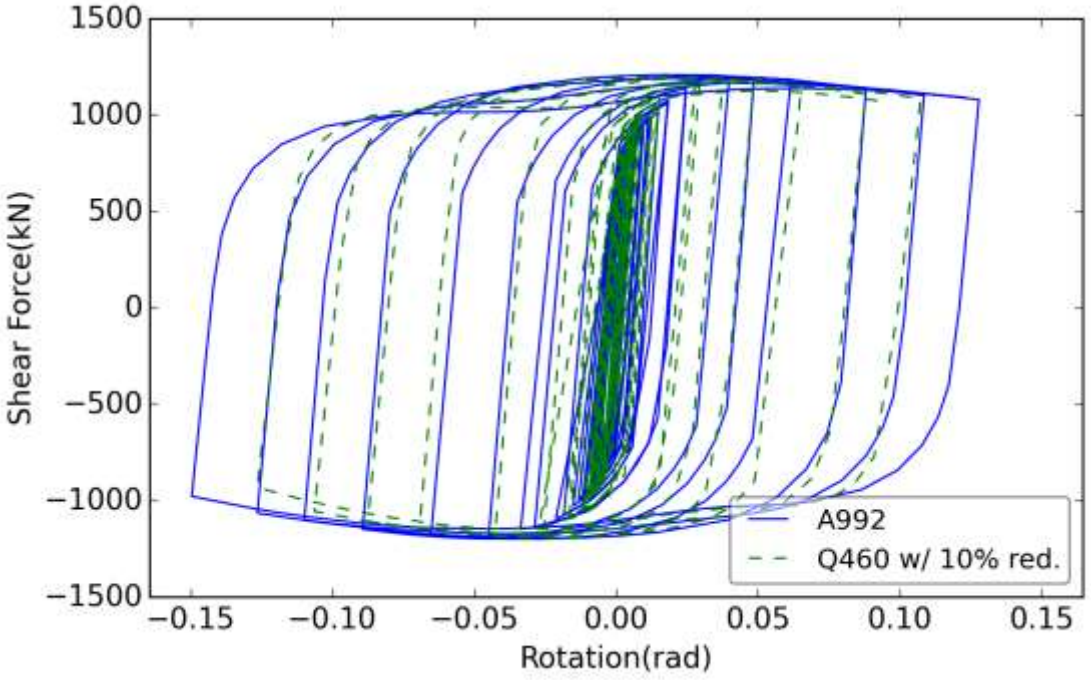

Figure 4-12 Comparison of W14x68 (ρ=1.2) with A992 and Q460 (10% reduction) under cyclic loading

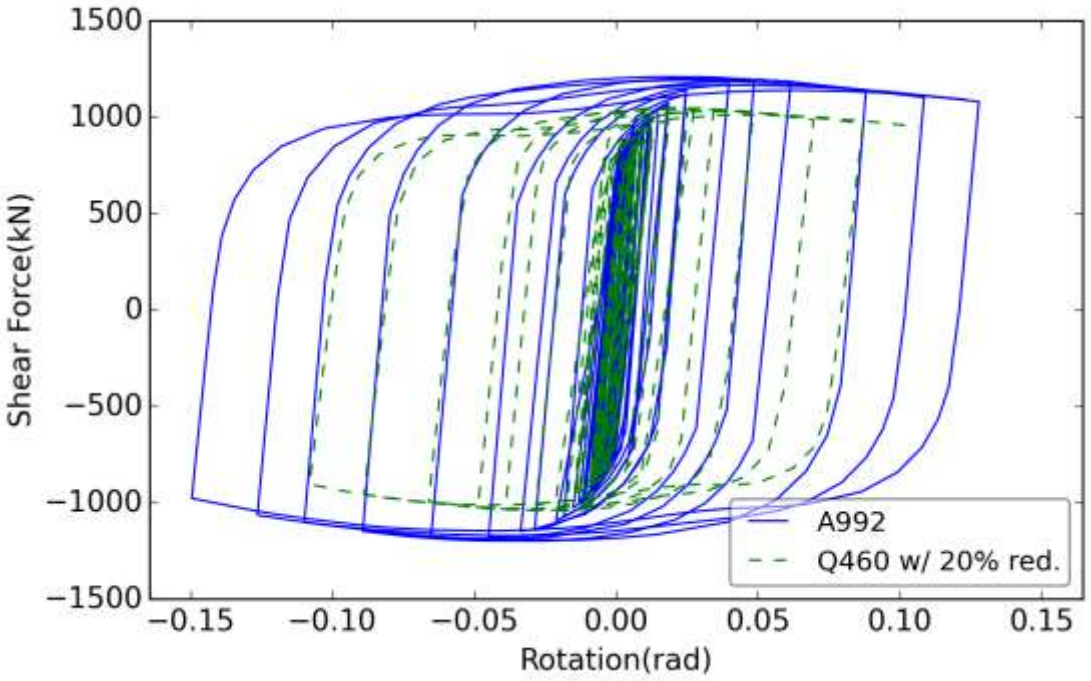

Figure 4-13 Comparison of W14x68 (ρ=1.2) with A992 and Q460 (20% reduction) under cyclic loading

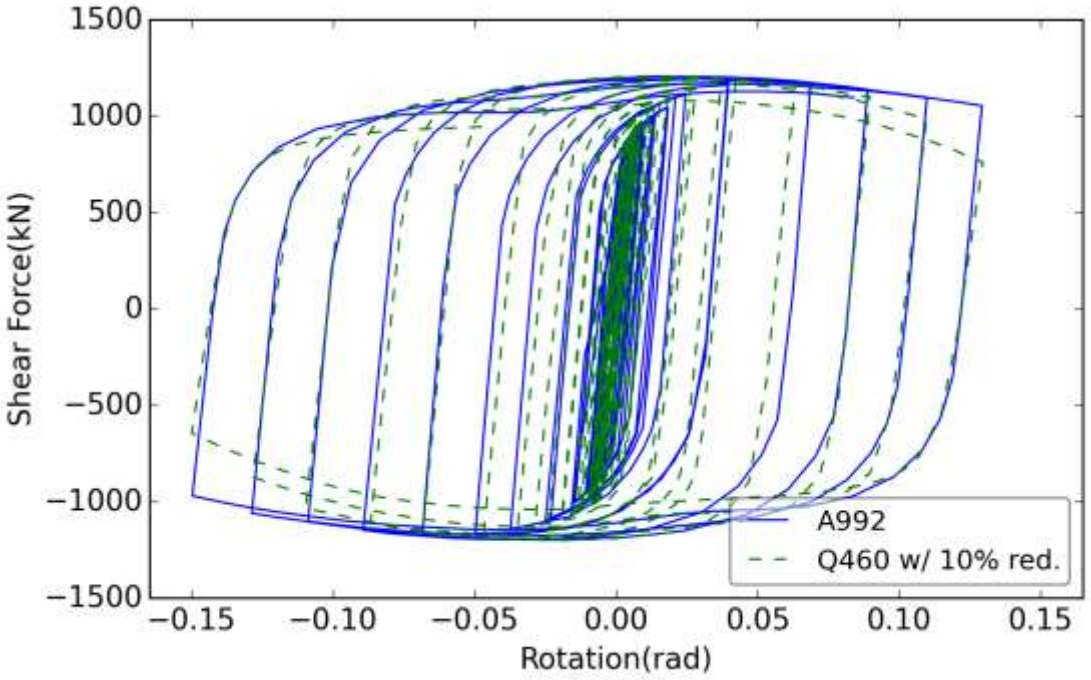

Figure 4-14 Comparison of W14x68 (ρ=1.4) with A992 and Q460 (10% reduction) under cyclic loading

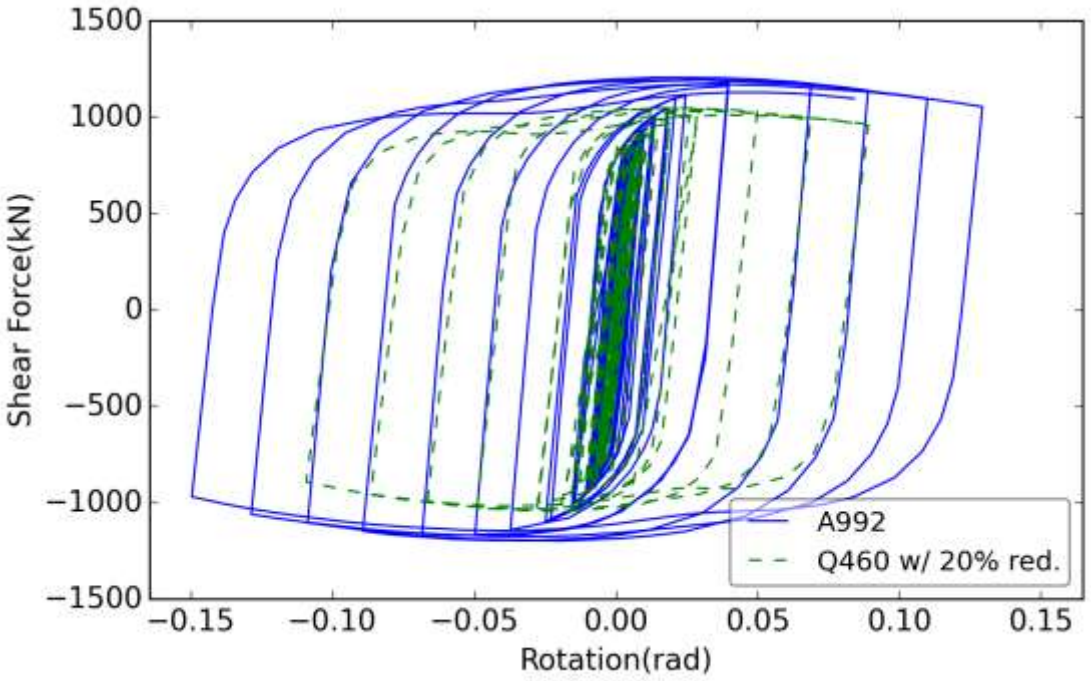

Figure 4-15 Comparison of W14x68 (ρ=1.4) with A992 and Q460 (20% reduction) under cyclic loading

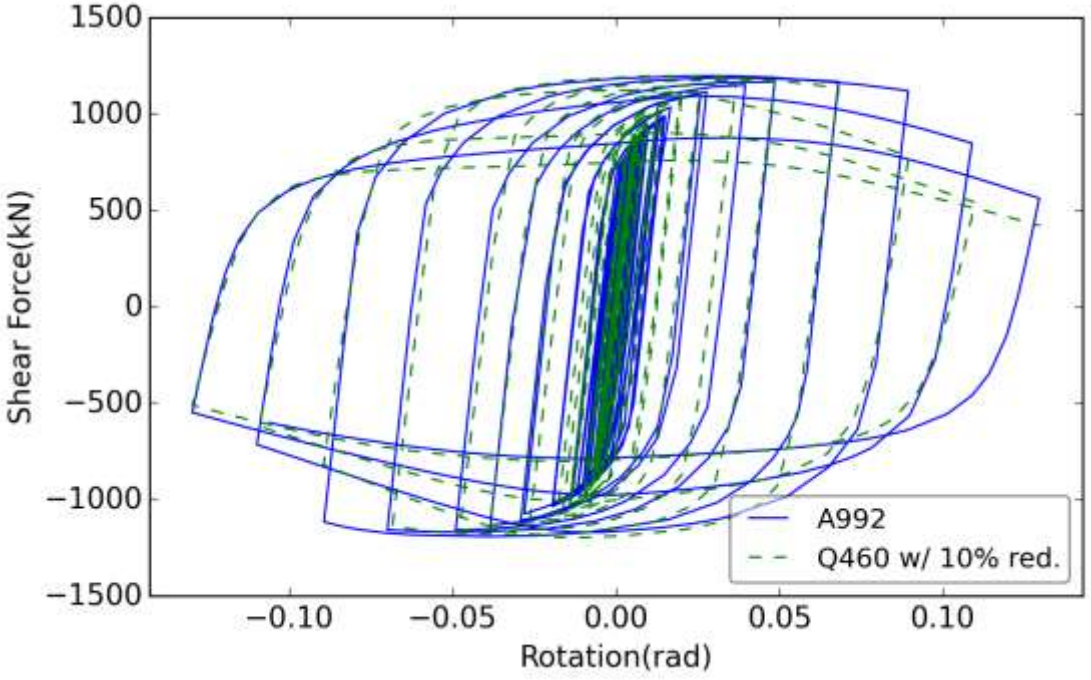

Figure 4-16 Comparison of W14x68 (ρ=1.6) with A992 and Q460 (10% reduction) under cyclic loading

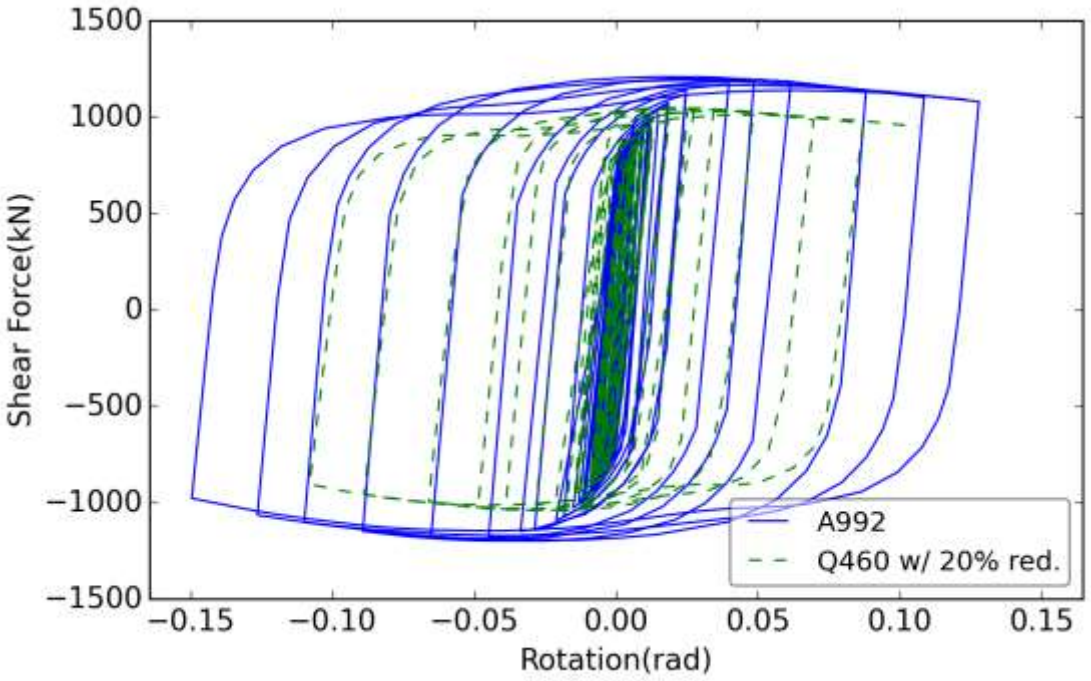

Figure 4-17 Comparison of W14x68 (ρ=1.6) with A992 and Q460 (20% reduction) under cyclic loading

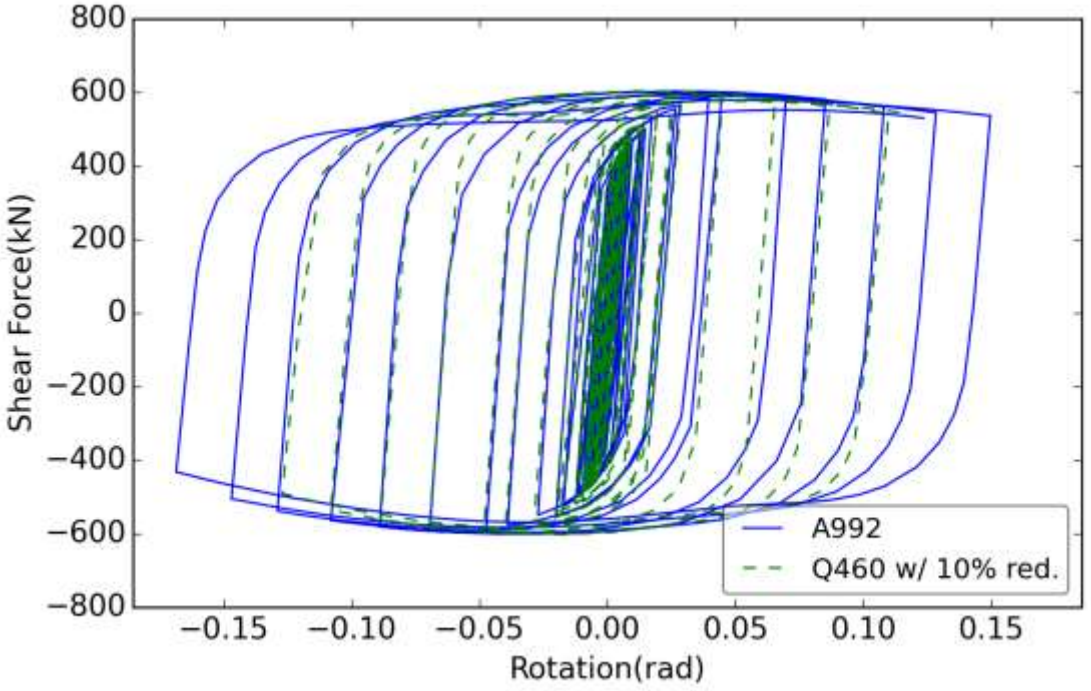

Figure 4-18 Comparison of W10x33 (ρ=1.07) with A992 and Q460 (10% reduction) under cyclic loading

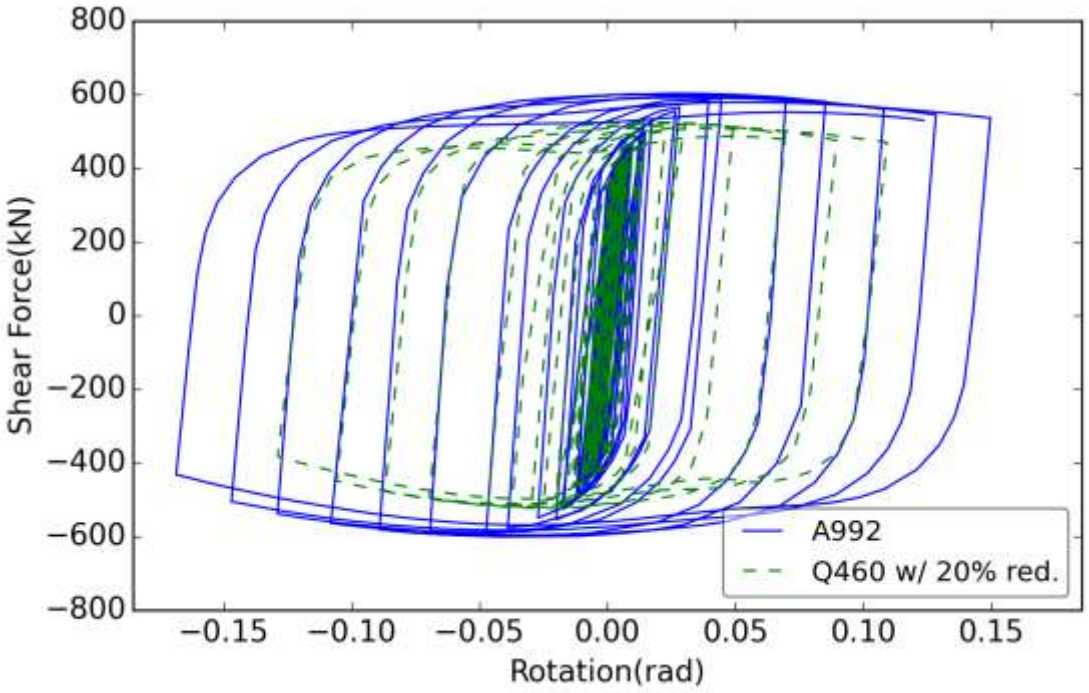

Figure 4-19 Comparison of W10x33 (ρ=1.07) with A992 and Q460 (20% reduction) under cyclic loading

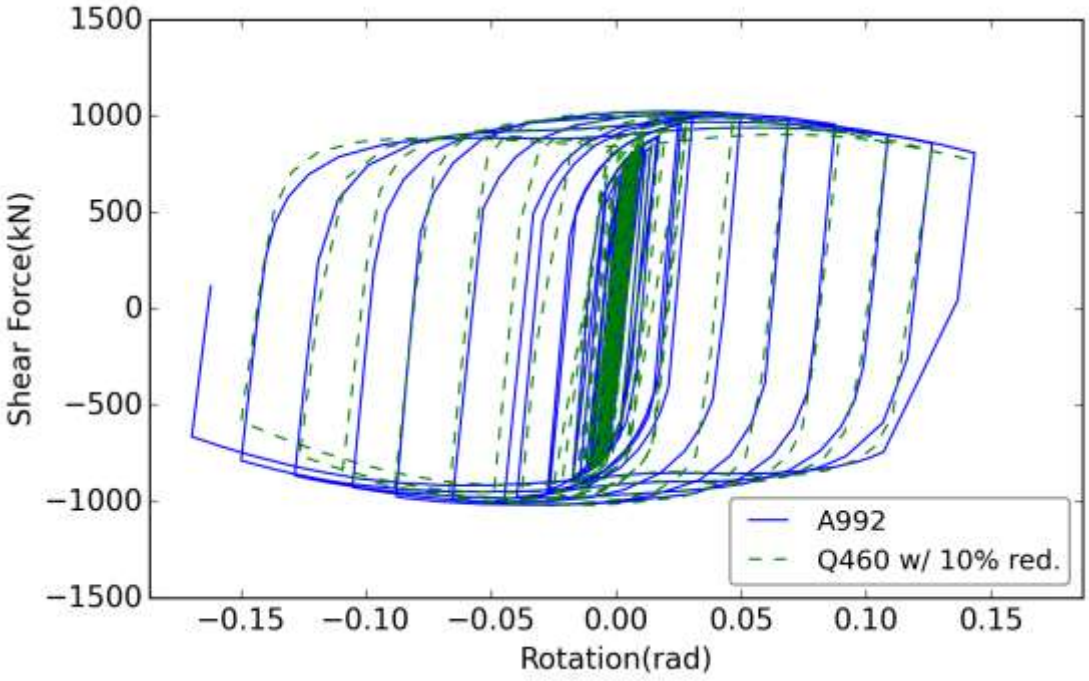

Figure 4-20 Comparison of W10x68 (ρ=1.2) with A992 and Q460 (10% reduction) under cyclic loading

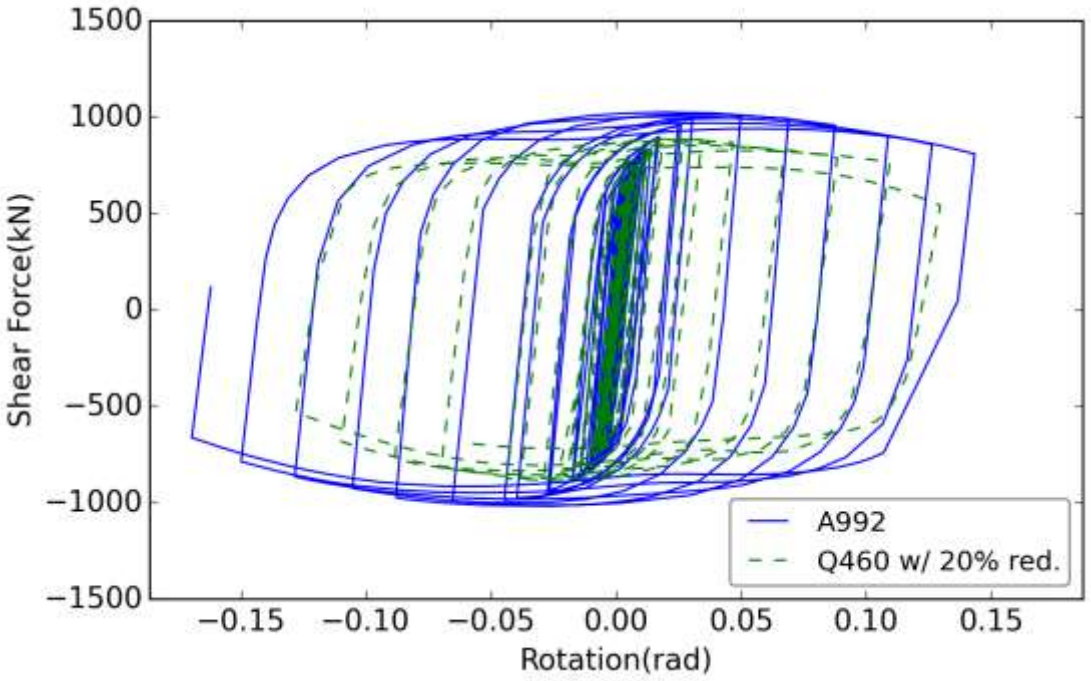

Figure 4-21 Comparison of W10x68 (ρ=1.2) with A992 and Q460 (20% reduction) under cyclic loading

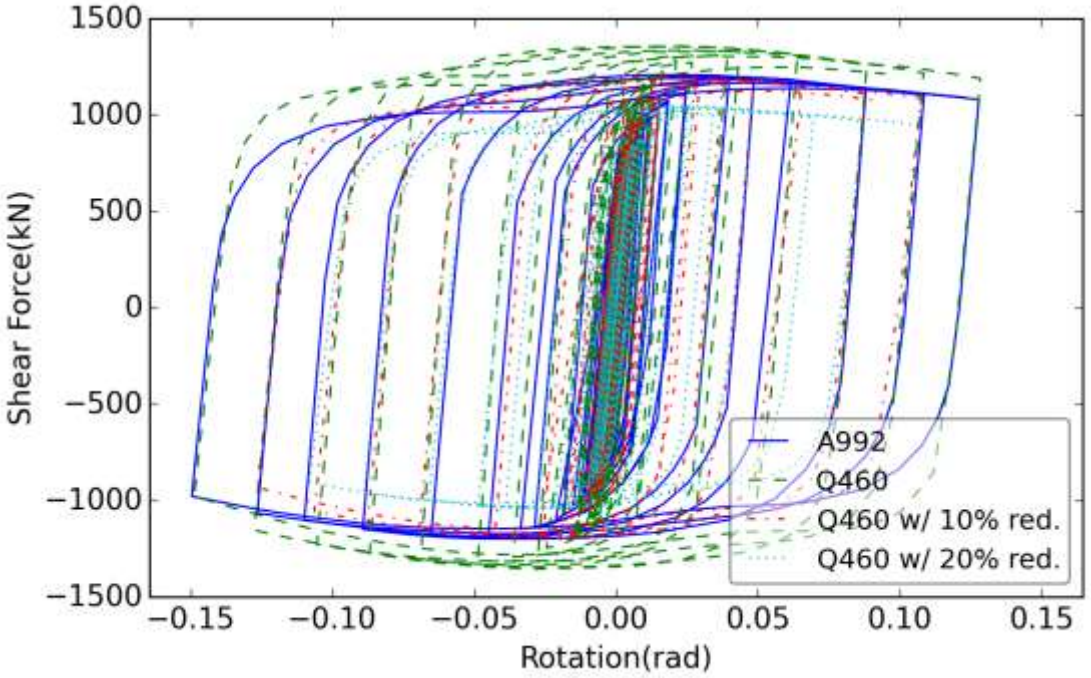

Figure 4-22 Comparison of different variations of W14x68 (ρ=1.2)

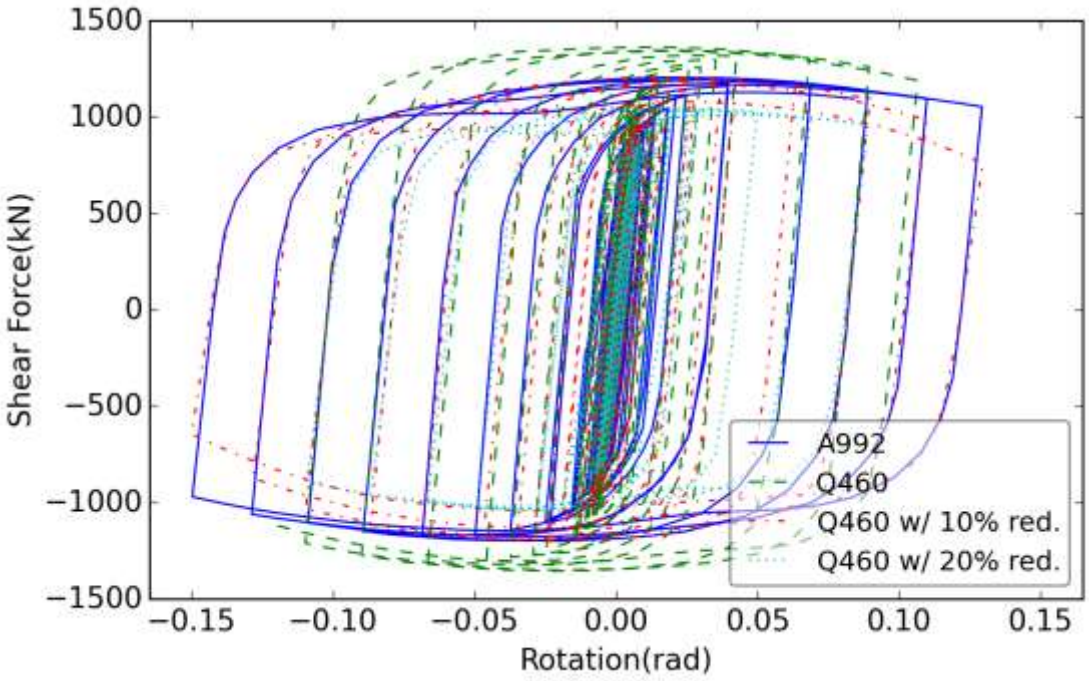

Figure 4-23 Comparison of different variations of W14x68 (ρ=1.4)

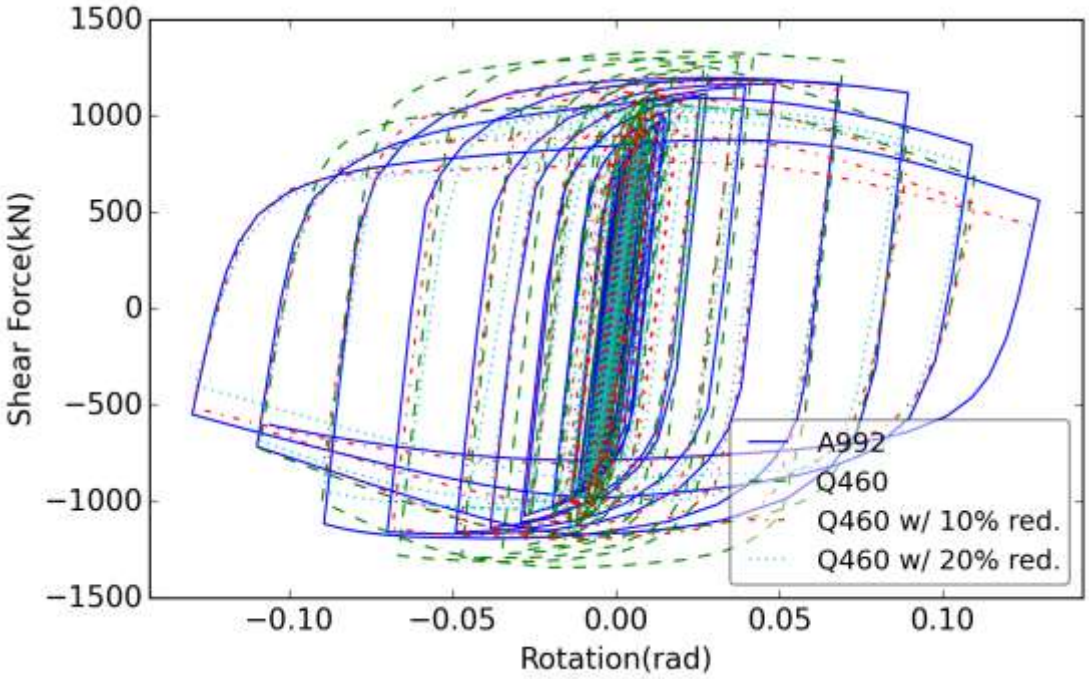

Figure 4-24 Comparison of different variations of W14x68 (ρ=1.6)

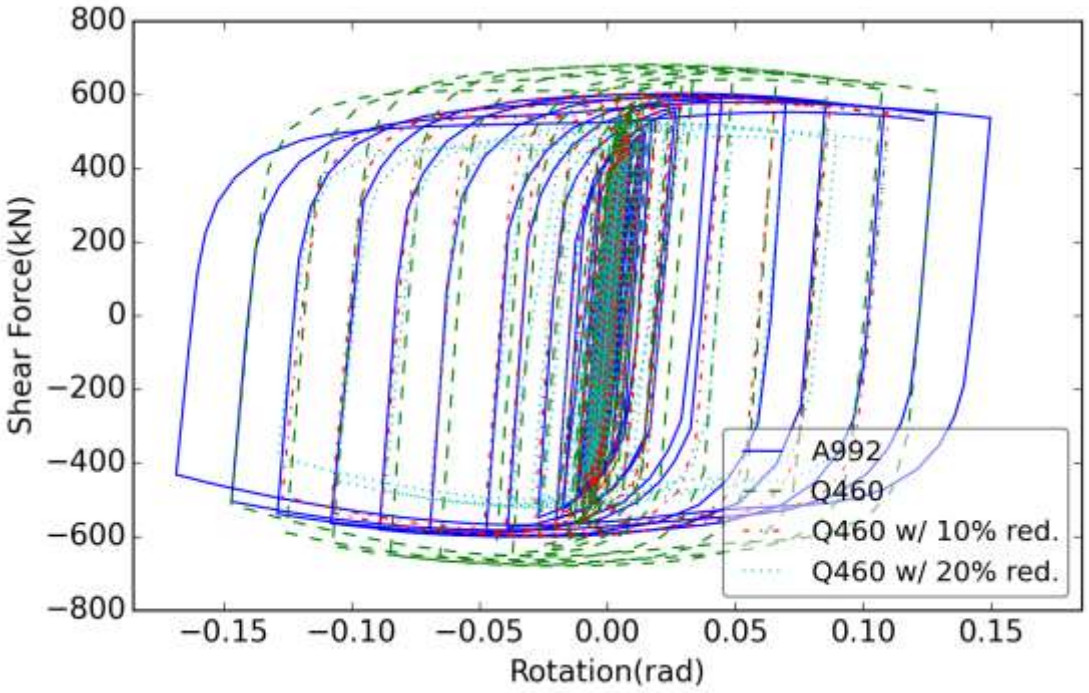

Figure 4-25 Comparison of different variations of W10x33 (ρ=1.07)

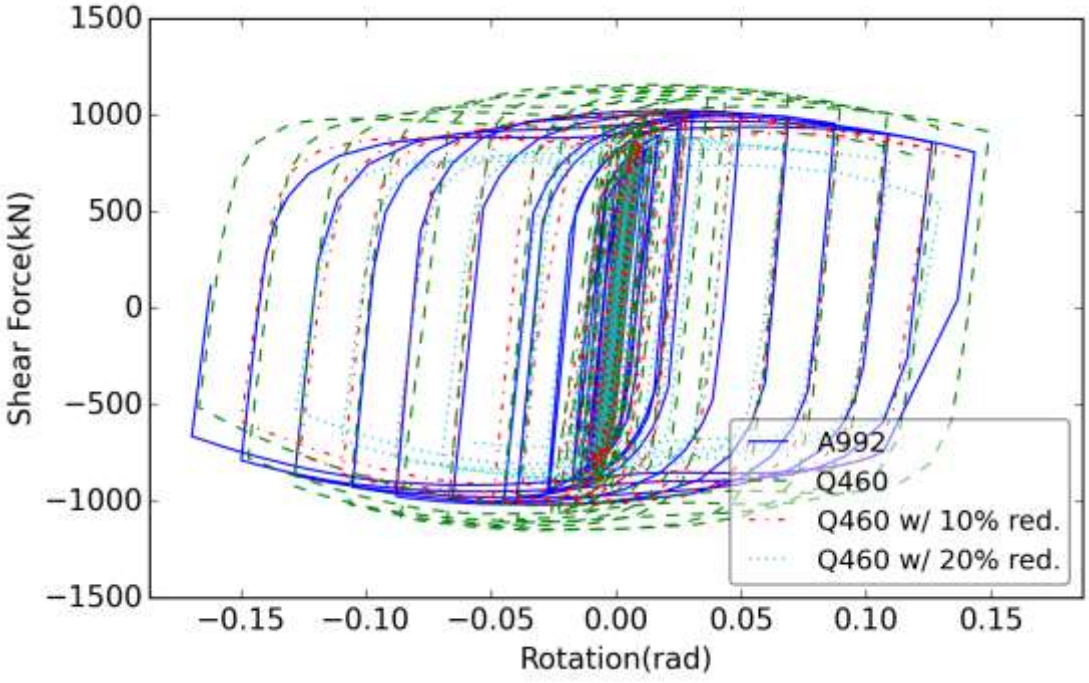

Figure 4-26 Comparison of different variations of W10x68 (ρ=1.2)

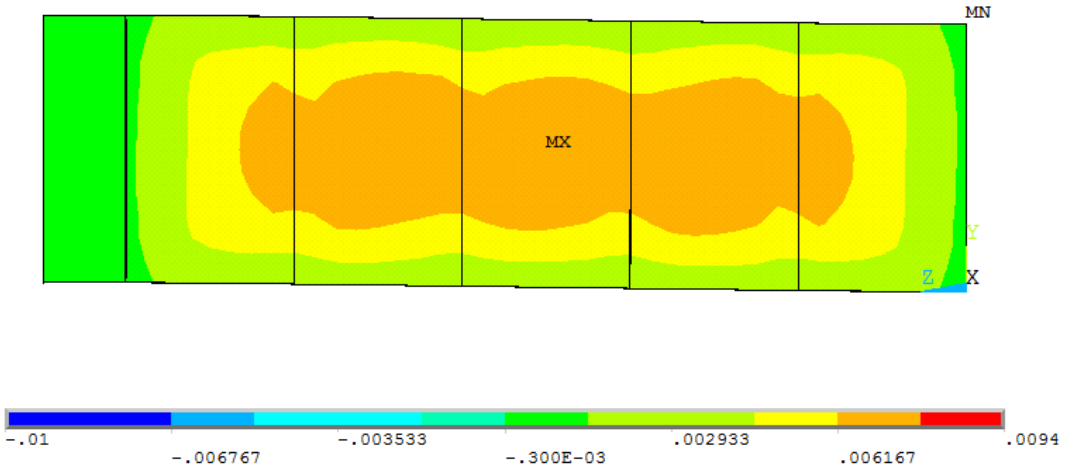

Figure 4-27 Plastic shear strain contour of A992 shear link W14x68 (ρ=1.2) at γ=0.015 rad

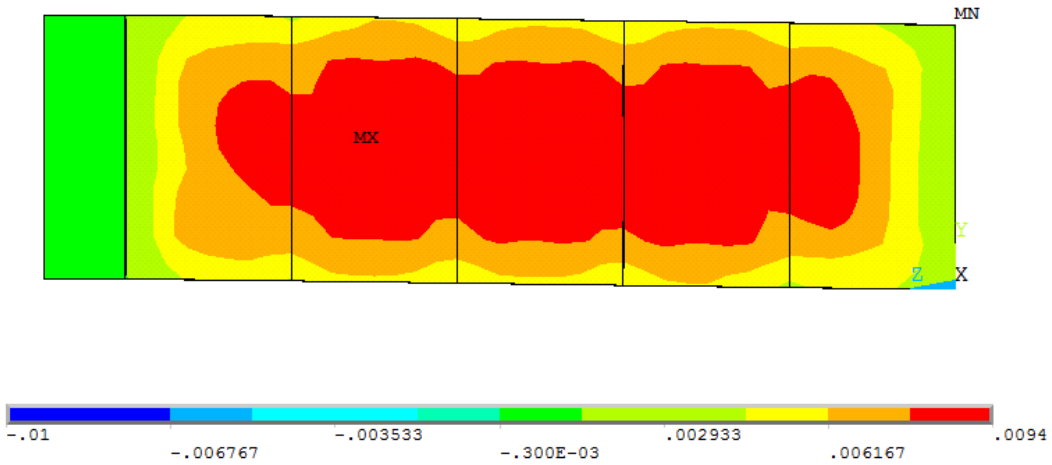

Figure 4-28 Plastic shear strain contour of Q460 shear link W14x68 (ρ=1.2) at γ=0.015 rad

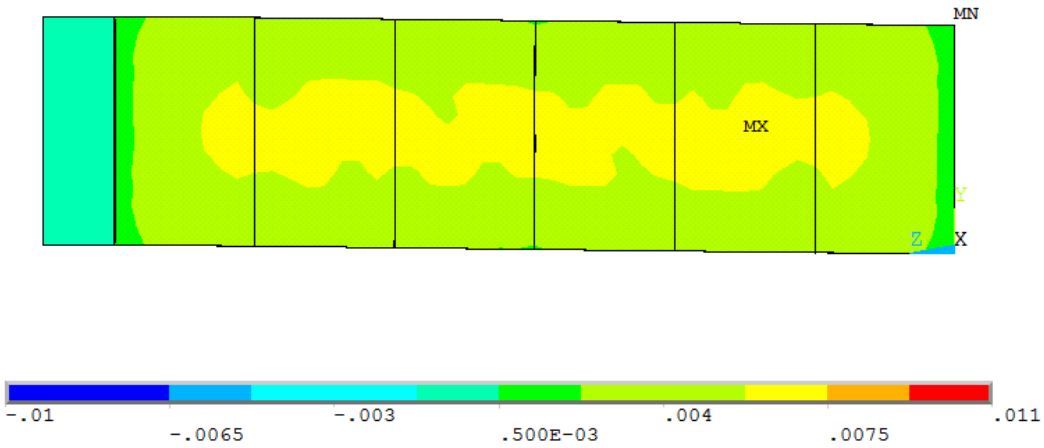

Figure 4-29 Plastic shear strain contour of A992 shear link W14x68 (ρ=1.4), at γ=0.015 rad

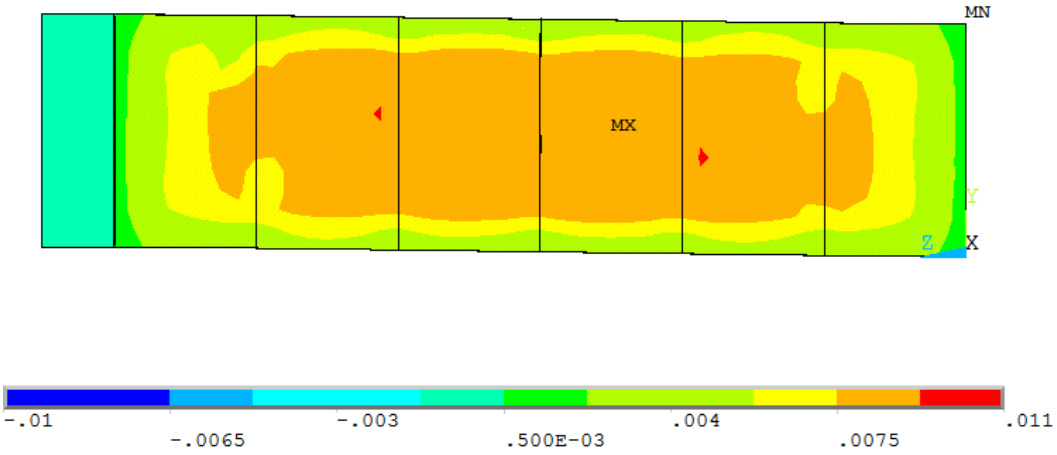

Figure 4-30 Plastic shear strain contour of Q460 shear link W14x68 (ρ=1.4), at γ=0.015 rad

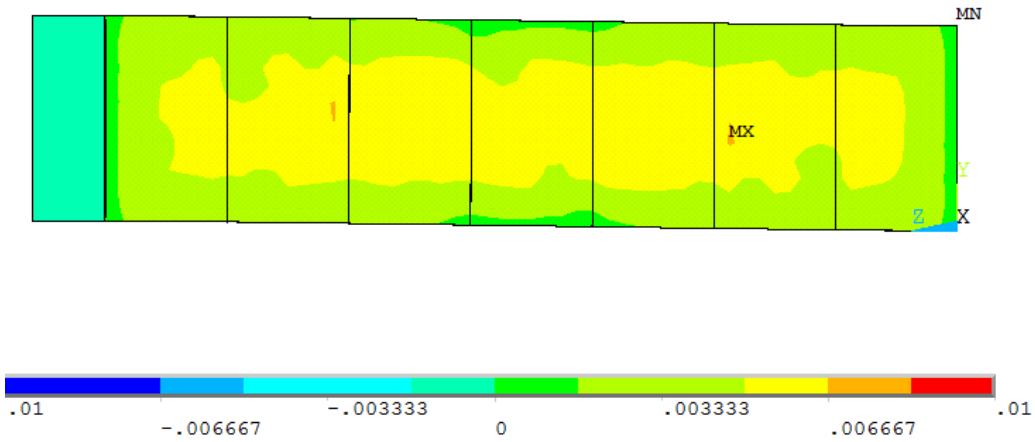

Figure 4-31 Plastic shear strain contour of A992 shear link W14x68 (ρ=1.6), at γ=0.015 rad

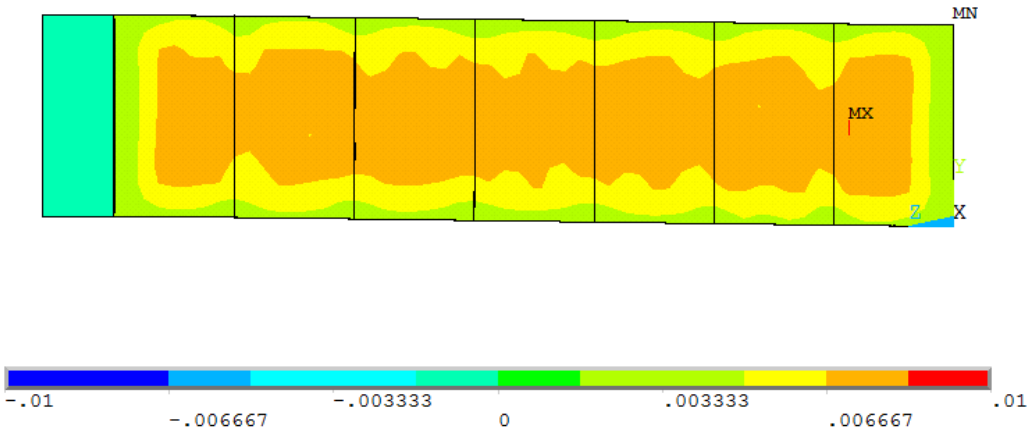

Figure 4-32 Plastic shear strain contour of Q460 shear link W14x68 (ρ=1.6), at γ=0.015 rad

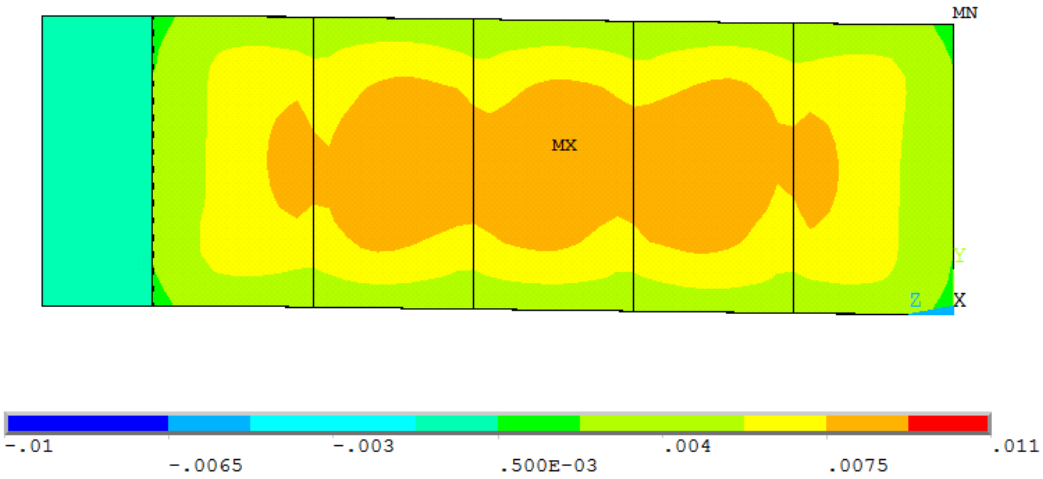

Figure 4-33 Plastic shear strain contour of A992 shear link W10x33, at γ=0.015 rad

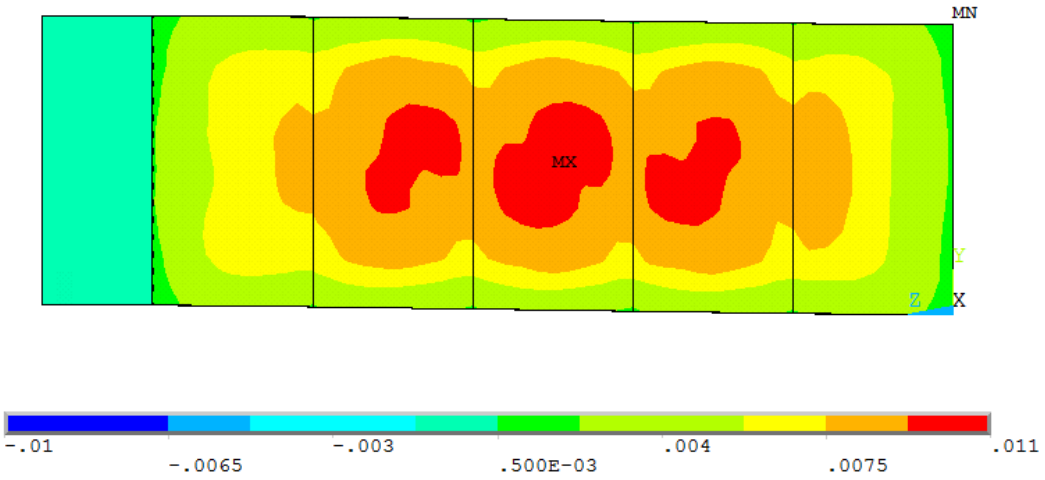

Figure 4-34 Plastic shear strain contour of Q460 shear link W10x33, at γ=0.015 rad

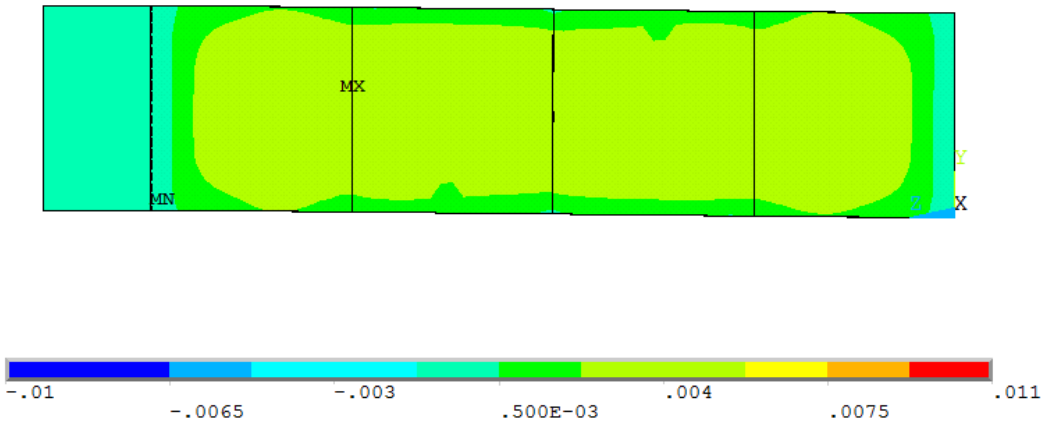

Figure 4-35 Plastic shear strain contour of A992 shear link W10x68, at γ=0.015 rad

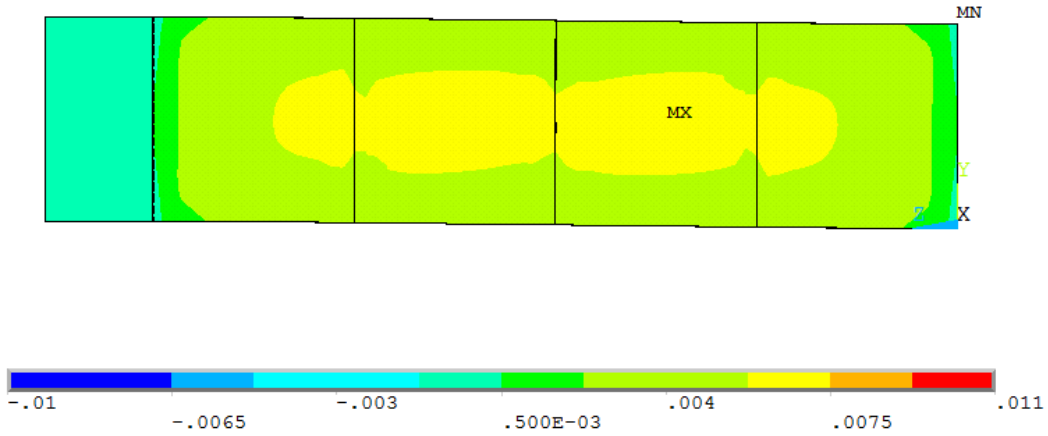

Figure 4-36 Plastic shear strain contour of Q460 shear link W10x68, at γ=0.015 rad

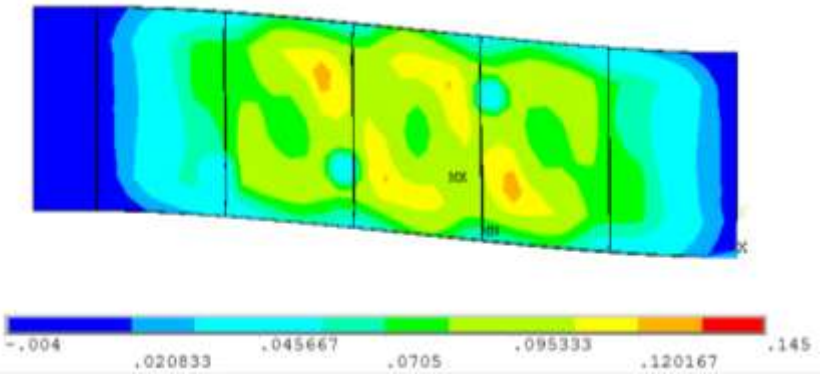

Figure 4-37 Plastic shear strain contour of A992 shear link W14x68 (ρ=1.2) at around γ=0.10 rad

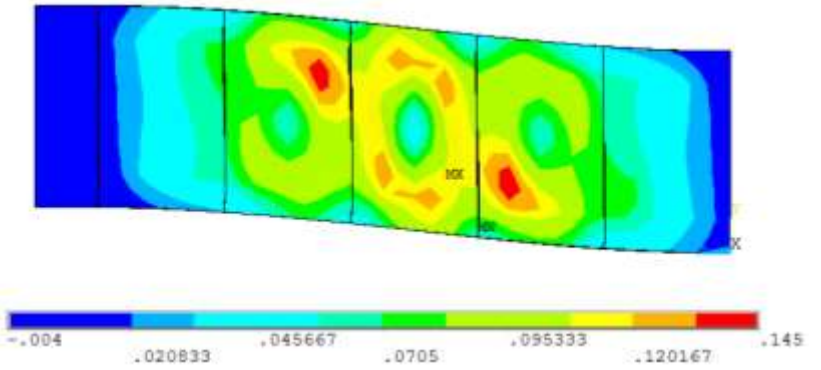

(a)

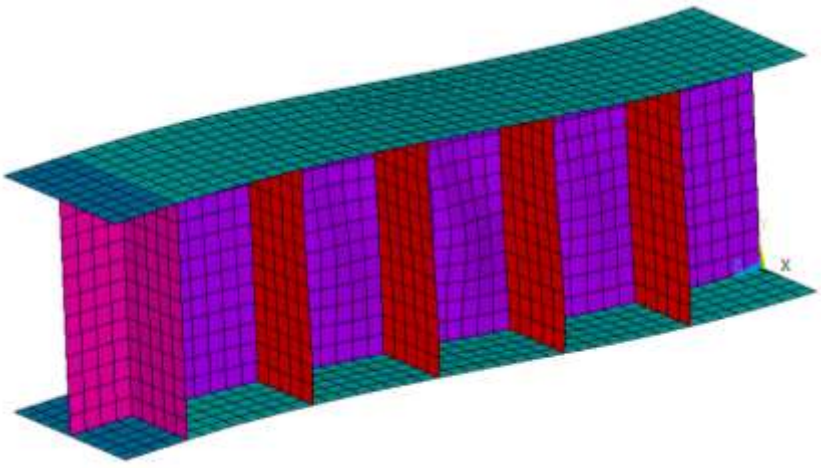

(b)

Figure 4-38 (a) Plastic shear strain contour; (b) Deformed shape of Q460 shear link W14x68 (ρ=1.2) at around γ=0.10 rad

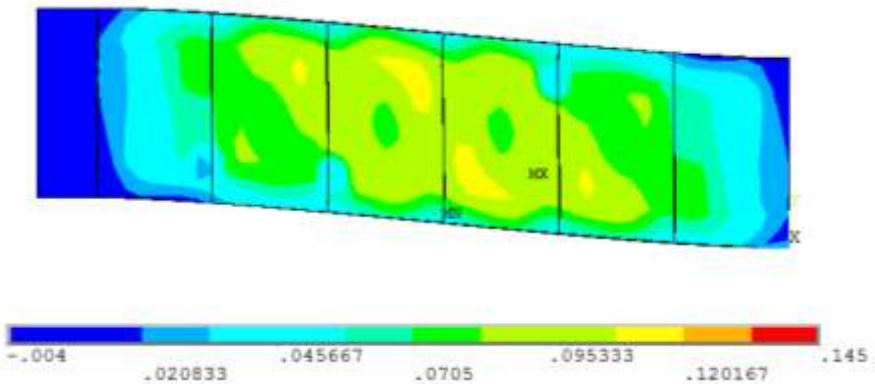

Figure 4-39 Plastic shear strain contour of A992 shear link W14x68 (ρ=1.4), at around γ=0.10 rad

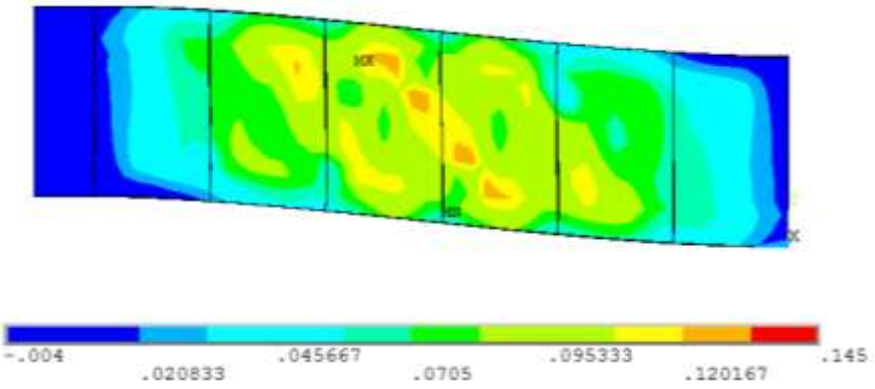

(a)

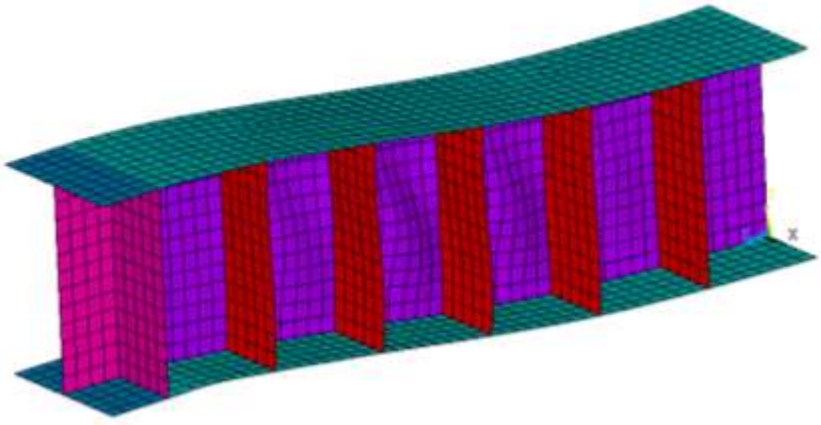

(b)

Figure 4-40 (a) Plastic shear strain contour; (b) Deformed shape of Q460 shear link W14x68 (ρ=1.4), at around γ=0.10 rad

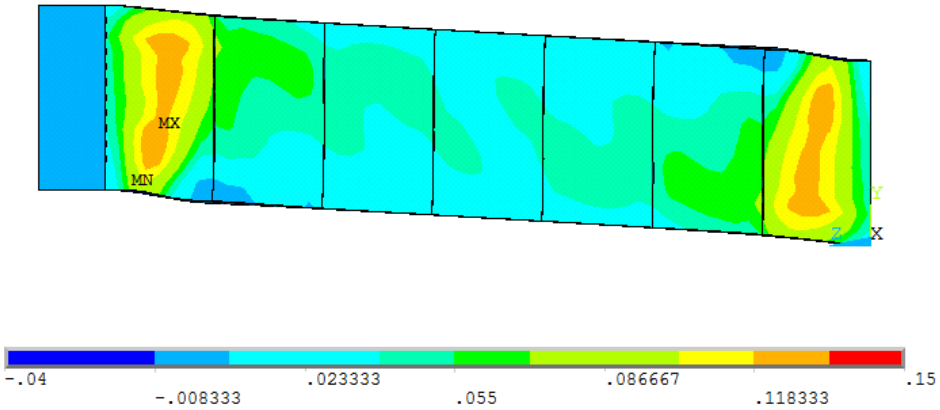

Figure 4-41 Plastic shear strain contour of A992 shear link W14x68 (ρ=1.6), at around γ=0.10 rad

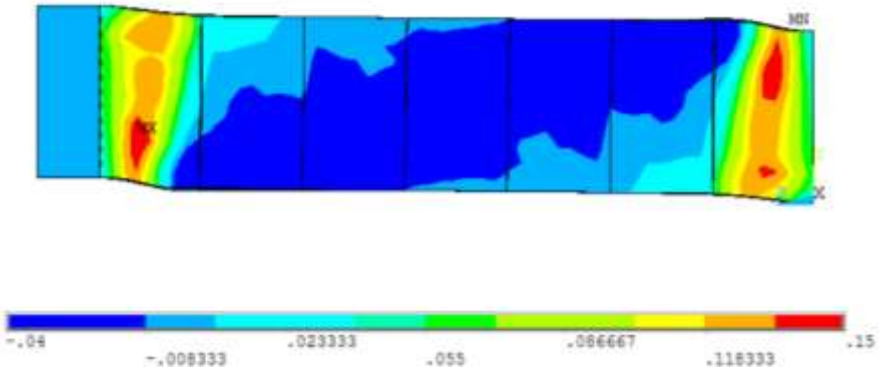

(a)

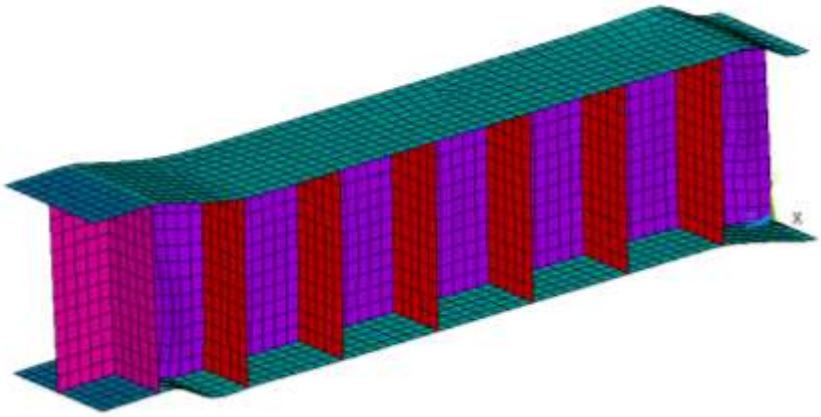

(b)

Figure 4-42 (a) Plastic shear strain contour; (b) Deformed shape of Q460 shear link W14x68 (ρ=1.6), at around γ=0.10 rad

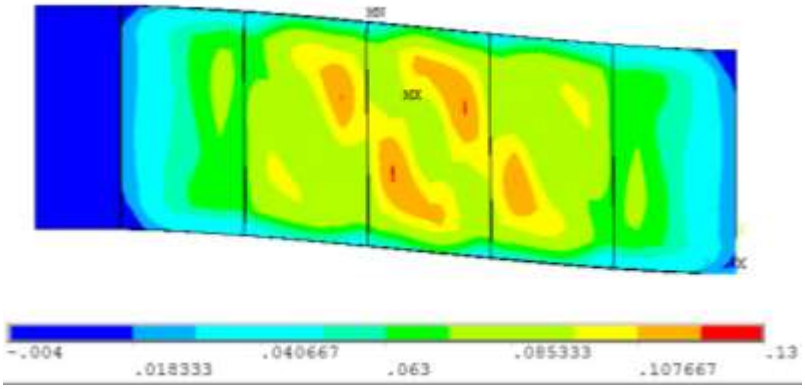

Figure 4-43 Plastic shear strain contour of A992 shear link W10x33, at around γ=0.10 rad

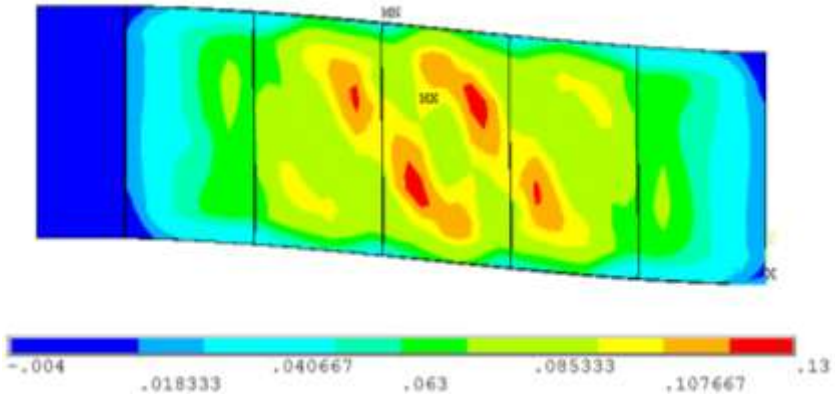

(a)

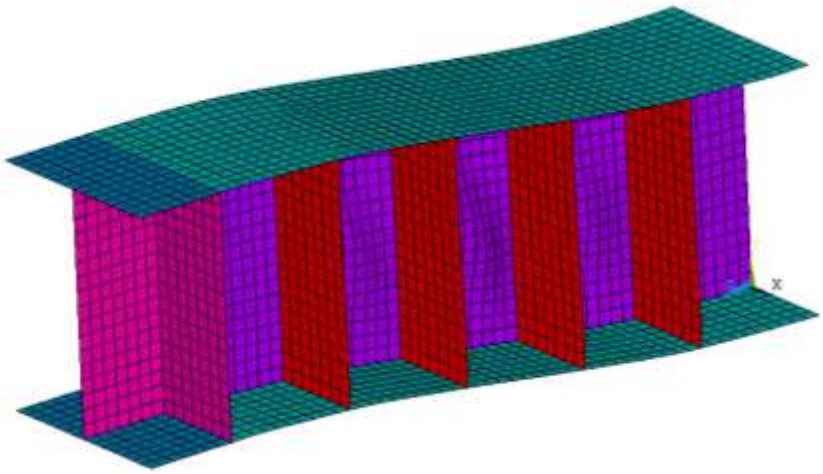

(b)

Figure 4-44 (a) Plastic shear strain contour; (b) Deformed shape of Q460 shear link W10x33, at around γ=0.10 rad

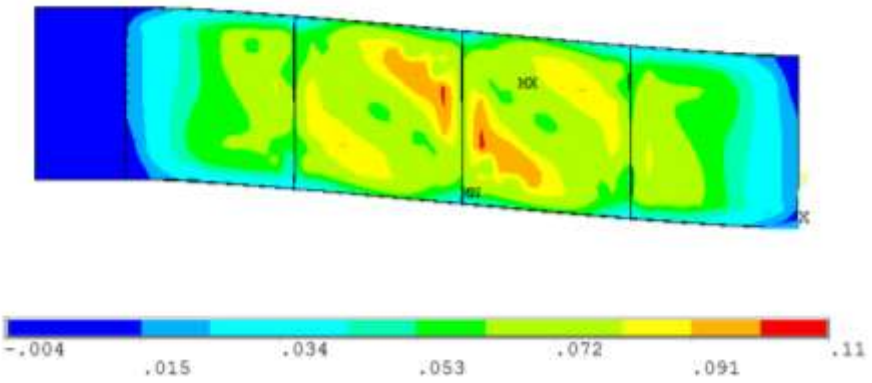

Figure 4-45 Plastic shear strain contour of A992 shear link W10x68, at around γ=0.10 rad

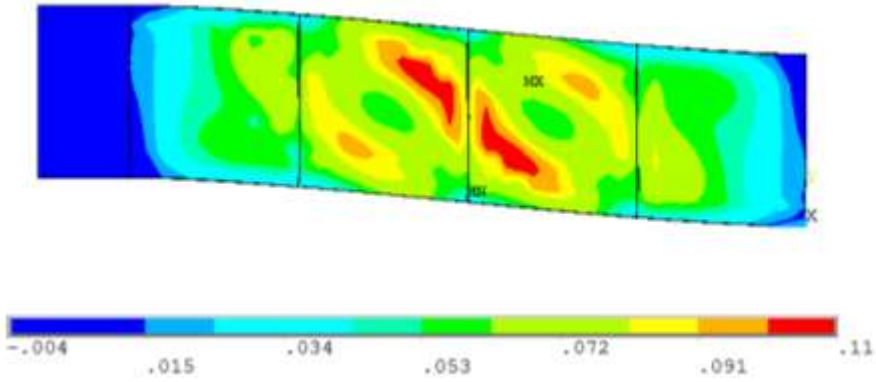

(a)

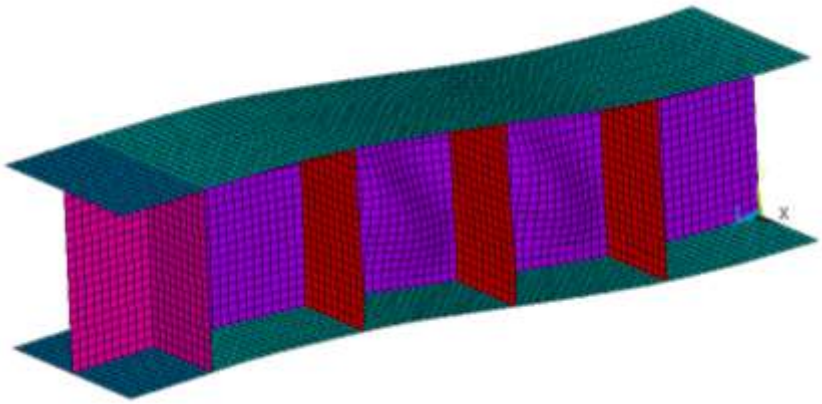

(b)

Figure 4-46 (a) Plastic shear strain contour; (b) Deformed shape of Q460 shear link W10x68, at around γ=0.10 rad

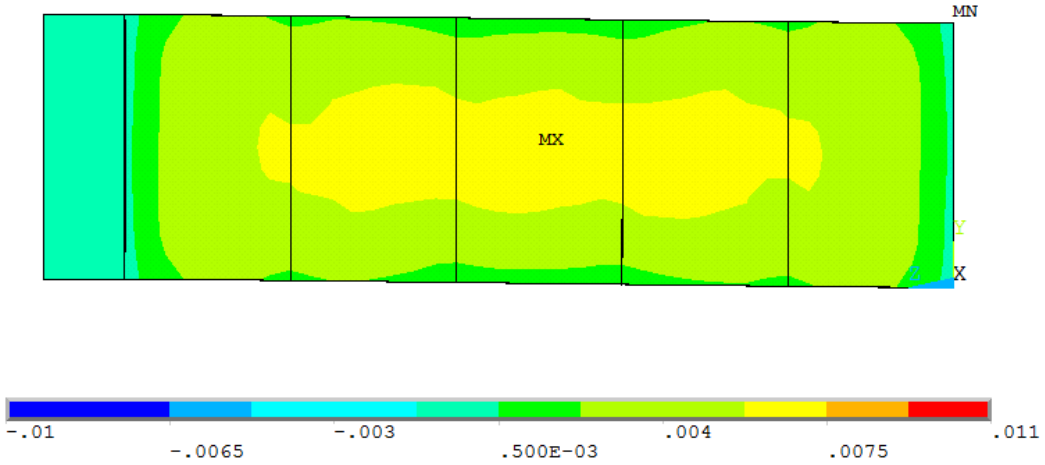

Figure 4-47 Plastic shear strain contour of Q460 shear link W14x68 (ρ=1.2), 10% red. at γ=0.01rad

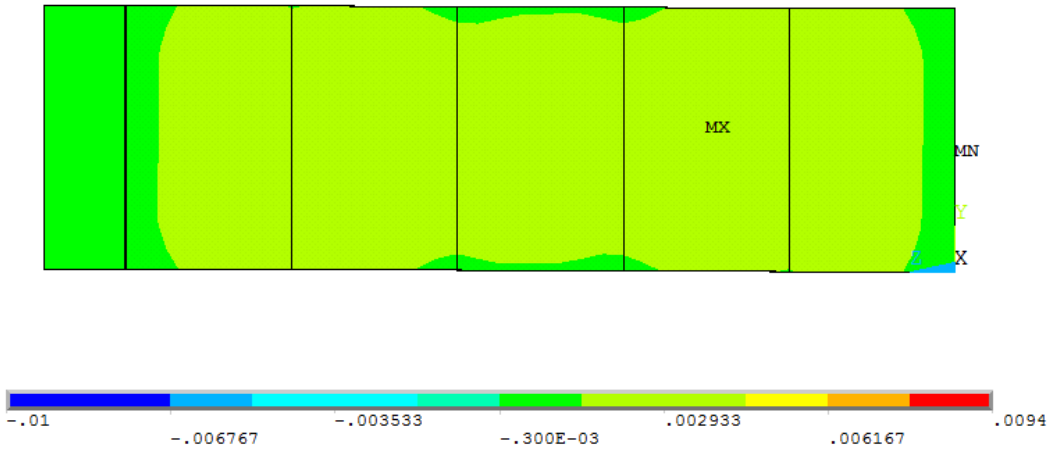

Figure 4-48 Plastic shear strain contour of Q460 shear link W14x68 (ρ=1.2), 20% red. at γ=0.01 rad

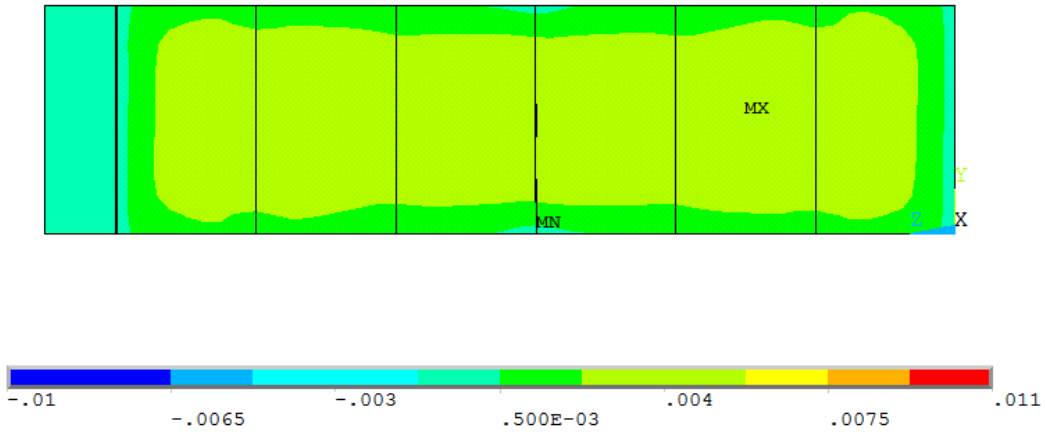

Figure 4-49 Plastic shear strain contour of Q460 shear link W14x68 (ρ=1.4), 10% red. at γ=0.01 rad

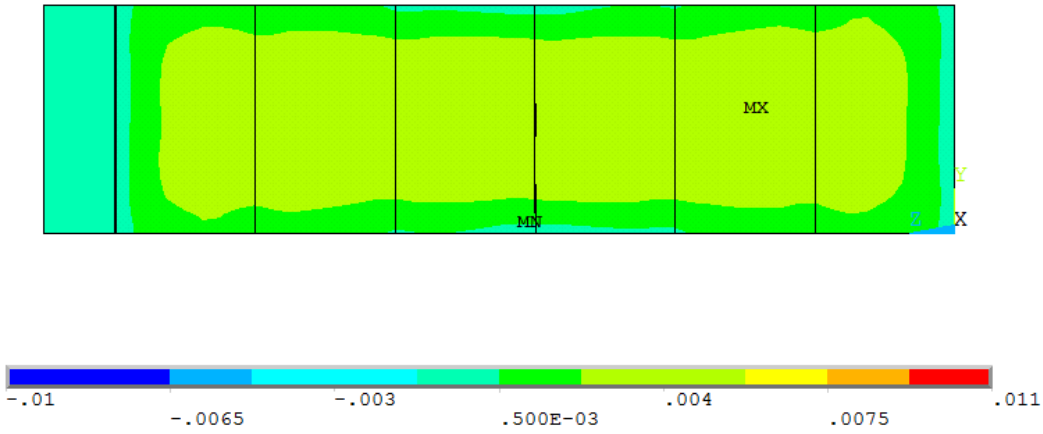

Figure 4-50 Plastic shear strain contour of Q460 shear link W14x68 (ρ=1.4), 20% red. at γ=0.01 rad

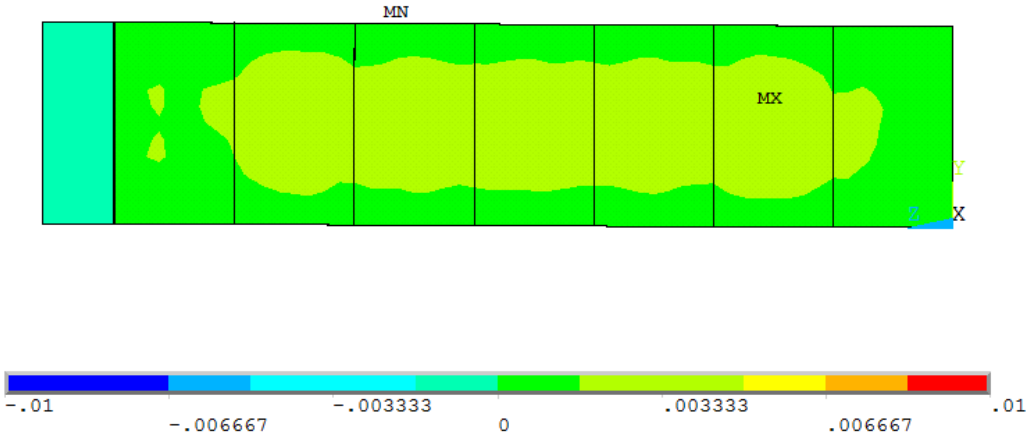

Figure 4-51 Plastic shear strain contour of Q460 shear link W14x68 (ρ=1.6), 10% red. at γ=0.01 rad

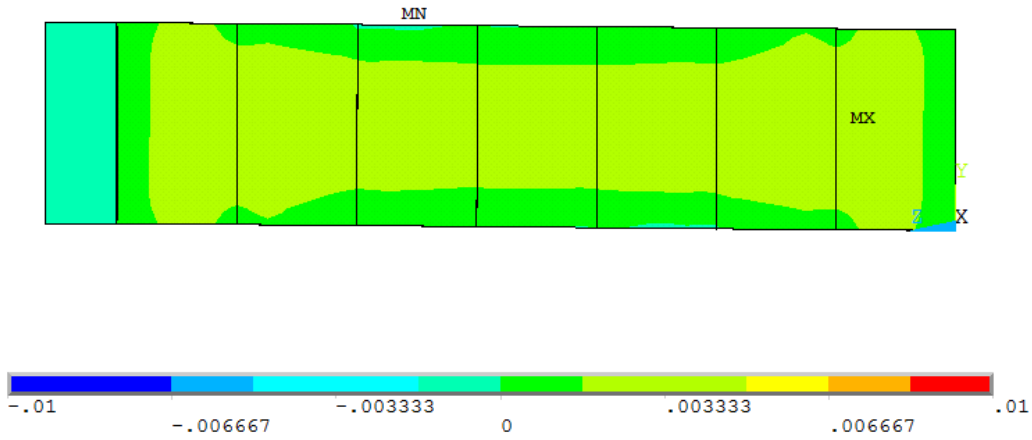

Figure 4-52 Plastic shear strain contour of Q460 shear link W14x68 (ρ=1.6), 20% red. at γ=0.01 rad

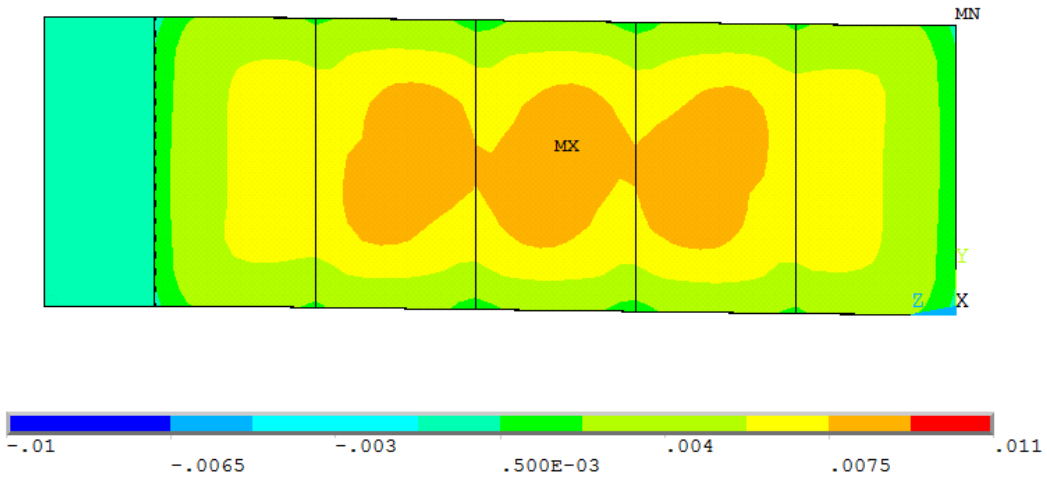

Figure 4-53 Plastic shear strain contour of Q460 shear link W10x33, 10% red. at γ=0.01 rad

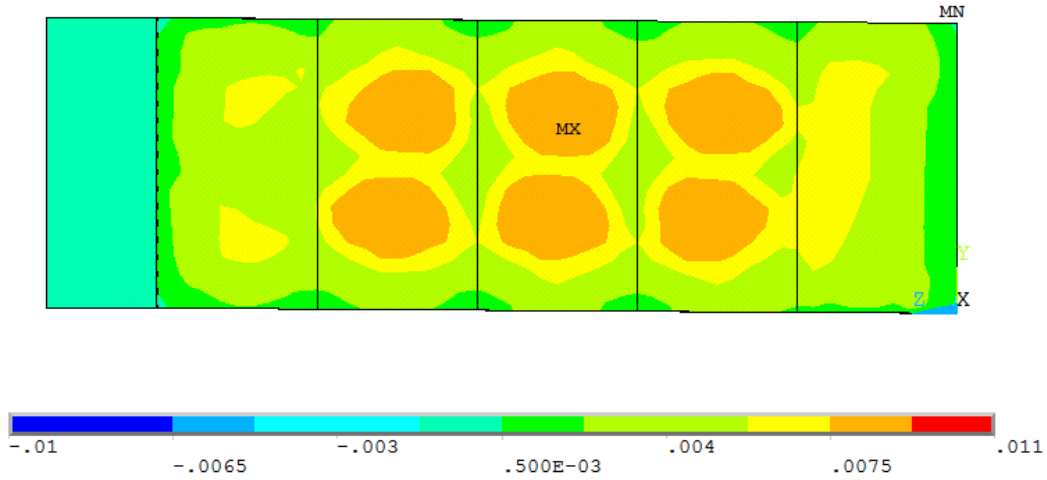

Figure 4-54 Plastic shear strain contour of Q460 shear link W10x33, 20% red. at γ=0.01 rad

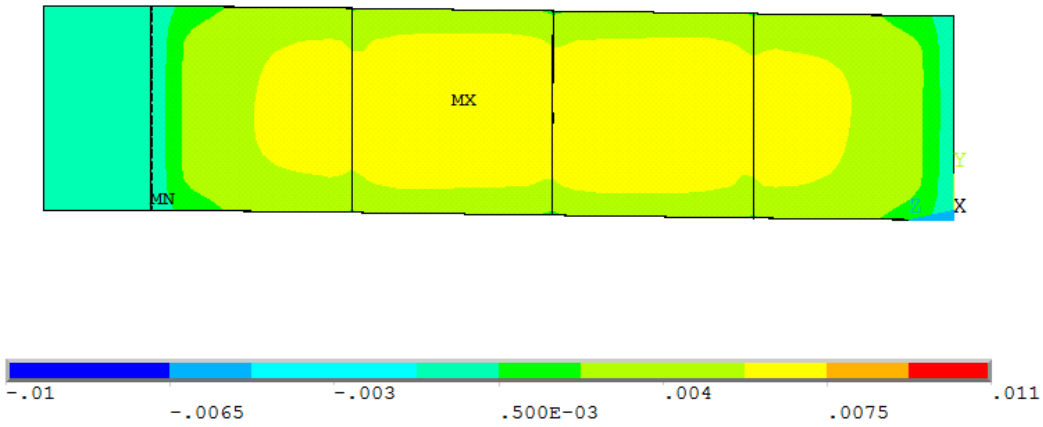

Figure 4-55 Plastic shear strain contour of Q460 shear link W10x68, 10% red. at γ=0.01 rad

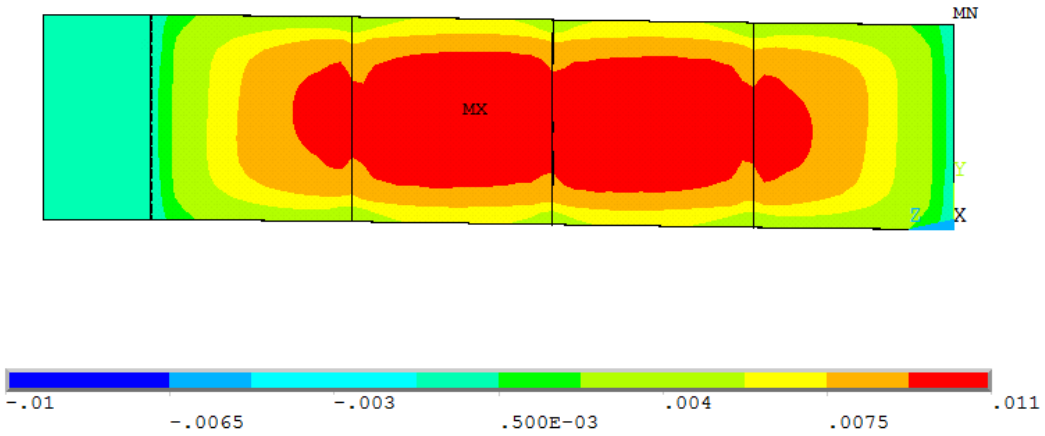

Figure 4-56 Plastic shear strain contour of Q460 shear link W10x68, 20% red. at γ=0.01 rad

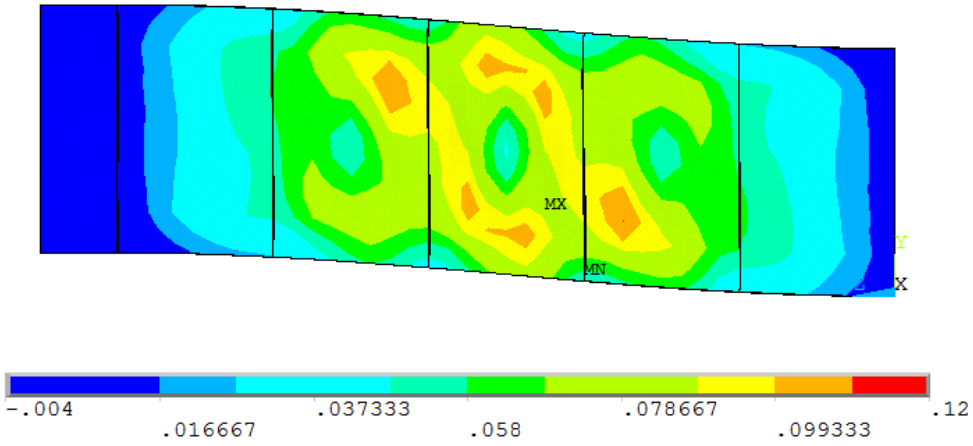

Figure 4-57 Plastic shear strain contour of Q460 shear link W14x68 (ρ=1.2), 10% red. at around γ=0.08 rad

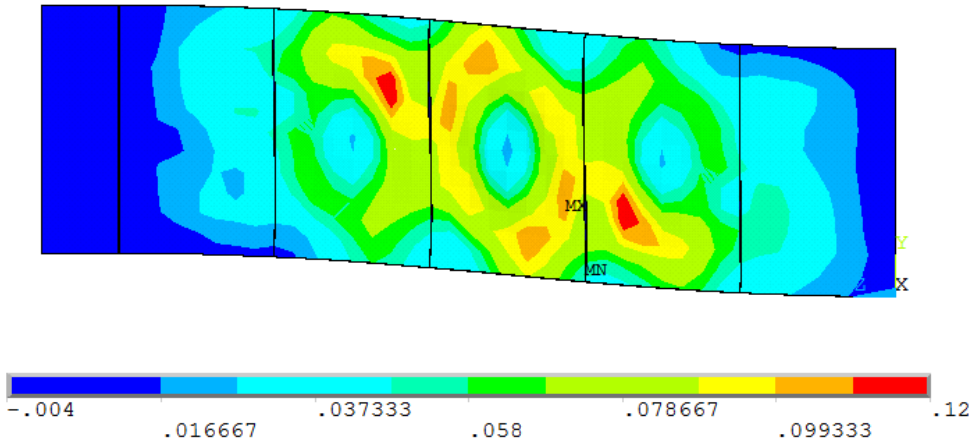

Figure 4-58 Plastic shear strain contour of Q460 shear link W14x68 (ρ=1.2), 20% red. at around γ=0.08 rad

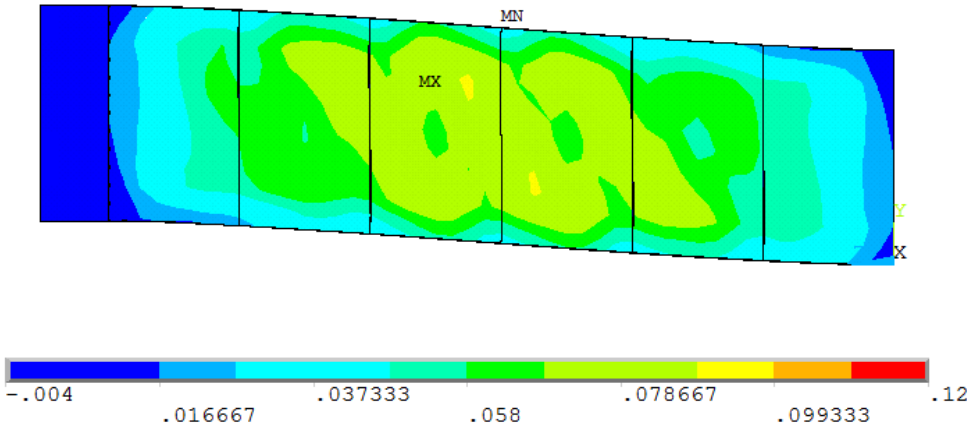

Figure 4-59 Plastic shear strain contour of Q460 shear link W14x68 (ρ=1.4), 10% red. at around γ=0.08 rad

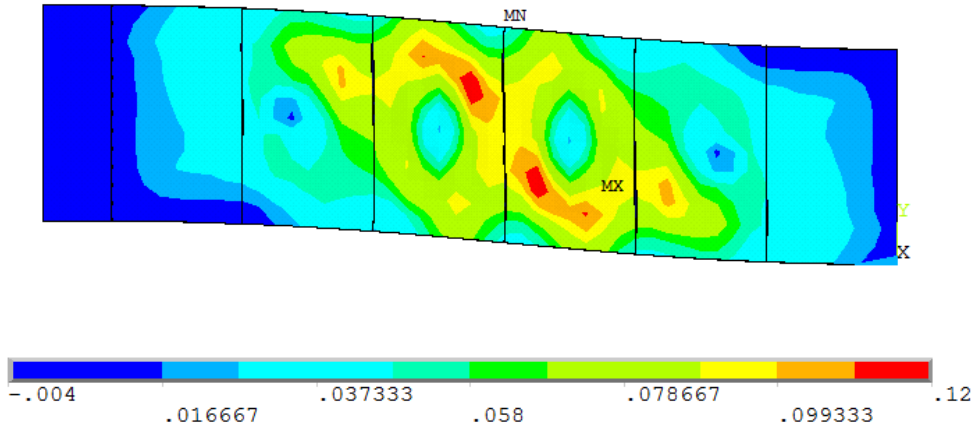

Figure 4-60 Plastic shear strain contour of Q460 shear link W14x68 (ρ=1.4), 20% red. at around γ=0.08 rad

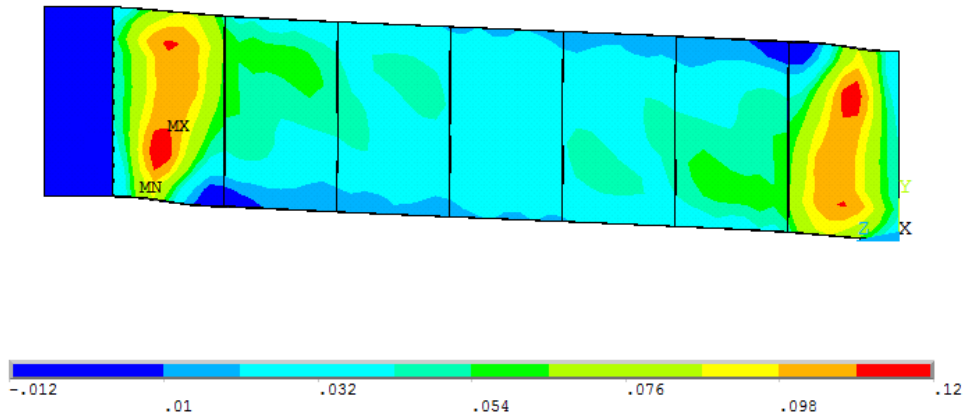

Figure 4-61 Plastic shear strain contour of Q460 shear link W14x68 (ρ=1.6), 10% red. at around γ=0.08 rad

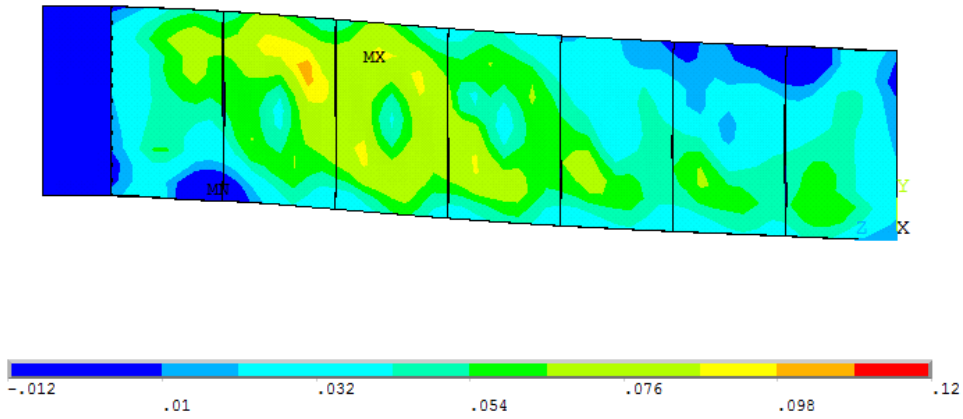

Figure 4-62 Plastic shear strain contour of Q460 shear link W14x68 (ρ=1.6), 20% red. at around γ=0.08 rad

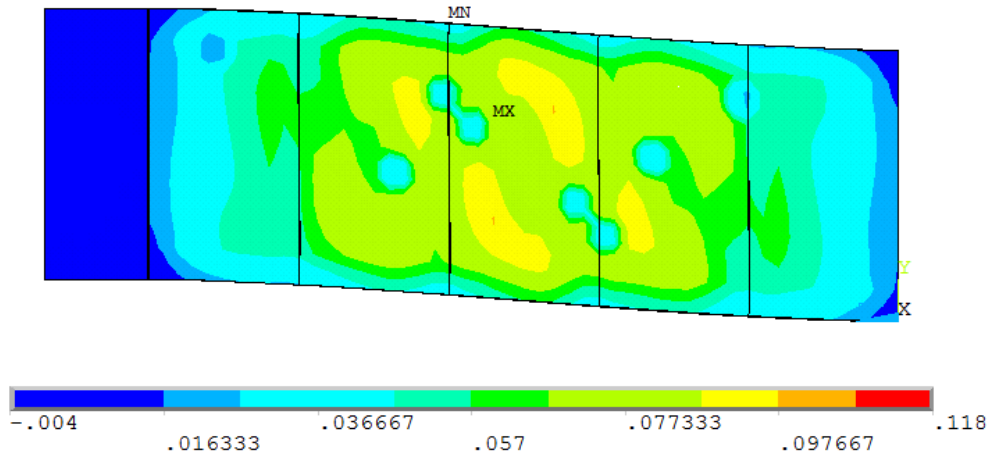

Figure 4-63 Plastic shear strain contour of Q460 shear link W10x33, 10% red. at around γ=0.08 rad

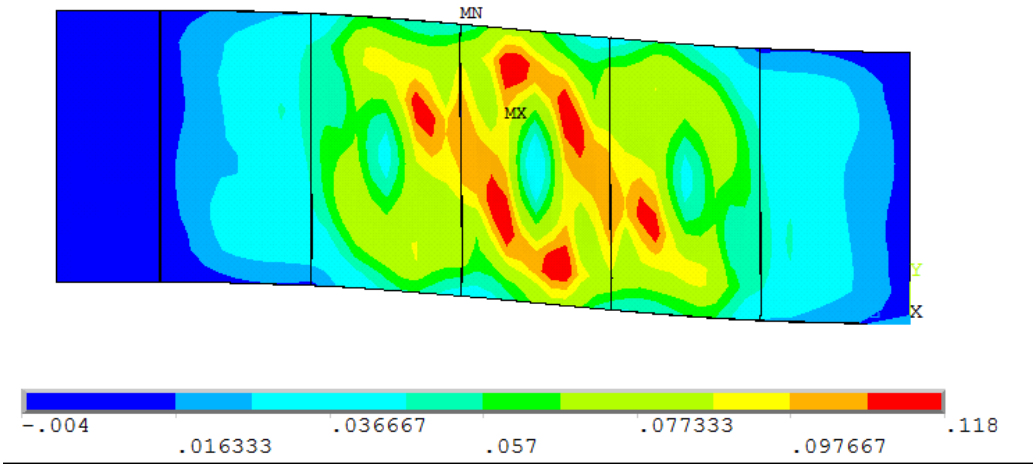

Figure 4-64 Plastic shear strain contour of Q460 shear link W10x33, 20% red. at around γ=0.08 rad

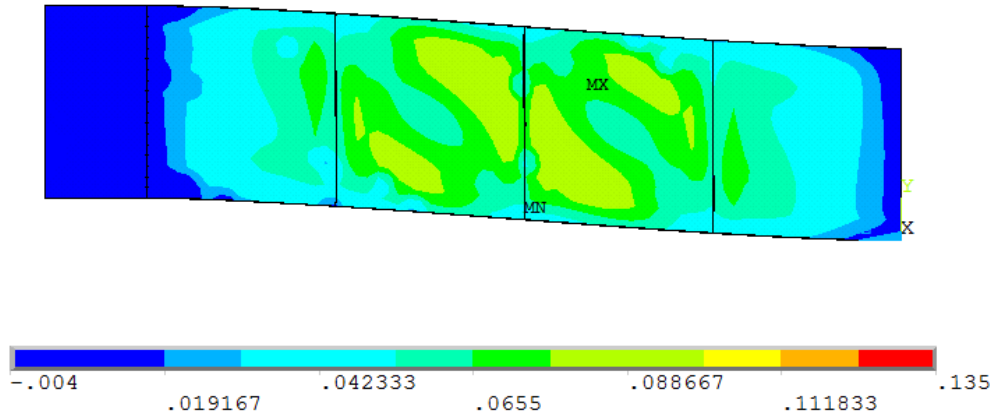

Figure 4-65 Plastic shear strain contour of Q460 steel shear link W10x68 with 10% section reduction at around γ=0.08 radians

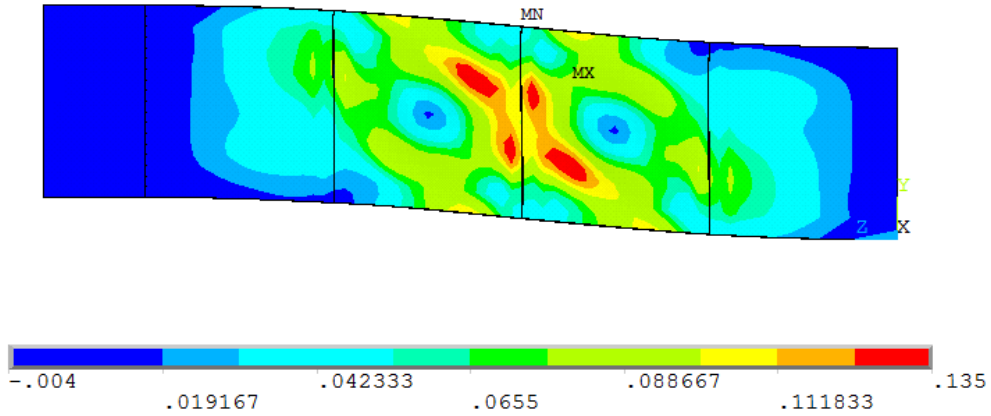

Figure 4-66 Plastic shear strain contour of Q460 shear link W10x68, 20% red. at around γ=0.08 rad

CHAPTER 5: CONCLUSIONS AND FUTURE WORK

5.1 Conclusions

EBFs are an important seismic force resisting system in the modern buildings, where shear links play a crucial role to provide the ductility and absorb the energy inflicted to the building by earthquake ground motion. In this study, the seismic performance of shear links made of Q460 high strength steel is investigated with numerical simulation.

In order to perform numerical simulation based parametric study on shear links models, ANSYS command line suit is utilized, which can be used to build and test a shear link section with user specified parameters.

The five initial shear link specimens are designed, each was made from different steel grades including ASTM A992 (345MPa) steel and Q460 (460MPa) high strength steel. An additional set of 10 shear link specimens made of high strength steel are designed to have a 10% and 20% size reduction in section area compared with the corresponding unreduced shear link specimen. Finite element models of all these 20 shear link specimens are built in ANSYS software. We used ANSYS command line tool to automate and accelerate the simulation of models in ANSYS and discussed core snippet of the code.

Five performance indices are evaluated to quantitatively assess the seismic behavior of Q460 steel shear links subjected to cyclic lateral load and varying axial force: stiffness, ductility, shear strength, over-strength factor, energy dissipation, and failure mode. Based on the numerical simulation results, the following conclusion can be drawn:

1. By using Q460 high strength steel for shear links, smaller over-strength factor values and higher energy dissipation capacity are achieved compared to corresponding A992 steel shear links. Although reduced ductility due to local buckling is observed in Q460 steel shear links, this can be alleviated by adding more stiffeners. All shear links made of Q460 steel considered in this study can achieve 0.08 radian inelastic link rotation.
2. When the section size of Q460 steel shear links is reduced by 10%, the performance is comparable to that of corresponding A992 steel shear links with no section reduction. However, further section size reduction to 20% lead to deteriorated performance. It is expect that additional section reduction would be made possible by using even higher strength steel like A100 or Q510 steel for shear links. Section size reduction and thus weight reduction is important to replaceable shear link replacement when manual installation might be necessary due to lack of heavy lifting equipment after strong earthquakes.
3. When varying cyclic axial load is applied in additional to cyclic lateral loading, the seismic performance tends to deteriorate compared with the corresponding case without axial load. This can be explained by the observed web local buckling in most of the numerical simulation cases.

In general, the numerical simulation results reveal that shear links made of Q460 high strength steel have satisfactory performance compared with A992 steel shear links, with additional benefits of material saving and weight reduction, often desired

features for sustainable steel construction and replaceable fuse elements in seismic resistant structures.

5.2 Future work

The goal of this study is to investigate the potential benefits of shear links made of Q460 high strength steel. With steel grade of higher strength, it is likely to achieve comparable seismic performance with further reduced shear link section. It is noted that ultra-high strength steel, such as ASTM A100 or Q510, are currently available. It would be interesting to look at the seismic behavior of shear links made of ultra-high strength steel and potential further weight reduction.

The current numerical simulation study did not consider two effects in finite element modeling: fracture initiation and residual stress in heat affected zone. Under certain conditions, the ultimate behavior of shear links might be controlled by fracture development. It is suggested that future study should include fracture initiation criteria and residual stress modeling in numerical simulation and calibrated with experimental data to further improve the accuracy of numerical simulation results.

BIBLIOGRAPHY

AISC. (2010). “Seismic provisions for structural steel buildings.” *ANSI/AISC 341-05*. Chicago, IL.

ANSYS Mechanical APDL. ANSYS Academic Teaching Introductory. ANSYS, Inc. (2013).

Chaboche, J. L. (1986). Time-independent constitutive theories for cyclic plasticity. *International Journal of Plasticity*, 2(2), 149-188.

Chen, Y., and Lu, X. (2015). New replaceable coupling beams for shear wall structures. *15WCEE*, Lisbon, Portugal, Paper-ID, 2583, 24-28.

Corte, G.D., D'Aniello, M., and Landolfo, R. (2013). “Analytical and numerical study of plastic overstrength of shear links.” Journal of Constructional Steel Research., 82:19–32.

Dai, G., Wang, F., Shi, G., and Shi, Y. (2012). “Comparison of Monotonic and Cyclic Performances of Structural Steel Q345 and Q460.” *Industrial Architecture,* Vol. 42, No.1. 13 - 17

Dastmalchi, S. (2014). “Numerical Study of Axial Load Effect on the Seismic Behavior of Shear Links.” *Master Thesis*. http://hdl.handle.net/1903/15865

Dusicka, P., Itani, A. M., and Buckle, I. G. (2004) "Finite element investigation of steel built-up shear links subjected to inelastic deformations." *Earthquake Engineering and Engineering Vibration* 3.2: 195-203.

Dusicka, P., Itani, A. M., and Buckle, I. G. (2010). "Cyclic Behavior of Shear Links of Various Grades of Plate Steel." *J. Struct. Eng. ASCE.*, 136(4): 370-8.

A.J. Fussell, K.A. Cowie, G.C. Clifton, and N. Mago. (2014). Development and research of eccentrically braced frames with replaceable active links. *NZSEE Conference.* 1 - 13

Green, P. S., Sause, R., & Ricles, J. M. (2002). Strength and ductility of HPS flexural members. *Journal of Constructional Steel Research*, 58(5), 907-941. Chicago

Li, R., Zhang, Y., and Tong, L. (2014). "Numerical study of the cyclic load behavior of AISI 316L stainless steel shear links for seismic fuse device." *Frontiers of Structural and Civil Engineering.*, 10.1007/s11709-014-0276-4, 414-426.

Lu, X., Chen, Y., and Jiang. H. (2013). Research progress in new replaceable coupling beams. *Journal of Earthquake Engineering and Engineering Vibration*. Vol. 33 No. 1. pp 8 - 15

Mansour, N., Christopoulosew, C., & Tremblay, R. (2011). Experimental validation of replaceable shear links for eccentrically braced steel frames. *Journal of Structural Engineering*, 137(10), 1141-1152.

Okazaki, T., and Engelhardt, M. D. (2007). "Cyclic loading behavior of EBF links constructed of ASTM A992 steel." *J. of Construction Steel Research*. 63:751–765.

Park, R. (1989). "Evaluation of Ductility of Structures and Structural Assemblages from Laboratory Testing." *Bulletin of the New Zealand National Society for Earthquake Engineering,* Vol. 22, No. 3.

Richards, P. W., and Uang, C. M. (2005). "Effect of flange width thickness ratio on eccentrically braced frame link cyclic rotation capacity." *J. Struct. Eng. ASCE,* 131(10): 1546-52.

Shi, G., Shi, Y., and Wang. Y. (2009). "Analysis on Overall Buckling Behavior of Ultra-high Strength Steel Columns by ANSYS." *Journal of Jilin University,* Vol. 39, No.1. 113-118

Shi, G., Wang, F., Dai, G., Wang, Y., and Shi, Y. (2011). "Cyclic Loading Tests on High Strength Steel Q460C." *Journal of Southeast University,* Vol. 41, No.6. 1259-1265

Shi, G., Wang, M., Bai, Y., Wang, F., Shi, Y., and Wang, Y. (2012a). "Experimental and modeling study of high-strength structural steel under cyclic loading." *Engineering Structures* 37 (2012): 1-13.

Shi, G., Wang, F., Dai, G., Wang, Y., and Shi, Y. (2012b). "Experimental Study of High Strength Structural Steel Q460D under Cyclic Loading." *China Civil Engineering Journal,* Vol. 45, No.7. 48-55

Shi, Y., Wang, M., and Wang, Y. (2012). "Experimental Study of Structural Steel Constitutive Relationship under Cyclic Loading." *Journal of Building Materials,* Vol. 15, No.3. 293 - 300

Wang, Y, Li, G., Cui, W., Chen, S., and Sun, F., (2015). Experimental investigation and modeling of cyclic behavior of high strength steel, *Journal of Constructional Steel Research*, Volume 104, 37-48.